THE SUPPLY OF NUTRIENTS TO THE SUBSURFACE CHLOROPHYLL MAXIMUM IN TEMPERATE SHELF SEAS

Thesis submitted in accordance with the requirements of the University of Liverpool for the degree of Doctor of Philosophy

By

Charlotte Anne June Williams

Department of Earth and Ocean Sciences

University of Liverpool

August 2013

Abstract

The supply of nutrients to the subsurface chlorophyll maximum in temperate shelf seas

Charlotte A. J. Williams

Shelf seas are believed to play an important role in the oceanic export of carbon (C). The combination of enhanced primary productivity partly induced by highly energetic mixing, together with the euphotic zone being in close proximity to the seabed, make the shelf seas highly efficient region for biological C sequestration. The high productivity observed in shelf seas also has high economical significance by supporting >90% of the global fish catch.

A subsurface peak in biomass, termed the subsurface chlorophyll maximum (SCM), at the base of the thermocline occurs as a result of phytoplankton being nitrate limited in the surface layer. The SCM is believed to be responsible for as much primary production as the spring bloom. The turbulent supply of nutrients across the thermocline, driven by the internal tide and wind-driven inertial oscillations, is believed to support growth at the SCM. However, although inertial oscillations are recognised as an important mixing mechanism, the turbulent flux of nitrate that they supply has not yet been estimated.

In this thesis the importance of diapycnal fluxes of nutrients, particularly those generated by wind-driven inertial oscillations, is investigated in terms of sustaining productivity in the SCM, using a Lagrangian numerical model, observational and experimental approaches. The results in this study indicate that diapycnal nitrate fluxes limit new production at the SCM, and mixing generated by wind-driven inertial oscillations play a key role in supporting primary production at the SCM. In addition, this study demonstrates that the background nitrate flux, as well as transport of nitrate via dinoflagellate migration, are too low to sustain primary productivity at the SCM Our observations demonstrate that wind-driven

large, short-lived dissipation events increase the daily nitrate flux to the SCM by a factor of at least 17, supplying the SCM with ~33% to 71% of the nitrate required for new production in shelf seas during summer. Thus it is intermittent mixing events which must supply the required nitrate for new production at the SCM. Using an experimental approach, a wind event was simulated in order to estimate the impact of mixing of water from the SCM and BML on primary and secondary production in the SCM. Nutrients were assimilated rapidly and phytoplankton production increased as expected. However, up to two thirds of the C fixed was exuded as DOC and there was a significant increase in bacterial activity. As well as supplying nutrients to the SCM, we show that diapycnal mixing may also be important in redistribution plankton, especially bacteria, which subsequently impacts both the inorganic and organic nutrient pools. Thus the sensitivity of the SCM, in terms of autotrophy and heterotrophy, to diapycnal mixing is highlighted.

This study highlights the importance of short-lived events in supplying nutrients to the SCM. Concluding that these are likely undersampled and also not well represented in shelf sea models. In addition, this thesis demonstrates that there is a need to consider secondary as well as primary production to fully understand the C cycle in the shelf sea.

Declaration

I certify that the work described in this thesis is my own except where otherwise stated and has not previously been submitted for any degree at this or any other University.

Charlotte. A. J. Williams

Acknowledgements

I would like to thank my supervisors, Jonathan, Claire and Tom for the time, support, and knowledgeable advice they have given me over the years. I am so incredibly grateful. Jonathan: thank you for all of the discussions which have always led on to interesting scientific ideas, and always inspiring in me a new way of understanding and dissecting science. Claire: I cannot thank you enough, I am so appreciative of the time you have invested in me, the support you have provided me over the past years has been beyond the call of duty. I definitely wasn't a natural in the lab when I started, so also thank you for teaching me everything I know.

I am also very grateful to Mattias Green of Bangor University for his invaluable input to the first paper manuscript, Alex Poulton of the National Oceanography Centre Southampton for patiently teaching me how to identify phytoplankton, as well as Jo Hopkins, Benny Lincoln, Yueng Lenn, Matthew Palmer, Jeff Polton, and Anna Hickman for their help with data and interesting discussions. I have been fortunate to work in a supportive, multidisciplinary department, where staff have always shown great interest in all research projects and given fantastic feedback in presentations. So thank you to Ric Williams, Harry Leach, George Wolff, Pascal Salaun, Rachel Jeffreys and the rest of the Nicholson building staff for all of the stimulating discussions they have provided.

I've been extremely lucky to do my PhD alongside Clare, Lucy, Nuala, Kasia, Nick, Anouska and Matt, who have become great friends and I hope will remain so. Thank you especially to Lucy, Sarah, Nuala and Kasia for being there for a tea break and a calming chat whenever things got a tad stressful. But mostly I want to thank Clare Davis, you have not only been the best PhD office buddy ever, but an immediate and firm best friend. I want to stress that you are stuck with me for life. As are Steve, Steph, Sarah, Katy, Abi, Colette and Amy, you've all been fantastic and a great support over these years.

I have saved thanking my family until the end, this is due to me struggling to express how grateful I am to them for everything. I can't, but I can tell you how much I love you all, and how everything I have achieved (including this entire thesis) is down to having you as my eternally supportive, loving and proud family. Gemma, my sister and best friend, thank you for your continuous and selfless support. George and Rob, cheers boys. Most importantly, Mum and Dad, I think I won the lottery of life having you both as parents, your guidance and encouragement is the reason I have accomplished all that I have up until now. Thank you.

For Mum and Dad,

Contents **Page**

Table of contents **Page**

Table of contents **Page**

List of figures **Page**

List of tables **Page**

1. Introduction

1.1 The oceanic carbon pump

The amount of carbon dioxide (CO_2) in the atmosphere has increased by more than 30% since pre-industrial times and is increasing at a rate of on average 0.4% per year (IPCC, 2001). The ocean is a significant sink for atmospheric carbon dioxide (Siegenthaler and Sarmiento, 1993) and is estimated to take up approximately a quarter of anthropogenic carbon (C) emissions (Canadell et al., 2007). Furthermore, the global oceans are also an enormous C reservoir, storing 50 times more C than the atmosphere (IPCC, 2001). Thus, fully comprehending the processes which may affect oceanic C dynamics is vital in terms of understanding the global C cycle.

C in the ocean can be transported from the surface to the deep ocean by two key processes, the solubility pump and the biological pump (Volk and Hoffert, 1985). The solubility pump is the combination of physical and chemical processes that transport CO_2 from the atmosphere to the ocean exterior as dissolved inorganic C (DIC). The solubility of CO_2 from the atmosphere to the sea surface is strongly related to temperature, with increased solubility occurring at lower sea surface temperatures. Subduction and thermohaline circulation in the ocean then act to transport DIC from the surface ocean to depth.

The biological pump involves the assimilation of DIC by autotrophic species. Marine phytoplankton are primary producers which assimilate DIC and 'fix' it into organic C via photosynthesis. The near-surface partial pressure of CO_2 (pCO_2) is reduced as a result of phytoplankton uptake of CO_2 in the surface, sunlit (euphotic) zone. The gradient in CO_2 concentrations between the atmosphere and sea surface is thus increased, driving an air-sea flux of CO_2. The C fixed during photosynthesis is either partitioned into phytoplankton biomass as particulate organic carbon (POC), where it is then made available to higher trophic levels, or into the dissolved pathway as dissolved organic carbon (DOC). When phytoplankton are eaten or die, a portion of the C fixed into biomass (POC) sinks as marine snow and is removed from the surface euphotic zone. However, subduction of DOC by ocean currents can also be an important C export pathway in some areas of the ocean (Hopkinson et al., 2002; Hopkinson and Vallino, 2005; Williams, 1995). The physical and biological processes that affect C fixation by phytoplankton and the rate of organic C export, are termed the biological pump.

There is almost 20 times more DIC in the ocean than organic C in the water column and in the top 1 m layer of the seabed sediments (IPCC, 2001). Though the solubility pump dominates the transport of CO_2 from the atmosphere to the ocean exterior as dissolved inorganic C (DIC), some of the DIC in the oceanic interior results from remineralisation of both POC and DOC that have arrived there via the biological pump. Furthermore, atmospheric CO_2 in the last glacial maximum is thought to have been influenced by changes in the biological pump (Sigman and Boyle, 2000). The biological pump also varies on smaller temporal scales, and the fixation of inorganic C by phytoplankton determines the flow of C through marine food webs.

Phytoplankton cell size plays an important role in determining the fate of organic C, whether it is transferred to higher trophic levels or is exported to the deep ocean (Legendre and Rivkin, 2002). Communities of large phytoplankton (>5 µm) are considered important for the export of particulate organic carbon (POC), as large cells sinks faster (Legendre and Rivkin, 2002). Larger cells are also more likely to be grazed directly by zooplankton and fish larvae. Comparatively, small cells (< 5 µm) play an important role in what is known as the microbial loop, where C and nutrients are recycled and a significant fraction of C is partitioned into the dissolved pool (Azam et al., 1983). Additionally, the transport of recalcitrant DOC from the euphotic zone to ocean interior has been acknowledged as an important long-term carbon storage mechanism, termed the 'microbial carbon pump' (Jiao et al. 2010). The community structure of phytoplankton therefore influences both C sequestration and the transfer of C to higher trophic levels.

Phytoplankton require sufficient light and nutrients in order to photosynthesise and fix C. In nutrient deplete regions phytoplankton communities are generally dominated by small-celled species (Munk and Riley, 1952; Chisholm, 1992), whereas large cells are associated with nutrient replete environments (Pingree et al., 1976). The supply of nutrients to the euphotic zone will determine the amount of C fixed in an area as well as the phytoplankton community that reside there, and consequently the rate of C export. Nutrients may be supplied externally to the euphotic zone via circulation and mixing mechanisms as well as atmospheric dust, riverine, sedimentary sources in the coastal zone. Nutrient supply to the euphotic zone in shelf seas is primarily determined by circulation and mixing mechanisms in

the ocean. Many physical mixing processes are either intensified within, or unique to, ocean boundaries (Jahnke, 2010). In particular the boundary between the coastal and deep ocean, known as the shelf seas, plays host to amplified physical mixing mechanisms, and is considered to be particularly important for the transport of C (as either dissolved or particulate matter) to the deep ocean (Tsunogai et al., 1999).

The oceanographic region of interest for this thesis is shelf seas, and the processes which may influence their role in the biological pump.

1.2 The importance of shelf seas

Shelf seas are the boundary between the coastal and deep ocean. They are typically less than 200 m deep and contribute approximately 9% of the global ocean surface area (Simpson and Sharples, 2012). Large changes in ocean depth are observed at the steep shelf sea edge, influencing the physical processes that occur in shelf seas. Shelf seas are considered to be crucial regions for C fixation, contributing to between 16 and 30% of global marine primary production (Wollast, 1998; Simpson & Sharples, 2012). Consequently, as high productivity regions the shelf seas may have a significant impact of air-sea C fluxes, ocean C storage and the export of C (Tsunogai et al., 1999; Muller-Karger et al., 2005; Borges, 2005; Jahnke, 2010). Shelf seas have been identified as net sinks of CO_2 (Frankignoulle et al, 2001; Borges, 2005; Borges et al., 2005; Chen and Borges, 2009), particularly those located in temperate latitudes (Frankignoulle and Borges., 2001; DeGrandpre et al., 2002; Thomas et al., 2004).

Tsunogai et al. (1999) formulated the idea that the solubility and biological pumps interact with shelf sea hydrography in a mechanism referred to as the continental shelf sea pump. The continental shelf restricts the convection of cooling water, resulting in the production of cold dense water in shelf seas which can cascade off the shelf into the deep ocean (Tsunogai et al., 1999; Wobus et al., 2011). This process acts to promote the solubility pump and increase DIC storage. Additionally, the increased biological productivity characteristic of shelf seas serves to amplify C storage via the biological pump (Jahnke, 2010).

New production in the open ocean is currently estimated to be 2.9 Pg C y^{-1} (Liu et al., 2000), of which just 10% (0.31 Pg C y^{-1}) is believed to settle to the seafloor

(Muller-Karger et al., 2005). In contrast, new production in shelf seas is estimated to be 3.7 Pg C y^{-1} (Walsh, 1991; Liu et al., 2000) of which more than 16% (0.62 Pg C y^{-1}) is believed to settle to the sea floor (Muller-Karger et al., 2005). Additionally, some new production estimates and estimates of the export ratio suggest that shelf seas may be more than 3 times more efficient at exporting C than the open ocean (Jahnke, 2010), this is partly due to the close proximity of the euphotic zone to the seafloor sediments in the relatively shallow shelf sea environment.

In addition to supporting a significant fraction of the global biological C pump, enhanced primary production in shelf regions supports important commercial fisheries and marine mammals (Fernandez et al., 1993; Wishner et al., 1988). Globally the shelf seas support over 90% of fish catches (Young et al, 2001; Pauly, 2002)

Considering the relatively small area that they cover, shelf seas evidently contribute disproportionately to global primary production, marine fisheries and C export. The dynamic hydrography of shelf seas influences the supply of light and nutrients to phytoplankton and is responsible for them being such highly productive regions. A high proportion of mechanical energy is dissipated in shelf seas, making them physically energetic areas with vigorous stirring (Simpson and Sharples, 2012). As well as receiving inputs of freshwater from river discharge and rainfall, shelf seas in temperate latitudes will also experience periods of intense solar heating which alter their vertical structure. Temperate shelf seas therefore experience seasonality in both water column structure and primary production.

1.2.1 Patterns of primary production in shelf seas

The vertical structure of a temperate shelf sea is the result of a 'heating-stirring' competition (Simpson and Bowers, 1984). When mixing energy from the wind and tides is strong enough to overcome the buoyancy inputs from fresh water and solar energy the water column will be vertically mixed. However, if the solar energy from the sun is strong enough to overcome the destabilising mixing energy the water column will become vertically layered, or 'stratified'. During winter months the water column is vertically well mixed as a result of the dissipation of energy from the wind and tides, as well as a loss of heat energy to the atmosphere. During summer the radiant energy from the sun received by the ocean is larger. In some

temperate shelf seas this solar buoyancy input is large enough to stabilise the water column and prevail over wind and tidal stirring causing a thermal stratification of the water column. The water column is divided into two vertical layers; the wind-mixed surface layer and the barotropic-tidally mixed bottom layer (BML). The two layers are separated by a sharp gradient in temperature (and density) known as the thermocline (and pycnocline). Stratification persists throughout the summer until heat losses via decreased radiant energy and atmospheric transfer destabilise the water column, and it becomes fully mixed again. In shallow areas of the shelf sea with high mechanical energy input, increased solar heating during summer may not

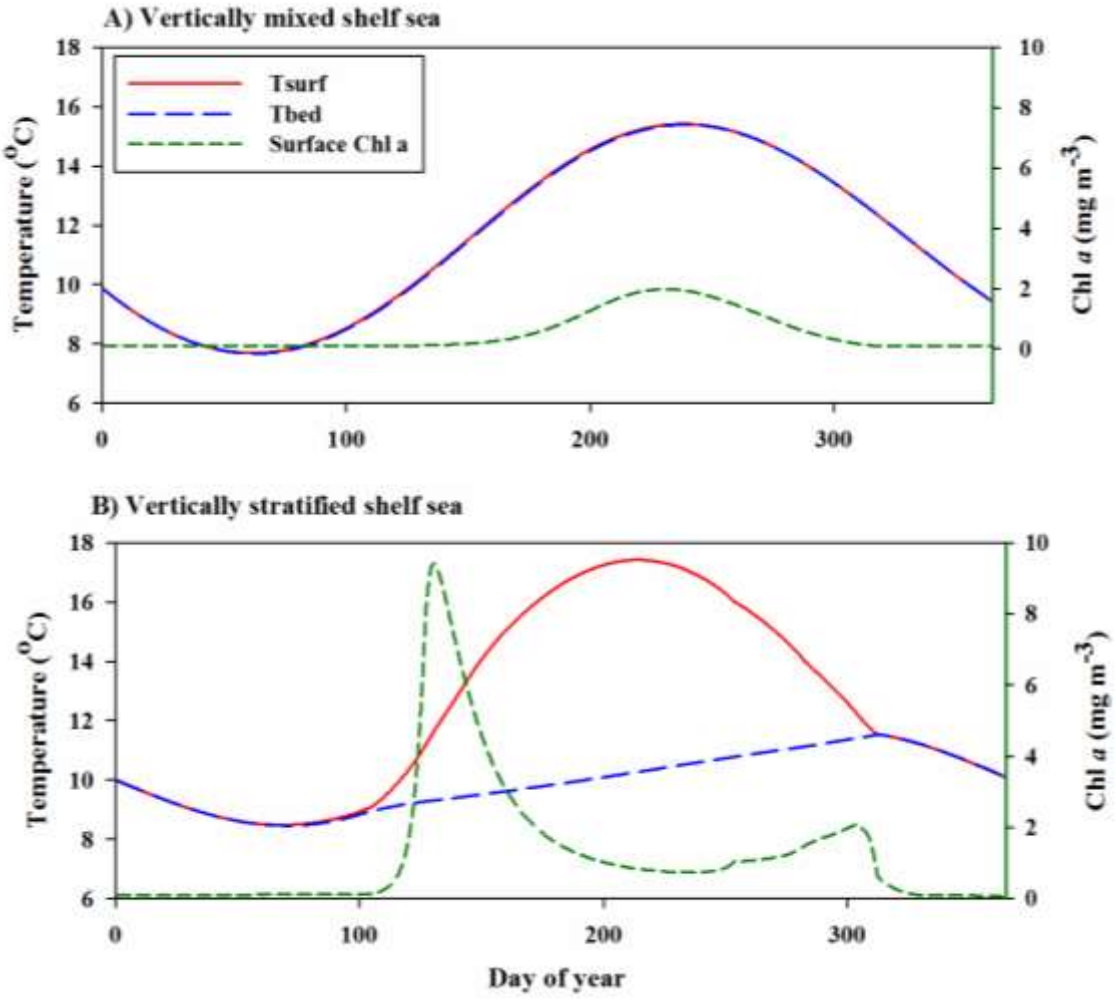

Figure 1.1: Seasonal surface layer temperature (red solid line), bottom layer temperature (blue long dashed line), and surface chlorophyll *a* concentrations for A) a vertically well-mixed temperate shelf sea, and B) a vertically stratified shelf sea from the Simpson and Sharples (2012) textbook numerical model.

be sufficient to stabilise the water column and it will remain vertically mixed throughout the year. Seasonally stratified shelf seas are separated from well-mixed water columns by tidal fronts, the position of which is dependent on water column depth and the strength of tidal and wind stirring (Simpson and Hunter, 1974).

The seasonal cycle in temperate shelf seas is important in terms of the light and nutrients that phytoplankton experience and thus is crucial for patterns in primary production. Figure 1.1 demonstrates the seasonal cycle of water column structure and surface chlorophyll in both well-mixed and stratified shelf seas using a numerical model which accounts for the heating and stirring competition (Simpson and Sharples, 2012). In well-mixed shelf seas, and during winter in stratified shelf seas, phytoplankton are turbulently mixed throughout the water column. Despite experiencing vertically homogenous nutrient replete conditions, the phytoplankton growth is limited by light and thus low production and low surface chlorophyll concentrations are observed (Fig. 1.1a).

At the onset of stratification however (Fig. 1.1a), phytoplankton which inhabit the surface mixed layer are presented with optimal conditions of ample nutrients in a stable, well-lit region of the water column and rapid phytoplankton growth occurs (Lalli and Parsons, 1993; Fig. 1.1b). This event is known as the spring bloom (Sverdrup, 1953; Pingree and Pennyquick, 1975), and is believed to be responsible for approximately 50% of the annual primary production in stratified shelf seas (Hickman et al., 2012). The spring bloom rapidly depletes inorganic nutrients in the surface layer, with the thermocline acting as a physical barrier between the surface and bottom mixed layer for nutrients, salt and phytoplankton cells (Sharples et al., 2001). As a result, phytoplankton in the surface become nutrient limited and their growth deteriorates, leaving a nutrient-limited, low-biomass surface layer (Fig. 1.2a) where rates of primary production are largely reliant on recycled nutrients. At the base of this surface layer, within the seasonal thermocline, a layer of higher concentrations of phytoplankton is frequently seen (e.g. Fig. 1.2a). This subsurface chlorophyll maximum (SCM) is a well-documented feature in temperate shelf seas (Pingree et al., 1978; Holligan et al., 1984; Sharples et al., 2001). Over the summer stratified season the phytoplankton in the SCM fix about the same amount of C as that fixed by the spring bloom (Hickman et al., 2012). Estimates of global primary production and phytoplankton biomass using satellites are based on measurements of

sea surface chlorophyll (e.g., Behrenfield & Falkowski, 1997), they are unable to detect the SCM. Therefore, using satellite data to examine and quantify changes in global primary production using satellites may be missing a considerable fraction of the water column primary production. Fully comprehending the processes and mechanisms that influence the existence of the SCM, and the production that occurs there, is therefore vital in terms of accurately quantifying global primary production.

1.2.2 The subsurface chlorophyll maximum

The SCM exists because there is sufficient light for photosynthesis along with a weak 'leakage' of nutrients from the nutrient replete BML (Pingree et al., 1977; Sharples et al. 2001). However, it is important to note that the ability of some motile species (particularly dinoflagellates) to swim in response to resource requirements may also allow them to actively form a phytoplankton layer (Margalef, 1978; Simpson and Sharples, 2012), this is particularly important in less energetic regions such as in Monterey Bay (Steinbuck et al., 2009; see also Chapter 2).

Considering the profile in Fig. 1.2a, and using a typical PAR attenuation coefficient for the Celtic Sea of 0.1 m^{-1} suggests that the light at the peak of the SCM is about 5% of that incident on the sea surface. While this is a low level of light, the stability of the thermocline allows phytoplankton to adapt to it and photosynthesise (e.g. Moore et al., 2006). The focus of this thesis is on the weak supply of nutrients to this phytoplankton layer, and the consequences of the nutrient supply for C fixation.

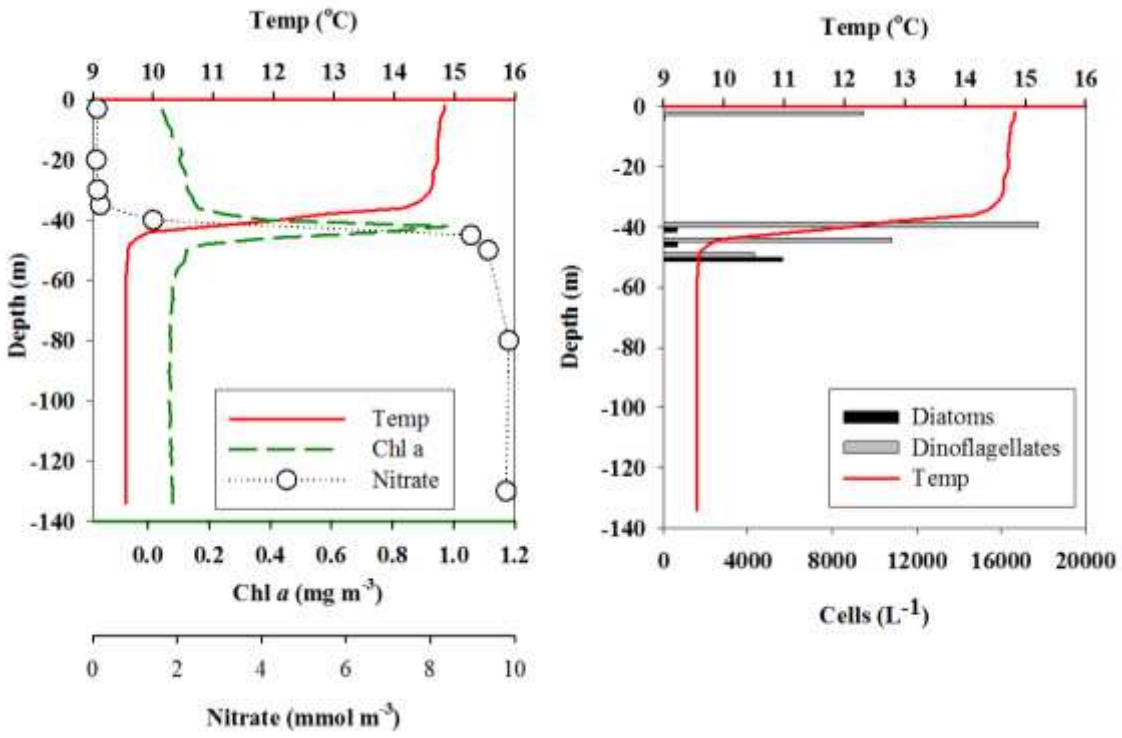

Figure 1.2: Vertical profiles of A) temperature (red solid line), chlorophyll *a* (green dashed line) and nitrate (open circles on dotted line), and B) diatoms (black bar), dinoflagellates (grey bar) and temperature (red solid line) taken from the Celtic Sea on 16th June 2010 (RRS Discovery, Research cruise D352, CTD43). See Chapter 3 for methods on data collection for temperature, chlorophyll *a* and nitrate. Samples for cell abundance of diatoms and dinoflagellates were taken from Niskin bottles on the CTD and preserved with Lugol's iodine, where they were later settled for enumeration following the Utermohl method (Utermohl, 1934).

Nitrate is generally considered the limiting nutrient to phytoplankton in temperate shelf seas and is depleted to below limits of analytical detection (e.g. less than 0.1 μM for nitrate) in the surface mixed layer following the spring bloom (Simpson and Sharples, 2012; Fig. 1.2a). In contrast, the nitrate concentration in the BML is relatively high (e.g., Sharples et al., 2001; Rippeth et al., 2009). As the vertical gradient in nitrate is partially a result of the thermal stratification, temperature and nitrate generally have a strong relationship in temperate shelf seas (e.g., Williams et al., 2013; see Chapter 2). Thus the thermocline reflects with the position of the vertical nitrate gradient, or 'nitracline' (Fig. 1.2a), and the SCM will be positioned at the base of both, where there is a supply of cold, nutrient rich BML water (Sharples et al., 2001).

The fraction of primary production fuelled by inorganic nitrogen (nitrate, nitrite or ammonium) involves the assimilation of inorganic C (Dugdale and Goering, 1967). Primary production consists of new production, which is supported by externally supplied nutrients (i.e. nitrate); and regenerated production, which is supported by internally recycled nutrients (i.e. nitrite and ammonium). However, only production fuelled by nitrate (i.e. new production) results in net carbon fixation, and thus is considered to be important for C sequestration in shelf seas. Nitrogen and C are generally assumed to be assimilated into cells at the 'Redfield ratio' of 6.6:1 (Redfield, 1958). This means that for every 16 moles of nitrogen assimilated 106 moles of C will also be assimilated by phytoplankton, as this is the average ratio of C and nitrogen found within phytoplankton cells. For a given rate of supply of nitrate, it is possible to estimate the amount of potential C fixed through new production by multiplying the amount of nitrate supplied by 6.6. It is important to note that nutrient ratios are widely acknowledged to vary between phytoplankton species (Tett et al., 1985; Arrigo 2005). The C:N ratio in phytoplankton has been shown to range between 6:1 and 20:1 (Goldman et al., 1979). However the assumption of Redfield stoichiometry is a useful value that applies to a mixed phytoplankton communities on average (Goldman et al., 1979).

Phytoplankton species composition in shelf seas during the spring bloom is dominated by large-celled diatoms (Rees et al., 1999). In contrast, the summer community in the SCM is layered, potentially as a response to vertical changes in the spectral properties of light (Hickman et al., 2009). The SCM peak is mostly made up of small-celled flagellates and motile dinoflagellates (e.g., Figure 1.2b). Large-celled diatoms are generally seen towards the base of the thermocline (e.g., Moore et al., 2006; Hickman et al., 2009; Simpson and Sharples, 2012), where they experience higher nitrate concentrations (Fig. 1.2b). The phytoplankton community at the SCM is assumed to assimilate any nitrate that may be supplied from the BML as the surface nitrate concentrations are very low (Sharples et al., 2001; Rippeth et al., 2009; Fig. 1.2a). Therefore, a measurement of the nitrate supply from the BML to the SCM represents a measurement of a limiting factor to primary production in summer shelf seas.

1.3 *The turbulent supply of nitrate to the SCM*

The leakage of nutrient rich BML water across the thermocline is thought to support phytoplankton nitrate requirements in the SCM, and is commonly referred to as the diapycnal nitrate flux (e.g., Sharples et al. 2001; 2007; Rippeth et al. 2009). The diapycnal nitrate flux, J_{NO3}, may sustain the SCM during summer (e.g., Rippeth et al. 2009), and set a limit on summer 'new' (i.e., driven by nitrate) production (e.g. Sharples et al., 2001). Furthermore, CO_2 drawdown has been linked to the diapycnal flux of nutrient rich water to the SCM (Kitidis et al., 2012). Turbulent vertical nutrient flux has been estimated by several authors (Seiwell, 1935; Coste, 1971; Jamart et al., 1977; Eppley et al., 1979) by means of turbulent mixing coefficients. The magnitude of this diapycnal nitrate flux (Eq. 1.1) is dependent on mixing at the thermocline and the strength of the nitrate gradient ($\delta NO_3/\delta z$):

$$J_{NO_3} = K_z \frac{\delta NO_3}{\delta z} \qquad [\text{mmol m}^{-2}\ \text{s}^{-1}] \qquad [1.1]$$

where K_z ($m^2\ s^{-1}$) is the turbulent eddy diffusivity.

The turbulent eddy diffusivity is a measure of turbulent mixing in the water column. The following section describes where this parameter comes from, how it is measured and the physical processes which enhance mixing, thus diapycnal nitrate fluxes.

1.3.1 Parameterising mixing in the ocean.

Turbulence is generated wherever there is a gradient in currents, referred to as current shear. Shear can be generated when fluid moves along a fixed boundary, such as the seabed. Alternatively, shear can be set up across the thermocline as a result of wind-driven flows in the surface layer or internal waves propagating along the density discontinuity. The process that can generate thermocline mixing will be discussed in more detail below. Whether or not shear at the thermocline can generate instabilities and mixing can be parameterised using the Richardson number (Eq. 1.2), which considers the ratio of the buoyancy and the shear squared:

$$Ri = \frac{N^2}{S^2} \qquad [\text{dimensionless}] \qquad [1.2]$$

The buoyancy frequency, N^2, is dependent on the vertical density (ρ) structure, i.e. the stratification, of the water column:

$$N^2 = \frac{-g}{\rho}\frac{\partial \rho}{\partial z} \qquad [s^{-2}] \qquad [1.3]$$

where g is the acceleration due to gravity (9.81 m s^{-2}). The shear, S^2, is calculated as a sum of the shear components in the x- and y-direction:

$$S^2 = \left(\frac{\partial u}{\partial z}\right)^2 + \left(\frac{\partial v}{\partial z}\right)^2 \qquad [s^{-2}] \qquad [1.4]$$

Generally if Ri < 0.25 mixing will occur spontaneously as a result of the velocity shear being large enough to overcome the stabilising effect of vertical stratification.

As mentioned above, turbulent mixing is parameterised by the vertical diffusion coefficient, K_z (Eq. 1.5). This can be calculated as a function of the balance between turbulence production, the turbulent kinetic energy dissipation (ε, m^2 s^{-3}), and the work against buoyancy (Osborn, 1980):

$$K_z = \Gamma \frac{\varepsilon}{N^2} \qquad [m^2\, s^{-1}] \qquad [1.5]$$

Here Γ represents the mixing efficiency defined as the ratio of potential energy gain to dissipation and is dependent on the shear, stratification and turbulence. Osborn (1980) derived:

$$\Gamma = \frac{Ri_f}{(Ri_f + 1)} \qquad [\text{Dimensionless}] \qquad [1.6]$$

where the relevant flux Richardson number, Ri_f, represents the critical value of Ri where spontaneous turbulence will occur. Ri_f in not known accurately but is widely assumed to be ~0.25, making Γ approximate to 0.2. Thus Eq. 1.5 becomes:

$$K_z = 0.2\frac{(\varepsilon)}{N^2} \qquad [m^2\,s^{-1}] \qquad [1.7]$$

Figure 1.3: Rockland Velocity Microstructure Profiler (VMP). Photo courtesy of J. Polton

To quantify the turbulent eddy diffusivity within a water column we require some method for estimating the turbulent dissipation of energy, ε ($m^2\,s^{-3}$). In the context

of this study the turbulent dissipation can be estimated from direct measurements of the current shear on scales of the order of 1 cm (Eq. 1.8):

$$\varepsilon = 7.5\upsilon\overline{\left(\frac{du}{dz}\right)^2} \qquad [m^2\ s^{-3}] \qquad [1.8]$$

where υ is the kinematic viscosity of seawater ($m^2\ s^{-1}$), and *du/dz* is the (small scale) vertical shear. Such shear measurements are made using free-fall microstructure turbulence sensors (Fig. 1.3).

1.3.2 Sources of turbulence and mixing at the shelf sea thermocline.

Vertical mixing in shelf seas was initially believed to be dominated by the tidal currents and the frictional stress generated by the currents at the seabed. The positions of tidal mixing fronts (i.e., the boundary between mixed and stratified regions) have been shown to be predicted in the Irish Sea by considering only this boundary mixing by the tides (Simpson and Hunter, 1974). Additionally the wind was incorporated into shelf sea models as a surface boundary mixing mechanism to better predict the position and strength of thermocline (Simpson and Bowers, 1984). Considering both the wind and tide as boundary generated mixing processes the seasonality and position of the thermocline in shelf seas has been adequately predicted (e.g. Simpson and Bowers, 1984; Sharples et al., 2006) using turbulence closure scheme (TCS) models. This type of physical model uses a series of equations to describe the evolution of the flow of the water column (Simpson and Sharples, 2012). However, although boundary layer mixing in TCS may adequately explain the position of the thermocline, models using boundary mixing fail to account for other mixing processes occurring within the interior of the water column (Simpson et al., 1996).

While these missing mixing processes dissipate considerably less energy than tidal boundary-driven mixing, they are critical to understand because the mixing operates on important biogeochemical gradients in the water column.

The vertical diapycnal flux of nitrate at the base of the shelf sea thermocline in the absence of additional interior mixing processes is difficult to estimate as such a measurement requires an environment devoid of mixing other than that driven by tidal friction at the seabed. Sharples et al., (2001a), estimated this "background" flux to be 1 – 2 mmol m^{-2} d^{-1} in the western English Channel. In Chapter 3 a value for the western Irish Sea is calculated to be 0.3 mmol m^{-2} d^{-1} (Williams et al., 2013). There are two key sources of mixing at the thermocline that could significantly augment these daily nitrate supplies to the SCM, internal waves and internal oscillations.

Internal waves

Internal waves propagating along the thermocline are associated with current shear; if the shear is sufficiently large (i.e. Ri < 0.25) then the wave can become unstable, break and generate turbulence and mixing. In shelf seas the initial perturbation of the thermocline position that leads to the internal wave can be generated by flow across changes in topography (e.g. Moum & Nash, 2000). In tidally energetic shelf seas, internal tidal waves can be generated by the change in bathymetry experienced by the oscillatory tidal flows moving over the shelf edge (e.g. Baines, 1981; Sharples et al, 2007) or over banks on the shelf seabed (e.g. Palmer et al., 2013). As stratified tidal flow moves over the shelf edge or a bank into deeper water, the density interface experiences a depression (Fig. 1.4a). As the tidal flow reduces the depression of the thermocline is released, and propagates as an oscillation of the thermocline (Fig. 1.4b). As this wave moves into shallower water (e.g. on the shelf or over the bank), it steepens and can result in the generation of high frequency, internal solitons (Fig. 1.4c). The current shear associated with these solitons can provide an efficient mechanism for diapycnal mixing as the turbulence is generated at the pycnocline.

The nitrate flux driven by internal tides has been estimated as 12 mmol N m^{-2} d^{-1} on the northeast shelf of New Zealand (Sharples et al., 2001b). Assuming Redfield stoichiometry, this flux was estimated to support 100 g C m^{-2} y^{-1} of new production annually on the shelf. Off the Mauritanian shelf diapycnal nitrate fluxes driven by the internal tide have been measured at about 10 mmol m^{-2} d^{-1} (Schafstall et al., 2010). At the Celtic Sea shelf edge, the nitrate flux driven by the internal tide was shown to be highly variable over the fortnightly spring-neap tidal cycle, ranging

between 1 and 9 mmol m^{-2} d^{-1} for neap and spring tides respectively (Sharples et al. 2001b). The large flux during spring tides was estimated to be in excess of phytoplankton requirements, with the nitrate being utilised during more quiescent periods of low turbulence around neap tides. Further on the shelf of the Celtic Sea, tidal flows interacting with a seabed bank have been found to drive very large nitrate fluxes, reaching up to 50 mmol m^{-2} d^{-1} (Tweddle et al., 2013). Thus, estimates of the nitrate fluxes generated by the internal tide suggests that these fluxes can be 1 – 2 orders of magnitude greater than reported values of the background flux.

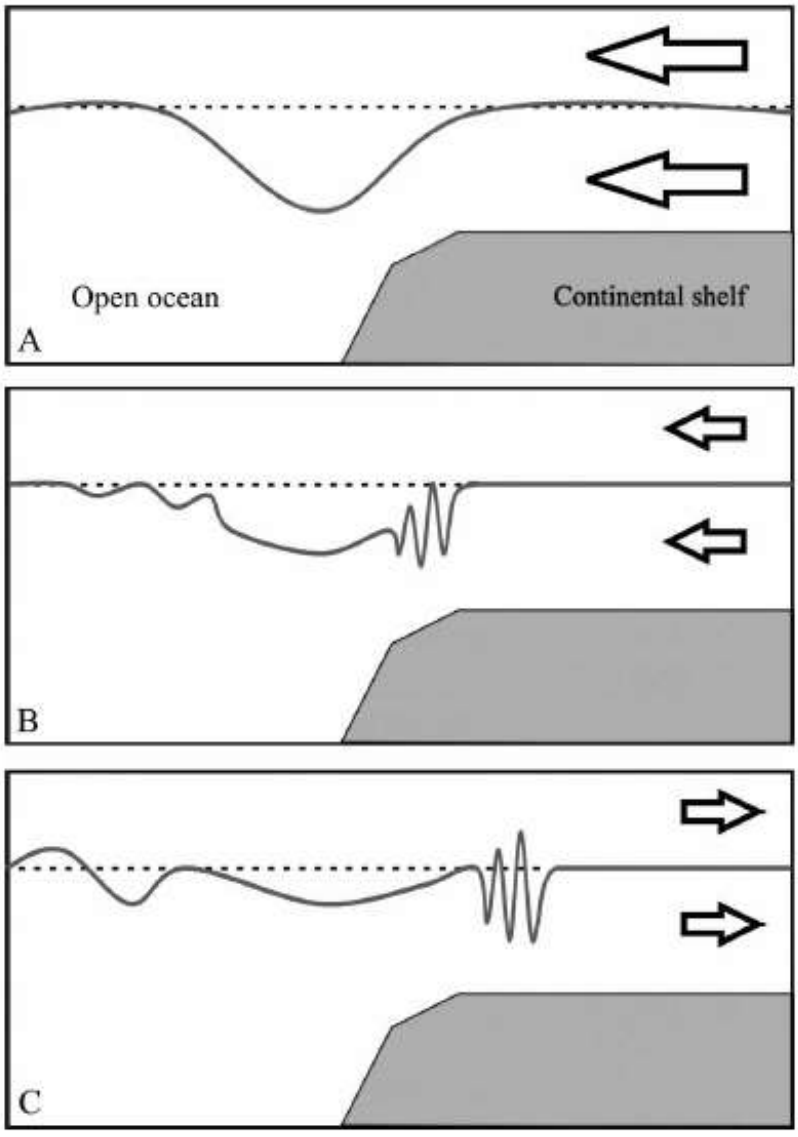

Figure 1.4: Taken from Sharples et al. 2007. A schematic illustration of the generation and dissipation of an internal tidal wave as described in text. The arrows indicate the direction and strength of the barotropic tidal currents.

Inertial oscillations

Inertial oscillations are the periodic motion of the ocean experienced by a sudden change in external forcing on the ocean surface, combined with the effect of the Earth's rotation (Krauss, 1979). A change in forcing is usually attributed to a change in wind-direction or magnitude (Gill, 1982; Rippeth, 2005). The forcing of wind over the sea surface will result in current shear at the sea surface, generating surface boundary layer mixing (i.e., section 1.3.3). Where there is vertical stratification in the ocean, a change in the forcing of the wind on the sea surface will also cause the surface mixed layer to oscillate like a slab over the BML. A short burst of wind stress will accelerate the surface mixed layer in the direction of the wind (Simpson and Sharples, 2012). A nice example of this phenomenon is provided by the measurements carried out in the North Pacific by van Meurs (1998) (Fig. 1.5). Van Meurs (1998) released 48 buoys drogued at 15 m depth to track the movement of the surface mixed layer over a month whilst storms occurred. The individual tracks of each buoy are shown in Figure 1.5. Although these tracks might look like individual eddies, they are in fact the movement of the whole surface layer, with the largest oscillations associated with the passing of a storm shortly after the buoys were released.

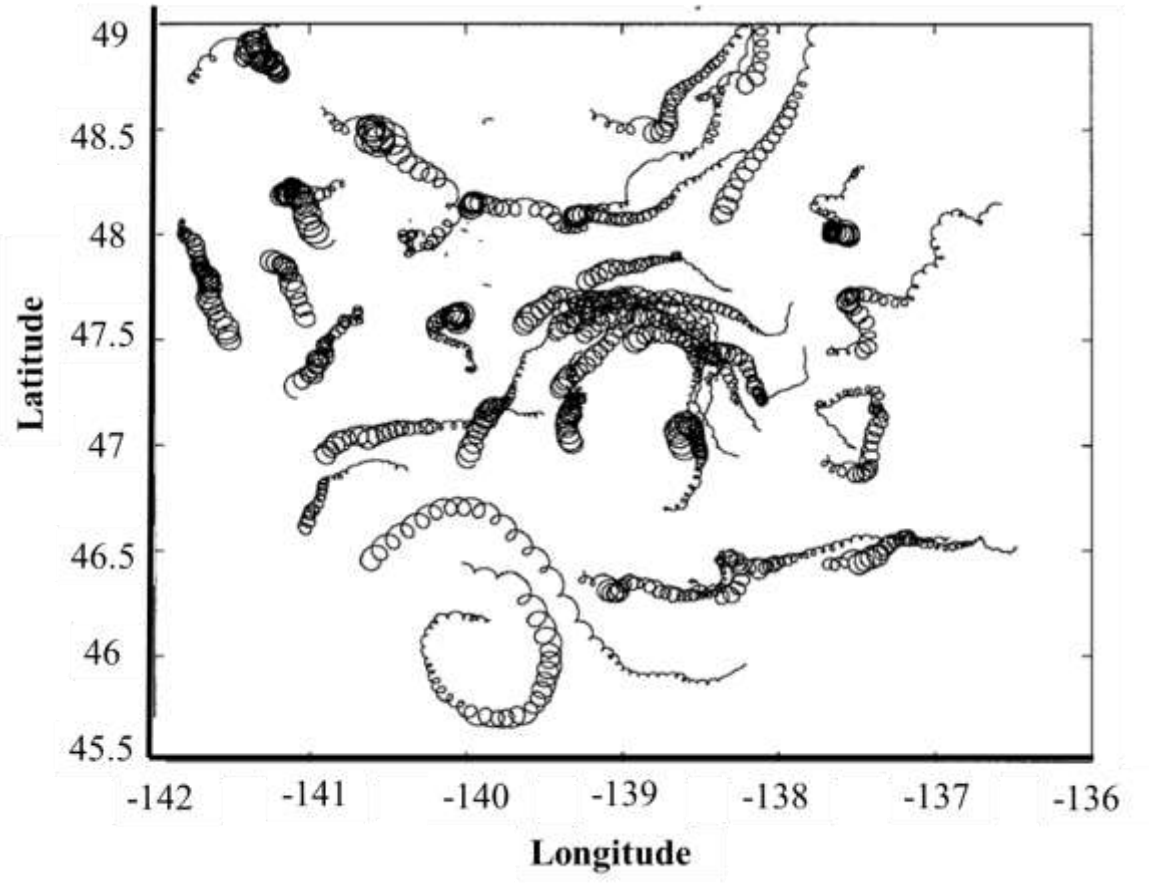

Figure 1.5: Taken from van Meurs (1998). Inertial oscillations in the North Pacific demonstrated by the tracks of 48 buoys drogued to 15m depth in the surface mixed layer.

The frequency of each oscillation is determined by the Coriolis parameter, and therefore the latitude of the region being considered:

$$\Omega_I = f/2л \qquad (s^{-1}) \qquad [1.10]$$

where f is the Coriolis parameter, $f = 2\omega sin\Phi$; and ω is the Earth's rotation rate, Φ represents latitude. The magnitude of the oscillation is determined by the strength of the forcing.

In stratified regions, the 'slab' motion' of the surface layer caused by the sudden forcing of wind generates shear at the thermocline and potential shear instabilities. Wind-driven inertial oscillations have been observed in stratified shelf seas (e.g., Simpson et al., 2002; Rippeth et al., 2002; Burchard and Rippeth, 2009).

Burchard and Rippeth (2009) found that when the shear direction at the thermocline aligned with the direction of the wind, large intermittent shear spikes at

the thermocline were observed in the North Sea. Furthermore, these shear spikes were associated with pulses of turbulent dissipation at the thermocline.

Inertial oscillations are well-documented physical processes that are considered to be an efficient diapycnal mixing mechanism as they input turbulence where the density gradient is at its largest (Simpson et al., 2002; MacKinnon and Gregg, 2005; Rippeth, 2005). Modelling by Sharples & Tett (1994) suggested that the SCM could only be supported if there was a diapycnal mixing mechanism available to transfer nitrate into the thermocline from the BML, with variability in the wind forcing identified as a likely source of the mixing. A recent study documented increased phytoplankton productivity following energetic inertial oscillations on the west coast of South Africa (Lucas et al., 2013). Moreover, diatom abundance was observed to increase following mixing caused by wind-driven inertial oscillations. As yet there are no direct estimates of the nitrate fluxes resulting from wind-driven inertial oscillations, despite their potential impact on diapycnal mixing and fluxes (Burchard and Rippeth, 2009). Recently, there has been increased scientific focus on how the changing climate may affect storm intensity and frequency. The frequency of wind events in the North Atlantic Ocean is determined by the position of the Jet Stream, and as the climate changes the position of the storm track is expected to change (Hu and Wu, 2004). In light of this, future changes in storm tracks may have important implications for the occurrence of inertial oscillations, and thus it is important to identify whether wind events are important in altering diapycnal nitrate supply.

1.4 Nitrate uptake below the SCM

The turbulent, diapycnal supply of nitrate is assumed to sustain the SCM (Sharples et al., 2001a; 2001b; Rippeth et al., 2005), as well as setting the limit on new production at the SCM (Sharples et al., 2007; Rippeth et al., 2009). However, it is possible that some phytoplankton may transport nutrients from the deeper water to the SCM as intra-cellular nutrients. In particular, motile dinoflagellates, a dominant phytoplankton group commonly seen in the shelf sea SCM (Holligan and Harbour, 1977) (Fig. 1.2b), may be able to take up BML nutrients and then swim upwards to the SCM. If this is a significant transport pathway for nutrients into the SCM, then

the assumption that an observation of diapycnal inorganic nutrient flux represents a measure of a limiter on new production could be undermined.

Certain adaptations are thought to allow dinoflagellates to compete and coexist with diatoms at the SCM (Fig. 1.2b), despite often having lower photosynthetic rates (Tang, 1995), higher metabolic costs and higher nutrient affinity (half saturation) coefficients (Smayda, 1997). In particular, dinoflagellates are able to migrate across temperature and nutrient gradients in order to assimilate nutrients (Eppley et al. 1968; Eppley and Harrison, 1975; Cullen and Horrigan, 1981). In a nutrient depleted system, Cullen and Horrigan (1981) observed the development of dinoflagellates in a SCM. The SCM developed when the phytoplankton intracellular nitrogen concentrations decreased as a response to nitrate deplete conditions, causing dinoflagellates to swim downwards. Furthermore, numerical studies suggest that dinoflagellates might be capable of reaccessing the thermocline from the BML in a tidally energetic shelf sea (Ross and Sharples, 2008). It is possible that a proportion of the SCM in shelf seas could be supported by nitrate acquired below the thermocline by dinoflagellates.

The nutrient concentration in the euphotic zone is relatively horizontally homogenous across the shelf sea, furthermore the external inputs of nitrogen is neglible away from the coast. Therefore it is the vertical supply of nutrients to the SCM that are likely to sustain it via two potential methods ; 1) diapycnal flux of nutrients from the BML to be taken up by the phytoplankton within the SCM, and/or 2) phytoplankton assimilation of nutrients in the BML, which are then transported via motility and turbulence into the SCM. If the ability of phytoplankton to assimilate BML nutrients and then regain access to the SCM is a dominant factor in the maintenance of the SCM, then this questions the basis of calculating the diapycnal flux of nutrients in shelf seas as a limiter of new production in the SCM.

1.5 Aims of this research

From this brief review it is evident that the supply of nitrate to phytoplankton in the SCM is important for summer production and net C sequestration in shelf seas. However, the processes that supply nitrate to the SCM have not been fully quantified. In particular, while inertial oscillations are well observed in the shelf sea

(Sherwin, 1987), there are no measurements of the nitrate flux that may result from them. Furthermore, there is no evidence of how the community at the SCM responds to mixing events in terms of primary production and community structure, despite this being vital for understanding the biological C pump. An additional interesting gap in shelf sea research is the importance of nitrate assimilation below the thermocline for SCM maintenance and production.

The aim of this study is to investigate the relative importance of background and event driven mixing on sustaining the subsurface chlorophyll maximum in shelf seas through the supply of nitrate. Particularly, this study aims to quantify the amount of nitrate supplied to the SCM via wind-driven inertial oscillations, how the SCM community responds to mix events of this scale. Thus, this thesis aims to assess the role of wind-driven inertial oscillations on summer production in shelf seas. An additional investigation of this thesis focuses on whether nitrate assimilation below the thermocline by dinoflagellates plays any role in SCM maintenance.

The overarching hypotheses of this thesis are as follows:

1) *In tidally energetic shelf seas, sustaining primary production in the SCM is controlled predominantly by diapycnal nitrate fluxes from the BML*.
2) *Diapycnal mixing events induced by wind-driven shear spikes will result in an enhanced supply of nitrate to the subsurface chlorophyll maximum.*
3) *This nitrate flux will stimulate primary production in the phytoplankton community at the SCM.*
4) *Wind-driven inertial oscillations are significant for annual production in shelf seas.*

In chapter 2 a modelling approach is used to investigate the relative importance of phytoplankton motility and nutrient acquisition below the thermocline to SCM maintenance. Thus this chapter outlines the importance of measuring the flux of nitrate to the SCM, which is the focus of chapters 3, 4 and 5.

Chapter 3 uses observations from the stratified western Irish Sea to quantify the background turbulent supply of nitrate and highlights the role of event driven mixing on sustaining the SCM.

In chapter 4, observations from the Celtic Sea are used to quantify the nitrate flux from wind-driven inertial oscillations. This chapter goes on to estimate the amount of summer production supported by wind-driven inertial oscillations.

In chapter 5, an experimental approach is used to assess the response of the phytoplankton and bacterial community at the SCM in terms of nutrient drawdown, primary and secondary production and the partitioning of organic C between particulate and dissolved phases to a large scale wind-driven mix event and isolation from diapycnal fluxes.

Chapter 6 brings together and summarises the findings from this thesis, and assesses the wider implications that this entire scientific study has. The short-falls of this work and implications for wider work are also discussed.

1.6 References

Arrigo, K. R. 2005. Marine microorganisms and global nutrient cycles. Nature. **437**: 349-355.

Azam, F., T. Fenchel, J. G. Field, J. S. Gray, L. A. Meyer-Reil, and F. Thingstad. 1983. The ecological role of water-column microbes in the sea. Mar. Ecol. Progr. Ser. 10: 257-263

Baines, P. G. 1982. On internal tide generation models. Deep. Sea. Res. 29(3A):307-338

Borges, A. V. 2005. Do we have enough pieces of the jigsaw to integrate CO2 fluxes in the coastal ocean? Estuar. 28:241-262.

Borges, A. V., B. Delille, M. Frankignoulle. 2005. Budgeting sinks and sources of CO2 in the coastal ocean: Diversity of ecosystems counts. *Geophys. Res. Lett*. **32**: L14601

Burchard, H. and T. P. Rippeth. 2009. Generation of Bulk Shear Spikes in Shallow Stratified Tidal Seas. Journal of Physical Oceanography 39(4): 969-985.

Canadell, J. G., C. LeQuere, M. R. Raupach, C. B. Field, E. T. Buitenhuis, P. Ciais, T. J. Conway, N. P. Gillett, R. A. Houghton, and G. Marland. 2007. Contributions to accelerating atmospheric CO2 growth from economic activity, carbon intensity, and efficiency of natural sinks. PNAS. 104(47):18866-18870.

Chen, C. T. A., and A. V. Borges. 2009. Reconciling opposing views on carbon cycling in the coastal ocean: continental shelves as sinks and near-shore ecosystems as sources of atmospheric CO2. Deep Sea Res II. 56(8-10), 578-590.

Chisholm, S. W. 1992. Phytoplankton size. In: Primary productivity and biogeochemical cycles in the sea. P. G. Falkowski and A. D. Woodhead (eds). Plenum Press, New York.

Coste, B. 1971. Les sels nutritifs entre la Sicile, la Sardaigne et al Tunisie. Cahlers Oceanographiques. 23:49-83.

Cullen, J. J. and S. G. Horrigan. 1981. Effects of nitrate on the diurnal vertical migration, carbon to nitrogen ratio, and photosynthetic capacityof the dinoflagellate *Gymnodinium splendens.* Mar. Biol. 62:81-89.

DeGrandpre, M .D., G. J. Olbu, C. M. Beatty, and T. R. Hammar. 2002. Air-sea CO2 fluxes on the US Middle Atlantic Bight. Deep Sea Res. Part II: Topic. Stud. In Oceanogr. 49(20):4355-4367.

Dugdale, R. C., and J. J. Goering. 1967. Uptake of new and regenerated nitrogen in primary productivity. Limnol. Oceanogr. **12**:196-206.

Eppley, R. W., O. Holm-Hansen, and J. Strickland. 1968. Some observations on the vertical migration of dinoflagellates. J. Phycology. 4: 333-340.

Eppley, R., and W. G. Harrison. Physiological ecology of *Gonyaulax polyedra*, a red water dinoflagellate in southern California. *In:* Proceedings of first international conference on toxic dinoflagellate blooms, 1974, pp 11-23. Ed. By V. R. LoCicero. Wakefield, Mass.: Massachusetts Technology Foundation. 1975.

Eppley, R., E. H. Renger, W. G. Harrison, and J. J. Cullen. 1979. Ammonium distribution in southern California coastal waters and its role in the growth of phytoplankton. Limnol. Oceanogr. 24(3): 495-509.

Fernandez, E., J. Cabai, J. L. Acuna, A. Bode, A. Botas, and C. Garciasoto. 1993. Plankton distribution across a slope-current induced front in the southern Bay of Biscay. J. Plankton Res. 15: 619-641.

Frankignoulle, M., and A. V. Borges. 2001. European continental shelf as a significant sink for atmospheric carbon dioxide. Global. Biogeochem. Cycles, 15: doi:10.1029/2000GB001307

Gill, A. E. Atmosphere-ocean dynamics. Academic Press. London 1982.pp 323-345.

Hickman, A. E., P. M. Holligan, C. M. Moore, J. Sharples, V. Krivstov, and M. R. Palmer. 2009. Distribution and chromatic adaptation of phytoplankton within a shelf sea thermocline. Limnol. Oceanogr. 54: 525-536.

Hickman, A. E., C. M. Moore, J. Sharples, M. I. Lucas, G. H. Tilstone, V. Kristsov, and P. M Holligan. 2012. Primary production and nitrate uptake in the seasonal thermocline of a stratified shelf sea. Mar. Ecol. Prog. Ser. **463**: 39-57.

Holligan, P. M., R. P. Harris, R. C. Newell, D. S. Harbour, R. N. Head, E. A. S. Linley, M. I. Lucas, P. R. G. Tranter, and C. M. Weekley. 1984. Vertical distribution and partitioning of organic carbon in mixed, frontal and stratified waters of the English Channel. Mar. ecol. Progr. Ser. 14:111-127.

Holligan, P. M., and D. S. Harbour. 1977. The vertical distribution and succession of phytoplankton in the western English Channel in 1975 and 1976. J. Mar. Biol. Assoc. 57: 1075-1093.

Hopkinson, C. S., and J. J. Vallino. 2005. Efficient export of carbon to the deep ocean through dissolved organic matter. Nature **433**: 142-145

Hopkinson, C. S., J. J. Vallino, and A. Nolin. 2002. Decomposition of dissolved organic matter from the continental margin. Deep-Sea Res. II **49**: 4461-4478

Hu, Z. Z., and Z. H.Wu. 2004. The intensification and shift of the annual North Atlantic Oscillation in a global warming scenario simulation. Tellus A 56:112–124

IPCC (2001) Contributions of Working Group I to the third assessment report of the intergovernmental panel on climate change. In: Houghton JG, Ding Y, Griggs DJ, Noguer M, van der Linden PJ, Dai X, Maskell K, Johnson CA (eds.) *Climate Change 2001: The scientific basis*. Cambridge University Press, Cambridge, pp. 185-237

Jahnke, R. A. 2010. Global Synthesis, p. 597-615. *In* K. K. Liu, L. Atkinson, R. A. Quinones and L. Talaue-McManus [eds.], Carbon and Nutrient Fluxes in Continental Margins: A Global Synthesis. Springer-Verlag.

Jamart, B. M., D. F. Winter, K. Banse, G. C. Anderson, and R. K. Lam. 1977. A theoretical study of phytoplankton growth and nutrients distribution in the Pacific Ocean off the northwestern U.S. coast. Deep. Sea. Res. 24:753-773.

Jiao, N., G. J. Herndl, D. A. Hansell, R. Benner, G. Kattner, S. W. Wilhelm, D. L. Kirchman, M. G. Weinbauer, T. Luo, F. Chen, and F. Azam. 2010. Microbial production of recalcitrant dissolved organic matter: long-term carbon storage in the global ocean. Nature Reviews Microbiology. 8(593-599).

Kitidis, V., N. J. Harman-Mountford, E. Litt, I. Brown, D. Cummings, S. Hartman, D. Hydes, J. R. Fishwick, C. Harris, V. Martinez-Vicente, E. M. S. Woodward, and T. J. Smyth . 2012. Seasonal dynamics of the carbonate system in the western English Channel. Cont. Sh. Res. **42**:30-40.

Krauss, W. 1979. Inertial waves in an infinite channel of rectangular cross section, Dtsch. Hydrogr. Z. 32: 248-266.

Lalli, C. M., and T. R. Parsons. Biological oceanography: an introduction. Second edition. Butterworth Heinmann. 1997.

Legendre, L., and R. B. Rivkin.2002. Pelagic food webs: responses to environmental processes and effects on the environment. Ecolog. Res. 17(2):143-149.

Liu, K-K., K. Iseki, and S.-Y. Chao. Continental margin carbon fluxes. In: The changing ocean carbon cycle (Eds. R. B. Hanson, H. W. Ducklow and J. G. Field), Cambridge University press, Cambridge, 2000.

Lucas, A. J. 2013. The influence of diurnal wind son phytoplankton dynamics in a coastal upwelling system off southwestern Africa. Deep sea Res. Part II. Topic. Stud. Oceanogr. (in press).

MacKinnon, J. A., and M .C. Gregg. 2005. Spring mixing: turbulence and internal waves during restratification on the New England shelf. J. Phys. Oceanogr. 35: 2425-2443.

Margalef, R. 1978. Life-forms of phytoplankton as survival alternatives in an unstable environment. Oceanol Acta, 134: 493-509

Moore, C. M., D. J. Suggett, A. E. Hickman, Y-N. Kim, J. F. Tweddle. J. Sharples. R. J. Geider, and P. M. Holligan. 2006. Phytoplankton photoacclimation and photoadaptation in response to environmental gradients in a shelf sea. Limnol. Oceanogr. 51(2):936-949.

Moum, J., and J. Nash. 2000. Topographically induced drag and mixing at a small bank on the continental shelf. J. Phys. Oceanogr. 30: 2049-2054

Muller-Karger, F. E., R. Varela, R. Thunell, R. Luerssen, C. Hu, and J. J. Walsh. 2005. The importance of continental margins in the global carbon cycle. Geophys. Res. Lets. 32: L01602, doi:10.1029/2004GL021346

Munk, W. H., and G. Riley. 1952. Absorption of nutrients by aquatic plants. J. Mar. Res. 11: 215-240.

Osborn, T. 1980. Estimates of the local rate of vertical diffusion from dissipation measurements. J. Phys. Oceanogr. **10**: 83-89, doi: 10.1175/1520-0485(1980)010<0083:EOTLRO>2.0.CO.

Palmer, M., M. E. Inall, and J. Sharples. 2013. The physical oceanography of Jones Bank: A mixing hotspot in the Celtic Sea. Progr. Oceanogr. (in press).

Pauly, D., V. Christensen, S. Guenette, T. J. Pitcher, U. R. Sumaila, C. J. Walters, R.Watson, and D. Zeller. 2002. Towards sustainability in world fisheries. Nature **418**: 689-695

Pingree, R. D., and L. Pennyquick. 1975. Transfer of heat, fresh water and nutrients through the seasonal thermocline. J. Mar. Biol. Assoc. 55(2):261-274.

Pingree, R. D., P. M. Holligan, G. T. Mardell, and R. N. Head. 1976. The influence of physical stability on spring, summer and autumn phytoplankton blooms in the Celtic Sea. J. Mar. Biol. Assoc. U.K. 56:845-873.

Pingree, R. D., L. Maddock, and E. I. Butler. 1977. The influence of biological activity and physical stability in determining the chemical distributions of inorganic phosphate, silicate and nitrate. J. Mar. Biol. Ass. 57:1065-1073.

Pingree, R. D., P. M. Holligan, and G. T. Mardell. 1978. The effects of vertical stability on phytoplankton distributions in the summer on the northwest European shelf. Deep Sea. Res. 25(11):1011-1016.

Redfield, A. C. 1958. The biological control of chemical factors in the environment. Amer. Scientist. **46**:205–221.

Rees, A. P., I. Joint, and K. M. Donald. 1999. Early spring bloom phytoplankton nutrient dynamics at the Celtic Sea shelf edge. Deep Sea Res. 46(2):483-510.

Rippeth, T. P. 2005. Mixing in seasonally stratified shelf seas: a shifting paradigm. Philos Trans A Math Phys Eng Sci. 363(1837): 2837-2854.

Rippeth, T. P., J. H. Simpson, R. J. Player, and M. Garcia. 2002. Current oscillations in the diurnal inertial band on the Catalonian shelf in spring. Cont. Sh. Res. 22:247-265.

Rippeth, T. P., P. J. Wiles, M. R. Palmer, J. Sharples, and J. Tweddle. 2009. The diapycnal nutrient flux and shear-induced diapcynal mixing in the seasonally stratified western Irish Sea. Cont. Sh. Res. **29**:1580-1587.

Ross, O. N., and J. Sharples. 2008. Swimming for survival: A role of phytoplankton motility in a stratified turbulent environment. J. Mar. Sys. 70(3-4): 248-262.

Schafstall, J., M. Dengler, et al. 2010. Tidal-induced mixing and diapycnal nutrient fluxes in the Mauritanian upwelling region. J. Geophys. Res. 115(C10).

Seiwell, H. R. 1935. The cycle of phosphorus in the western basin of the North Atlantic. Physic. Oceanogr. Metero. 3:1-56.

Sharples, J., and P. Tett. 1994. Modelling observations of the seasonal cycle of primary productivity: the importance of short-term physical variability. J. Mar. Res. 52:219-238.

Sharples, J., C.M. Moore, T. R. Rippeth, P. M. Holligan, D. J. Hydes, N. R. Fisher and J. Simpson. 2001a. Phytoplankton distribution and survival in the thermocline. Limnol. Oceanogr. **46**:486–496.

Sharples, J., C. Moore, and E. Abraham. 2001b. Internal tide dissipation, mixing, and vertical nitrate flux at the shelf edge of NE New Zealand. J. Geophys. Res. [Oceans]. **106:**14069–14081, doi:10.1029/2000JC000604.

Sharples, J., J. F. Tweddle, J. A. M. Green, M. R. Palmer, Y. Kim, A. E. Hickman, P. M. Holligan, C. M. Moore, T. P. Rippeth, J. H. Simpson, and V. Krivstov. 2007. Spring-neap modulation of internal tide mixing and vertical nitrate fluxes at a shelf edge in summer. Limnol. Oceanogr. **52**:1735–1747, doi:10.4319/lo.2007.52.5.1735.

Sherwin, T. J. 1987. Inertial oscillations in the Irish Sea. Cont. Sh. Res. **7**:191-213.

Siegenthaler, U., and J. L. Sarmiento. 1993. Atmospheric carbon dioxide and the ocean. Nature. 365:119-125.

Sigman, D. M., and E. A. Boyle. 2000. Glacial/interglacial variations in atmospheric carbon dioxide. Nature. 407:859-869.

Simpson, J. H., and J. R. Hunter.1974. Fronts in the Irish Sea. Nature **250**: 404-406

Simpson, J. H., and D. Bowers. 1984. The role of tidal stirring in controlling the seasonal heat cycle in shelf seas. Ann. Geophys. 2: 411-416

Simpson, J. H., W. R. Crawford, T. P. Rippeth, A. R. Campbell, and J. V. S. Cheok. 1996. The vertical structure of turbulent dissipation in shelf seas. J. Phys. Oceanogr. 26: 1579-1590.

Simpson, J. H., H. Burchard, N. R. Fisher, and T. P. Rippeth. 2002. The semi-diurnal cycle of dissipation in a ROFI: model measurement comparisons. Cont. Sh. Res. 22(11-13):1615-1628.

Simpson, J. H., and J. Sharples. 2012. Introduction to the shelf seas. In: Introduction to the physical and biological oceanography of shelf seas. Cambridge University Press, Cambridge, pp. 1-24

Smayda, T. J. 1997. Harmful algal blooms: their ecophysiology and general relevance to phytoplankton blooms in the sea. Limnol. Oceanogr. 42: 1137-1153.

Steinbuck, J., M. Stacey, M. A. McManus. O. M. Cheriton, and J. Ryan. 2009. Observations of turbulent mixing in a phytoplankton thin layer. Mar. Ecol. Progr. Ser. 378:55-69.

Sverdrup, H. U.1953. On conditions for the vernal blooming of phytoplankton. J. Cons. Int. Explor. Mer **18**: 287-295

Tang, Y. 1995. The allometry of algal growth rates. J. Plankton. Res. 17: 1325-1335.

Tett, P., S. I. Heaney, and M. R. Droop. 1985. The Redfield ratio and phytoplankton growth rate. J. Mar. Biol. Assoc. U.K. **65:** 487 – 504.

Thomas, H., Y. Bozec, et al. 2004. Enhanced open ocean storage of CO2 from shelf sea pumping. Science 304(5673): 1005-1008.

Tsunogai, S., S. Watanabe, and T. Sato. 1999. Is there a 'continental shelf pump' for the absorption of atmospheric CO2? Tellus. 51B:701-712.

Tweddle, J. F., J. Sharples, M. R. Palmer, K. Davidson, and S. McNeil. (2013). Enhanced nutrient fluxes at the shelf sea seasonal thermocline caused by stratified flow over a bank. Progr. Oceanogr. *In press*.

Utermöhl, H. 1931. Neue Wege in der quantitativen Erfassung des Planktons. (Mit besonderer Berücksichtigung des Ultraplanktons). *Verh. Int. Verein. Theor. Angew. Limnol.* **5**: 567–596

Van Meurs, P. 1998. Interactions between near-inertial mixed layer currents and the mesoscale: the importance of spatial variabilities in the vorticity field. J. Phys. Oceaongr. 28: 1363-1388.

Volk, T., and M. I. Hoffert. 1985. Ocean carbon pumps: analysis of relative strength and efficiencies in ocean driven atmospheric CO2 changes. In: Sandquist ET and Broecker WS (eds.) *The carbon cycle and atmospheric CO2: natural variations Archean to present*. AGU, Washington, pp. 99-110

Walsh, J. J. 1991. Importance of continental margins in the marine biogeochemical cycling of carbon and nitrogen. Nature. 350: 53-55/

Weston, K. (2005). "Primary production in the deep chlorophyll maximum of the central North Sea." Journal of Plankton Research 27(9): 909-922.

Williams, C. A. J., J. Sharples, M. Green, C. Mahaffey, and T. P. Rippeth. 2013. The maintenance of the subsurface chlorophyll maximum in the western Irish Sea. **3**: 61-73.

Williams, C. A. J., J. Sharples, C. Mahaffey, and T. P. Rippeth. (accepted). The wind driven pulses of nutrients to phytoplankton in stratified shelf seas. Geophy. Res. Let.

Williams, P. J. Le B. 1995. Evidence for the seasonal accumulation of carbon-rich dissolved organic material and the consequential effect on net C/N assimilation ratios. Mar. Chem. 51: 17-29.

Wishner, K. F., M. M. Gowing, C. Gelfman. 1998. Mesozooplankton biomass in the upper 1000m in the Arabian Sea: overall seasonal and geographic patterns, and relationships to oxygen gradients. Deep Sea Res II 45:2405-2432.

Wobus, F., G. Shapiro, M. A. M. Maqueda, and J. M. Huthnance. 2011. Numerical simulations of dense water cascading on a steep slope. J. Mar. Res. 69(2-3):391-415

Wollast, R. 1998. Evaluation and comparison of the global carbon cycle in the coastal zone and in the open ocean. In: Brink, K. H., Robinson, A. R. (Eds). The Sea, Vol 10. John Wiley and Sons, New York, 213 – 252.

Young, J. W., R. Bradford, T. D. Lamb et al. 2001. Yellowfin tuna (Thunnus albacares) aggregations along the shelf break off south-eastern Australia: links between inshore and offshore processes. Mar. Freshwater. Res. 52(4):463-474.

Chapter 2

How do phytoplankton in the sub-surface chlorophyll maximum acquire their nutrients?

2.1 Introduction

A persistent feature of shelf seas during summer stratification is the subsurface chlorophyll maximum (SCM), which occurs after nutrient uptake during the spring bloom depletes nutrients in the euphotic zone (Holligan and Harbour, 1977). The contribution of primary production in the SCM to the annual shelf sea primary production is of a similar magnitude to that observed in the spring bloom (Hickman et al. 2012). Furthermore, the primary production which is driven by nitrate ('new' production) at the SCM acts as an important sink of carbon dioxide in shelf seas (Kitidis et al. 2012). The turbulent, diapycnal supply of dissolved inorganic nitrogen from the nutrient replete BML is assumed to sustain the SCM (Sharples et al., 2001a; 2001b; Rippeth et al., 2005; Williams et al., 2013), as well as setting the limit on new production at the SCM (Sharples et al., 2007; Rippeth et al., 2009). Here this assumption is investigated by considering the possibility that phytoplankton might themselves transport significant quantities of nutrients from the deeper water to the SCM. In particular, motile dinoflagellates, commonly seen in the shelf sea SCM (Holligan and Harbour, 1977) may be able to take up BML nutrients and then swim upwards to the SCM.

Motile dinoflagellates are able to compete and coexist with diatoms at the SCM despite often having lower photosynthetic rates (Tang, 1995), higher metabolic costs and higher nutrient affinity (half saturation) coefficients (Smayda, 1997). These physiological disadvantages that dinoflagellates possess are believed to be offset by motility, in particular dinoflagellates are able to migrate to access deep inorganic nitrogen (hereafter N) pools when under nutrient stress (Eppley et al. 1968; MacIntyre et al., 1997; Inoue and Iseri, 2012), and are capable of luxury consumption of nutrients (Broekhuizen, 1999). This can be quantified by the internal stoichiometric ratio (cell C:N quota), and has been linked to dinoflagellate swimming behaviour in experiments (Kamykowski and Yamazaki, 1997). Furthermore, the cell C:N quota is an indicator of nutrient limitation and has been used to parameterise motility in numerical models (Broekhuizen, 1999; Ross and Sharples, 2007; 2008). In a nutrient depleted system, Cullen and Horrigan (1981) observed the development of an SCM when dinoflagellate intracellular C:N quotas increased as a response to nitrate deplete conditions, which caused dinoflagellates to swim downwards.

Observational evidence for the importance of dinoflagellate motility for SCM maintenance was recently highlighted in Monterey Bay (Steinbuck et al., 2009). . Concentrated thin layers of the dinoflagellate *A. Sanguiniea* were formed as a direct result of the phytoplankton swimming into deeper water to acquire nutrients, and then returning to the SCM to photosynthesise. The very weak tides, and subsequently weak turbulence, in Monterey Bay meant that the phytoplankton could control their position in the water column. Also, weak turbulence would mean weak diapycnal nutrient fluxes, and so the ability to swim down to access nutrients would be vital. In a contrasting environment which is tidally energetic, such as the Celtic Sea, it is likely that turbulent mixing will overcome phytoplankton motility within the BML. A numerical study by Ross and Sharples (2008) investigated the importance of motility in a tidally energetic shelf sea using a Lagrangian particle tracking model. BML turbulence eroded phytoplankton cells from the base of the SCM but also re-introduced cells to the SCM after they had spent some time in the nutrient-replete BML. This turbulence-mediated re-access to the SCM was found to be critical in sustaining the SCM, implying that nutrient uptake by the phytoplankton while in the BML could be an important nutrient source. The model suggested that this was the case for both motile and non-motile phytoplankton, though motility was advantageous in allowing nutrient-replete cells to swim further upward within the SCM following being mixed into the SCM base.

In two very different turbulent environments it thus appears that phytoplankton can transport nutrients from the BML into the SCM. In Monterey Bay re-access to the thermocline is entirely by motility, whereas in the tidally energetic Celtic Sea both motility and tidal turbulence are important. Thus it is possible that the SCM is partially sustained in a tidally energetic shelf sea by phytoplankton assimilation of nutrients in the BML, and then transported via motility and turbulence into the SCM. If the ability of phytoplankton to assimilate BML nutrients and then regain access to the SCM is a dominant factor in the maintenance of the SCM, then this questions the basis of interpreting the diapycnal flux of nutrients in shelf seas as a limiter of new production in the SCM.

This chapter focuses on addressing whether nutrient assimilation below the thermocline by motile phytoplankton plays any role in sustaining the SCM in a tidally energetic shelf sea. The aim of this chapter is to estimate the flux of nutrients

to the SCM via phytoplankton motility and thus assesses the importance of measuring diapycnal nitrate fluxes. The difficulty associated with measuring nutrient uptake and its subsequent transport by migrating dinoflagellates means that it would be virtually impossible to provide observational evidence of the role of BML nutrient uptake. It is viable, however, to use a numerical model to investigate nutrient assimilation and transport. A Lagrangian phytoplankton particle tracking model is ideal for tracking individual cell nutrient assimilation and trajectories (Woods and Barkmann, 1994; Broekhuizen, 1999; Ross and Sharples, 2004). Here we set out a series of numerical experiments using a documented 1D Lagrangian model which explicitly describes turbulence and motility (Ross and Sharples, 2007; 2008), the aim of which was to investigate whether N uptake below the thermocline by eroded phytoplankton plays a role in the SCM maintenance during summer. The study here is similar to that documented by Ross and Sharples (2008), who investigated the importance of motility for cells eroded from the SCM in terms of SCM maintenance in a tidally energetic shelf sea. Ross and Sharples (2008) found that cell motility was vital for sustaining the SCM biomass against tidal erosion, but did not comment on whether the flux of nutrients from below the thermocline via motile cells played a role in SCM maintenance. In this chapter, the internal nutrient status of cells is tracked to assess whether nutrient transport by eroded motile cells sustains the SCM in combination with SCM reaccess by the motile cells.

2.2 Methods

A 1D particle tracking numerical model (Ross and Sharples 2004; 2007; 2008) was used to investigate the relative importance of nutrient uptake by both motile and non-motile phytoplankton within the BML, followed by phytoplankton re-access to the SCM, and uptake by phytoplankton within the SCM. The model is based on three main components: 1) the physical model including turbulence, 2) a Lagrangian particle tracking component (Ross and Sharples, 2004), and 3) a biological component which determines the growth, nutrient uptake and swimming behaviour of individual phytoplankton cells as a function of their light and nutrient requirements (Ross and Sharples, 2007; 2008). A series of experiments were set up to assess the importance of N assimilation in the BML and cell reaccess in both motile (swimming speed = 0.1 mm s^{-1}) and neutrally buoyant, non-motile cells (swimming speed = 0 mm s^{-1}). A phytoplankton swimming speed of 0.1 mm s^{-1} was

selected for motile cells, this value represents the middle of the range of dinoflagellates swimming speed estimates (<0.1 – 0.5 mm s^{-1}; Eppley et al., 1967; Eppley et al., 1968).

2.2.1 The physical model

The physical model which was used to simulate a summer, stratified turbulent environment was based on a two equation κ-ε turbulence closure scheme (Canuto et al., 2001; Sharples et al., 2006), and was configured to be representative of a typical temperate shelf sea with relatively energetic tides (e.g. Simpson et al. 1996). The total water depth, *H*, in the 1-Dimensional model was 80 m (Table 2.1), the surface mixed layer consisted of the upper 20 m and was separated from the 50 m thick BML by a linear thermocline between 20 and 30 m depth. The tidal currents in the model were forced by an oscillating the sea surface slope at the period of the major lunar constituent of 12.42 h (M2), with a tidal current amplitude of about 0.75 m s^{-1}, corresponding to a near-spring tide condition in the Western English Channel (Sharples et al., 2001). A quadratic friction boundary condition at the seabed generated the vertical current shear, which yielded profiles of turbulent dissipation and eddy diffusivity (K_z). The strongest turbulence was generated at the bed and surface boundaries. Near the thermocline turbulence decreased rapidly and within the thermocline the diffusivity dropped to ~10^{-5} m^2 s^{-1} (Fig. 2.1), chosen as a typical value representing the mixing by internal waves (see Sharples et al., 2006 for details). Full details of the physical set up are provided with Ross and Sharples (2004; 2007; 2008). The physical model was run once to generate a 25 h time series (i.e. 2 full tidal cycles) of eddy diffusivity in mid summer which was then repeated over the model duration with a time step of 6 seconds. The K_z data were used in the repeating 25 h series to drive the Lagrangian particle tracking and biological components in the model.

2.2.2 Particle tracking

In each numerical experiment particles were treated as either motile (swim speed, w_p = 0.1 mm s^{-1}) or non-motile (w_p = 0 mm s^{-1}). Dinoflagellate swimming speed ranges from <0.1 to 0.5 mm s-1 (Eppley et al., 1967; Eppley et al., 1968), a speed of 0.1 mm s^{-1} is representative of a number of swimming speed estimates. The Lagrangian particle tracking component of the model incorporated the effects of

turbulence on the particles by using the K_z data in a random walk (described fully in Ross and Sharples, 2004). The model tracked 10,000 particles being mixed by the eddy diffusivities produced via the turbulence closure model outlined in section 2.2.1. Each particle initially consisted of 100,000 phytoplankton cells. Particles were distributed homogenously through the water column at the start of model runs. During each time step a particle was moved from its previous position (Z_n) to its new position (Z_{n+1}) following Eq. 1 (Hunter et al., 1993; Kamykowski et al. 1994; Visser 1997):

$$Z_{n+1} = Z_n + w_p\Delta t + K_z{}'(Z_n)\Delta t + R\left[\frac{2K_z(Z_n+\frac{1}{2}K_z{}'(Z_n)\Delta t)\Delta t}{r}\right]^{\frac{1}{2}} \quad [2.1]$$

where Z_n represents the vertical position of a particle at time n, w_p is the vertical swimming velocity, K_z is the turbulent eddy diffusivity, Δt is the time step (6 seconds), R is a random process of 0 mean and variance, and $K_z{}'=dK_z/dz$. The time step for Eq. 2.1 was chosen according to Eq. 8 in Ross and Sharples (2004) to ensure an error of less than 1% between particle accumulations and statistical variations at all times.

The cell swimming speed for motile cells was set as w_p =0.1 mm s^{-1} (approximately 8.5 m d^{-1}) which is in the middle of the range of estimates of the swimming speed of dinoflagellates (Eppley et al., 1968). Whether or not this moderate ability to swim could overcome the effects of turbulent mixing can be quantified using the Péclet number, *Pe*, defined as the ratio of the mixing time scale to the swimming time scale (Eq. 2.2):

$$Pe = \frac{L^2/K}{L/w_p} = \frac{w_p L}{K_z} \quad [2.2]$$

Here L is a suitable length scale, taken here to be the vertical distance a phytoplankton swimming at 0.1 mm s^{-1} could swim during 16 h of daylight. This is approximately 5.8 m. If *Pe* >>1 then motility should prevail and for *Pe*<<1 turbulent

mixing overcomes motility. Using the physical model to generate a K_z vertical profile (Fig. 2.1a), and with the chosen swimming speed of 0.1 mm s^{-1}, *Pe* is only larger than unity within the relatively quiescent thermocline (Fig. 2.1b). *Pe* is at least 2 orders of magnitude larger than unity further into the thermocline, thus motile cells will be able to swim within this region against the low levels of turbulence. Where tidally-driven bottom boundary mixing is high at the bed, *Pe* in the BML is approximately 2 orders of magnitude smaller than unity, thus indicating that motility will be overcome by turbulent mixing in the BML. If we consider a slow dinoflagellate swimming at 0.05 mm s^{-1} (thus capable of swimming 2.9 m in 16 h of daylight), $Pe < 1$ throughout the entire water column but ~10 in the relatively quiescent thermocline, thus motility will still prevail in this region. Comparatively, a dinoflagellate swimming at the upper estimate of swimming speeds (0.5 mm s^{-1}), would be capable of swimming approximately 29 m in 16 h daylight, and $Pe >> 1$ throughout the thermocline but closer to unity in the BML. For the ranges of swimming speeds, *Pe* is always greater than unity in the thermocline. The choice of 0.1 mm s^{-1} as the swimming speed is a reasonable estimate as it considers an environment where turbulence overcomes motility in part of the water column (the BML), as well as realistically allowing phytoplankton to be able to swim through the quiescent thermocline if positioned there.

The situation in a tidally energetic shelf sea (Fig. 2.1a and 2.1b), can be contrasted with the low turbulence environment of Monterey Bay, where motility has been shown to sustain phytoplankton thin layers (Steinbuck et al., 2009). Monterey Bay has weak tides and as a result K_z in the BML rarely exceeds 1×10^{-6} m^2 s^{-1} (Fig. 2.1c), which is almost 4 orders of magnitude smaller than K_z in the physical model set up for the Celtic Sea ($K_z>1\times10^{-2}$ m^2 s^{-1}; Fig. 2.1a). K_z in the Monterey Bay SCM is in the range of 1×10^{-7} and 1×10^{-5} m^2 s^{-1}, the higher estimate of which is close to the K_z values within the thermocline of the physical model for the experiments (Fig. 2.1a). Using the same swimming speed and length scale as quoted above together with the Monterey Bay K_z values provided by Steinbuck et al., (2009), *Pe* is greater than unity throughout the entire water column (Fig. 2.1d). Furthermore, in the

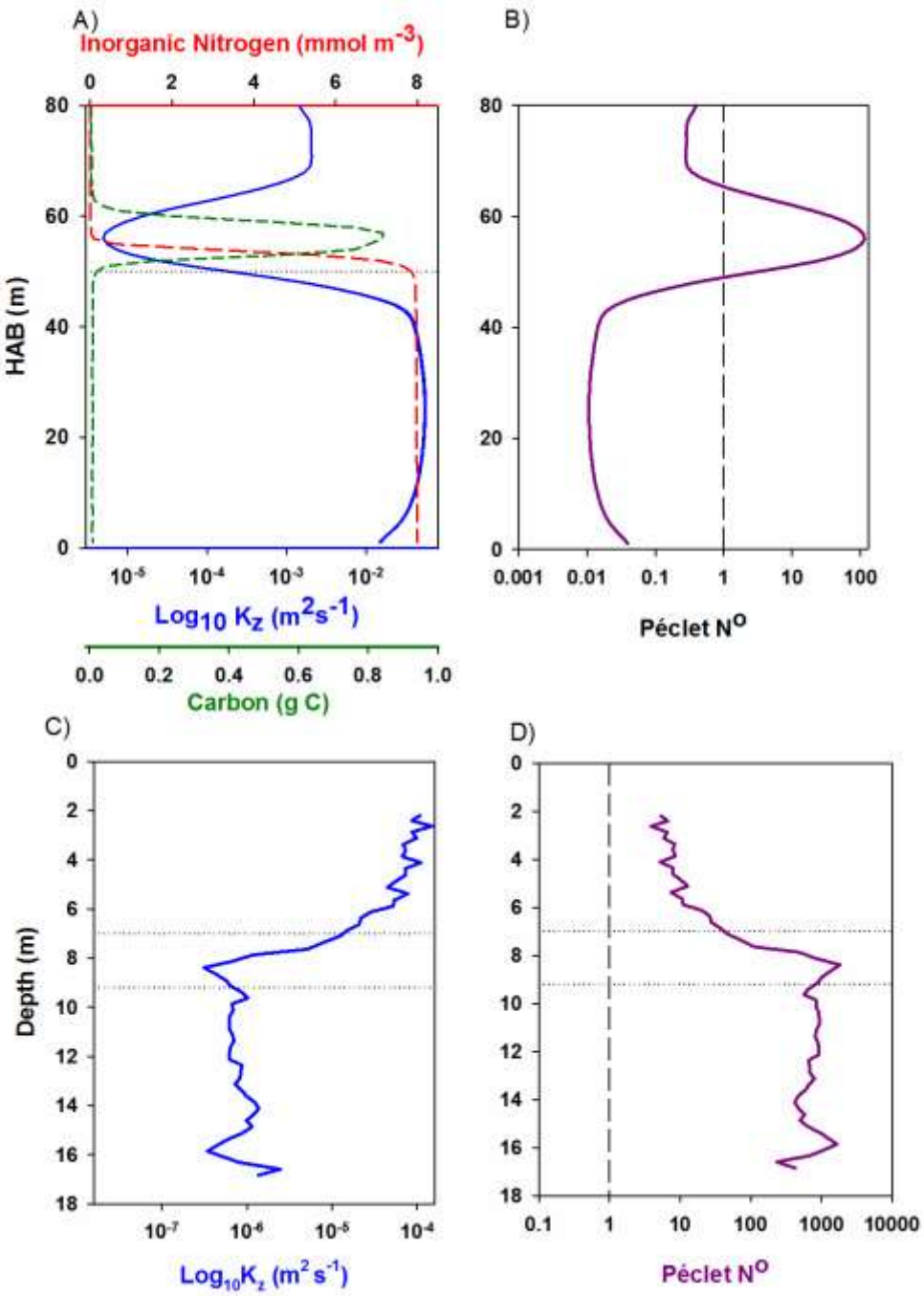

Figure 2.1: (a) Time averaged K_z (blue solid line), dissolved inorganic nitrogen (red long dashed line) and total carbon (green short dashed line), and (b) The Péclet number profile from the original 1D model (Ross and Sharples 2008) when run for 200 days. The dotted horizontal line in (a) indicates the base of the thermocline (z*). The dashed vertical line in (b) indicates the *Pe* threshold of 1. (c) Typical K_z profile as measured from Monterey Bay and (d) *Pe* for Monterey Bay (data provided by Steinbuck et al., 2009). The mean position of the top and bottom of the subsurface chl *a* layer have overlaid with been dotted lines in (c) and (d).

relatively quiescent BML *Pe*>>1, indicating that in this shelf sea environment motility would prevail against mixing. Hence, motile phytoplankton in this environment play a key role in the SCM maintenance and are highly capable of swimming below the SCM for nutrients and subsequently gaining reaccess to the SCM (Steinbuck et al., 2009). By contrast in the Celtic Sea, turbulence in the BML overwhelms phytoplankton motility; particle tracks shown later in this chapter illustrate how re-access to the SCM from the BML is driven by turbulent mixing, often after a particle has spent several days being mixed continuously within the BML.

2.2.3 The biological model

Production

Observations of swimming strategies of motile phytoplankton indicate that the nutrient status and light requirements of cells are important in determining swimming behaviour (Eppley et al., 1968; Cullen and Horrigan, 1981). The biological component of the model includes both photosynthetic and nutrient uptake components. Phytoplankton growth in the model was based upon the simple photo-acclimation model by Geider et al. (1998) as outlined in Eq. 2.3.

$$P = P_m \left[1 - exp\left(\frac{I.\propto^{chl}.\theta^c}{P_m}\right)\right] \quad \text{[dimensionless]} \qquad [2.3]$$

where P_m is the maximum growth rate of the cells (s^{-1}), α^{chl} represents the chlorophyll specific C assimilation rate (g C m^{-2} (g chl μE)$^{-1}$), and θ^C is the chlorophyll to carbon ratio of a cell (g Chl (g C)$^{-1}$) (See table 2.1). Following Ross and Sharples (2007; 2008), this chapter assumes that the maximum growth rate is a constant value. However this is flawed and it should be noted that the growth rate of phytoplankton is influenced by temperature, thus a vertically migrating/turbulently mixed phytoplankton would experience varying temperatures which would influence the potential maximum production rate. For simplicity P_m is assumed to be constant at a value of 2.174×10^{-5} s^{-1}, which represents the maximum growth rate at a reference temperature under nutrient replete conditions (Geider et al., 1997).

I is the light intensity (photosynthetically active radiation, PAR) at the particle depth which is calculated from a slightly modified version of the Beer-Lambert equation:

$$I(z) = I_0 \exp[-(k + k_s(z))(H - z)] \quad [2.4]$$

I_0 is the PAR at the sea surface, *H* is the total depth of the water column, *k* is the (background) light attenuation coefficient which is taken to be 0.09 m^{-1} (Table 2.1; Broekhuizen, 1999).

The parameter $k_s(z)$ is the absorption due to self-shading (Geider et al. 1998) and is dependent on a cell's individual position (z) and the amount of carbon above it:

$$k_s(z) = k_c \bar{C} \quad [2.5]$$

Where k_c is the carbon specific absorption coefficient taken as 0.0004 m^2 $(mg\ C)^{-1}$ (Broekhuizen, 1999), and $\bar{C}$ is the average carbon concentration in the water column between the cell position and the surface.

Nutrient uptake

Dissolved inorganic nitrogen (N; mmol m^{-3}) is the one nutrient considered in the model, justified because nitrate is generally observed to be the limiting nutrient in this type of environment. N is taken up and stored internally by the cells. Nutrient uptake (*U*) follows Michaelis-Menten kinetics:

$$U = U_m \left(1 - \frac{Q}{Q_{max}}\right) \frac{N}{K_N + N} \quad [2.6]$$

where *Q* is the cellular nitrogen-to-carbon ratio, which needs to remain above a subsistence quota of Q_{min} (Table 2.1) and below the maximum storage quota Q_{max} (e.g. Broekhuizen 1999; Broekhuizen et al. 2003). When a cell assimilates N the intracellular quota will increase, and when C is fixed via photosynthesis the cell quota will decrease. The maximum uptake rate (U_m) and half saturation constant (κ_N) describe the Michaelis-Menten curve of nutrient uptake.

The cellular nitrate levels are updated at each time step according to equation 2.7:

$$\frac{dN}{dt} = [U - r - G - Lr]N \quad [2.7]$$

Here U is the uptake of nitrate (Eq. 2.6), r is the respiration rate, and G is the grazing rate. Lr is the carbon dependent mortality rate, which is a fixed rate of 0.1 day^{-1} if C is less than a lower carbon threshold (C_{starve}), and Lr=0 otherwise. At an upper carbon level ($C_{fission}$) cells will divide and the number of cells per Lagrangian particle will double (Table 2.1). The rate of grazing in an environment is dependent on the concentration of prey, with increasing ingestion by predators occurring with increasing prey concentration (Holling, 1959). For simplicity in this model, a proportion (10%) of the total cells was removed due to the grazing rate (G) every day, though this assumes that the grazing rate is fixed which it would not be in the real environment. However, this chapter is focused on the role of motility for nutrient acquisition only and thus a fixed grazing rate is suitable for this purpose (Ross and Sharples, 2008).

The cell carbon, C, is calculated at each time step following a Droop-type function:

$$\frac{dC}{dt} = \left[P\left(1 - \frac{Q_{min}}{Q}\right) - r - G - Lr\right]C \quad [2.8]$$

Here P is the instantaneous production (Eq. 2.3), Each one of the 10,000 Lagrangian particles was initially made up of 2 mg C and represented 100,000 cells (2×10^{-6} mg C cell^{-1}). C losses due to grazing and mortality reduce the number of cells within each Lagrangian particle. For N_{part} particles, a particle was forced to divide into two if it carried more than $20/N_{part}$ of the total water column biomass, in order to ensure that no Lagrangian particle represented a disproportionately large fraction of the total biomass.

Inorganic nitrogen was modelled on a Eularian grid using the standard diffusion equation, where the nutrient concentration in each depth element changed according to:

$$\frac{dN_{tot}}{dt} = \frac{d}{dz}\left(K\frac{dN}{dz}\right) - UC_{tot\_i} + [r + \beta G]\widehat{N}_{tot} + \beta Lr\widehat{N_{tot}}^{starve} \quad [2.9]$$

where $\widehat{N}_{tot}$ denotes the total amount of cellular nitrogen at a particular depth, $\widehat{N_{tot}}^{starve}$ is the total cellular nitrogen content in the cells where $C<C_{starve}$, C_{tot_i} is the total amount of cellular carbon in the i-th depth element, thus UC_{tot_i} describes the uptake loss term for all cells at a particular depth. The term β is the fraction of the grazed and starved nitrogen that is recycled back into the water immediately. A simple method of including the re-supply of dissolved inorganic nitrogen to the water column, following nitrogen re-mineralisation in the bottom water and sediments, was implemented by forcing a fixed concentration of DIN_{bed} = 7 mmol m^{-3} at the seabed in the bottom model depth element.

Realistically there are trade-offs for motility (e.g. Litchman & Klausmeier, 2008). Motile phytoplankton are likely to have lower photosynthetic and growth rates (Tang, 1995), higher metabolic costs and higher nutrient affinity (Smayda, 1997).Furthermore many non-motile phytoplankton such as diatoms are capable of storing nutrients in their vacuoles (Lomas & Glibert, 2000). However, in this chapter phytoplankton parameters were set as the same for both motile and non motile cells (Table 2.1) in order to assess the role of motility for sub-thermocline nutrient uptake strategies.

Cellular quota driven swimming strategy

The swimming strategy of cells was determined by light-nutrient requirements using the following Eq. 3.0 (Broekhuizen, 1999; Liu et al., 2001; Broekhuizen et al., 2003):

$$w_p = \left\{ \begin{array}{c} -w_{p,}\ if\ Q < f_1 Q_{max} \\ w_{p,}\ if\ Q > f_2\ Q_{max}\ and\ I(z) > I_c \\ 0,\ if\ Q > f_2 Q_{max}\ and\ I(z) < I_c \end{array} \right\} \qquad [3.0]$$

where Q is the cellular N:C ratio. If Q falls below a certain fraction, f_1, of Q_{max}, the cell will start to become nutrient depleted and will swim towards higher nutrient concentrations (i.e. downwards). As the cells reach higher nutrient concentrations Q

starts to increase and once the cell N:C quota is above a certain fraction, *f2*, of the maximum storage quota ($Q>f_2\ Q_{max}$) the cell is nutrient replete and will begin to swim upwards towards higher light intensities. $f_2>f_1$ at all times. Cells require a light intensity above a certain threshold, I_c, in order to determine the upward direction, if the light intensity of a cell is below this threshold (i.e. at night or too deep) a nutrient replete motile cell will become neutrally buoyant (w_p=0).

Parameterisation of swimming strategy

The fractions f_1 and f_2 which dictate the swimming behaviour of cells as a function of their intracellular nutrient stoichiometry are particularly sensitive parameters in the model. If f_1 is too low then cells will swim up for longer until they eventually enter the more turbulent surface mixed layer, where $Pe<<1$ and cells will struggle to battle turbulence to re-enter the thermocline. If f_2 is too high it will force a cell to continue swimming downwards and is likely to become eroded from the thermocline via tidal turbulence. Ross and Sharples (2008) found that the parameter range for which an SCM was found to develop is approximately $0.6<f_1<0.8$ and $0.6<f_2<0.9$.

The choices of f_1 and f_2 are to some extent arbitrary, as there is no observational data to base them on. In this study the choices were made using an initial investigation to determine whether there were optimum fractions of the cell quota, which would result in maximum cell growth and survival of the SCM for a given motile species. Approximately 400 numerical experiments with the same initial conditions were performed for 200 model days but with varying f_1 and f_2. For these simulations 1000 Lagrangian particles were used with each particle consisting of 1,000,000 cells as this was less computationally expensive. Statistically robust model simulations require a high number of particles (Ross and Sharples, 2004), however model results when using 1000 particles were consistent with simulations using more particles.

The cumulative number of cells and production (g C) were calculated from each simulation (Fig. 2.2). Optimum values of cell quota turnaround fractions were identified for maximum growth and production. These were found to be f_1=0.75 and f_2=0.8 (Fig. 2.2). These values are within the range quoted by Ross and Sharples (2008) for SCM development. These optimum values were therefore used

throughout all of the numerical simulations (Fig. 2.2a and 2.2c). The maximum cell production and growth in non-motile cells was evidently unaffected by varying f_1 and f_2 as Eq. 3.0 did not apply to the neutrally buoyant cells.

Table 2.1: Model parameters and common symbols used in model and throughout text, modified from Ross and Sharples (2008). The sources are 1=Sharples (1999), 2= Broekhuizen (1999), 3=Sharples et al. (2001), 4=Geider et al (1998), 5=Ross and Sharples (2008), and 6=assumed.

Symbol	Description	Value/unit	REF.
α^{chl}	Chlorophyll specific C	1×10^{-5} g C m^{-2}(g chl µE) photons)$^{-1}$	4
C_{starve}	Cellular carbon starvation threshold	1×10^{-6} mg C	2
$C_{fission}$	Cellular carbon level for cell division	3×10^{-6} mg C	2
DIN_{bed}	Nitrogen concentration in bottom depth	7.0 mmol N m^{-3}	6
f_1	If $Q<f_1\ Q_{max}$ cell swims down	0.75	6
f_2	If $Q>f2\ Q_{max}$ cell swims up	0.8	6
G	Grazing rate	0.1 day^{-1}	6,5
H	Total water depth	80 m	6
I_c	Critical light intensity for phototaxis	0.1 µE m^{-2} s^{-1}	3
I_0	Midday surface PAR	1030 µE m^{-2} s^{-1}	6
k	Light attenuation co-efficient	0.09 m^{-1}	2
K	Vertical eddy diffusivity	m^2 s^{-1}	3
Lr	Mortality rate if $C< C_{starve}$	0.1 day^{-1}	6
P_e	Peclet number	-	-
P_m	Max. growth rate	2.174×10^{-5} s^{-1}	4
Q_{min}	Subsistence nitrogen-to-carbon quota	0.056 mg N (mg C)$^{-1}$	1
Q_{max}	Maximum nitrogen-to-carbon storage	0.28 mg N (mg C)$^{-1}$	1
r	Respiration rate (=mortality rate if $C< C$	0.1 day^{-1}	6
Δt	Model time step	6 s	6
T_D	Light period	16 h	6
θ^C	Chlorophyll to C ratio (Chl:C) of a cell	0.03 g Chl (g C)$^{-1}$	4
U_m	Maximum nitrogen uptake rate	0.5 mg N (mg cell.C d)$^{-1}$	2
w_p	Particle swimming velocity	10^{-4} m s^{-1} or 0 m s^{-1}	5,6
Z	Vertical position as height above bed (z>0)	m	6
z^*	Defined reaccess depth	50 m above bed	6
β	Fraction of grazed nitrogen that is recycled	0.5	6
κ_N	Nutrient affinity (half saturation constant)	0.3 mmol N m^{-3}	1

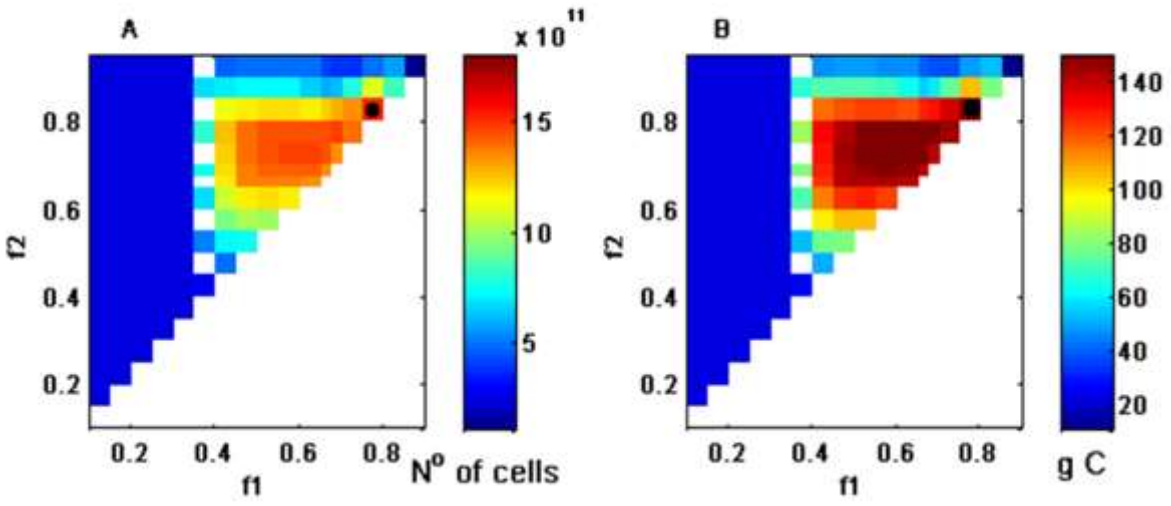

Figure 2.2: Motile a) total cell numbers and b) total production, for varying swimming turnaround fractions f_1 and f_2 over 200 day model simulations. Black circles indicate the maximum cell numbers and biomass.

2.2.4 Experiment design

The aim of experiments was to assess whether N uptake in the BML via cell motility is important for SCM maintenance. Therefore the model was modified in order to track and control the individual particle N uptake. Six model runs were set up, three of these were using motile cells, and three were using non-motile cells in order to investigate the relative importance of motility in nutrient uptake in comparison to a neutrally buoyant, non motile cell. For both the motile or non-motile species the following experiments were carried out, 1) a control, 2) particles were forced to stay in the BML once eroded, and 3) N uptake was controlled depending on a particle's vertical position. The reason for forcing the motile or non motile cells to stay in the BML once eroded in experiment 2 was to initially assess whether the SCM could sustain itself against tidal erosion if motile or non motile cells were unable to regain access to the SCM. This experiment therefore provided the basis of the main objection of the paper, if the SCM is unable to sustain itself against tidal erosion then it is cell raccess and/or nitrogen acquisition below the thermocline which sustains it. In experiment 3 the option of nutrient acquisition below the thermocline was restricted, thus eliminating this as a factor capable of sustaining the SCM and allowing this chapter to assess its importance. Experiments 1, 2 and 3 for motile or

non motile cells were all run for 200 model days, following a stable SCM formation (~40 days) this allowed the model to run for a period slightly longer than the SCM existence in observations (~120-130 days). This meant that the maintenance of the SCM, via cell reaccess and/or subthermocline nutrient uptake, in the model could be observed over a meaningful and realistic time period.

Experiment 1: Control (Reaccess allowed, free N uptake)

Experiment 1 acted as the control experiment, and was the default model set up following Ross and Sharples (2008). It was run for both motile cells and non motile cells in separate runs. If a particle found itself too deep, it could become tidally eroded from the thermocline. Eroded particles were able to gain re-access when tidal turbulence pushed the particle into the base of the thermocline, where $Pe<<1$ (Fig. 2.1b). N uptake was allowed anywhere in the water column, depending solely on the cell nutrient quota and Eqn. 5.

Experiment 2: Reaccess not allowed, free N uptake

Experiment 2 was modified after a steady model SCM was reached (40 days). It was run for both motile cells and non motile cells in separate runs. If a particle found itself at or below a certain threshold depth at the base of the thermocline (z^*=50 m) and became tidally eroded from the SCM, then it was forced to be unable to ever re-access the thermocline (Fig. 2.1a). The particles which became mixed out were still able to take up N and to respire, but they remained in the BML. These particles eventually died due to low light conditions and $C<C_{starve}$. This simple experiment has already been documented by Ross and Sharples (2008) who highlighted the importance of motility even in a relatively turbulent environment by demonstrating that particle re-access via swimming appeared to be vital in sustaining the SCM. If particles became mixed out and could not re-access the thermocline the SCM rapidly declined (<60 days) in both motile and non motile species. We revisit this experiment to investigate the role of BML N uptake in eroded particles which reaccess the thermocline.

Experiment 3: Reaccess allowed, BML N uptake prevented

Experiment 3 was set up so that after 40 model days run time if a non-motile or motile particle found itself at or below the specified depth at the base of the

thermocline, z* (50m above bed; Fig. 2.1) it was prevented from N uptake. However, the particle trajectories still responded to swimming and turbulence so that eroded particles were able to re-access to the thermocline. Thus phytoplankton particles behaved as in Experiment 1 in terms of how their trajectories were governed, but they could only acquire N from the nitracline. Experiment 3 was run for both motile cells and non motile cells in separate runs.

2.3 Results

2.3.1 SCM formation and maintenance

Experiment 1

A stable SCM developed within 2 days in Experiment 1 with motile particles (Fig. 2.3a) and within 10 days for the non motile particles (Fig. 2.3b) when no limitations on particle reaccess or N uptake were enforced in the model. Cell numbers typically exceeded 1×10^{8} cells m^{-3} and 5×10^{7} cells m^{-3} for the motile and non motile particles respectively. The tidal mixing eroded particles from the SCM. This resulted in a significant biomass of both motile and non-motile particles in the BML (previously documented by Ross and Sharples, 2008).

The swimming strategy of motile particles forced them to swim downwards to the base of the thermocline (where they could be eroded by tidal turbulence) when their cell quota decreased as a result of C assimilation. Particle erosion of the motile particles occurred on a diurnal rather than a semi-diurnal cycle. The cell intracellular N:C quota decreased during the light period whilst cells were photosynthesising, leaving the cells nutrient limited at the end of the day, and resulting in them swimming downwards for nutrients. This swimming behaviour produced a 2-day 'swath' pattern for the motile particles in the SCM as previously noted by Ross and Sharples (2008).

Motile cells were evidently more successful at sustaining a higher biomass at the SCM, whereas the non motile SCM was patchy, though still sustained for the 200 day duration of Experiment 1. Hence biomass was able to be sustained for both motile and non motile SCMs despite the turbulent erosion of particles. This

experiment thus reiterated what was already documented in Ross and Sharples (2008) and served as a control for experiments 2 and 3.

Experiment 2

Reaccess was denied to particles which were eroded below z* (50 m) after day 40 in Experiment 2. The SCM was therefore allowed to develop for both motile and non motile particles for 40 days before experimental conditions differed from those in Experiment 1. The high concentration of motile particles at the (1×10^{8} cells m^{-3}) was maintained until at least day 80 (Fig. 2.3c 40 days after SCM reaccess of BML particles was prevented. Following day 80, motile cell numbers began to decrease rapidly. The motile SCM was diminished by >90% to a thin (<5m) layer by day 110, indicating that growth alone could no longer sustain the SCM against periodic tidal erosion. By comparison, the non motile SCM population decreased within 60 days following the prevention of reaccess (Fig. 2.3d), and significant cell biomass was observed in the BML. Within 20 days of reaccess prevention (day 60), the non motile SCM had died out and could not recover from the tidal erosion of biomass.

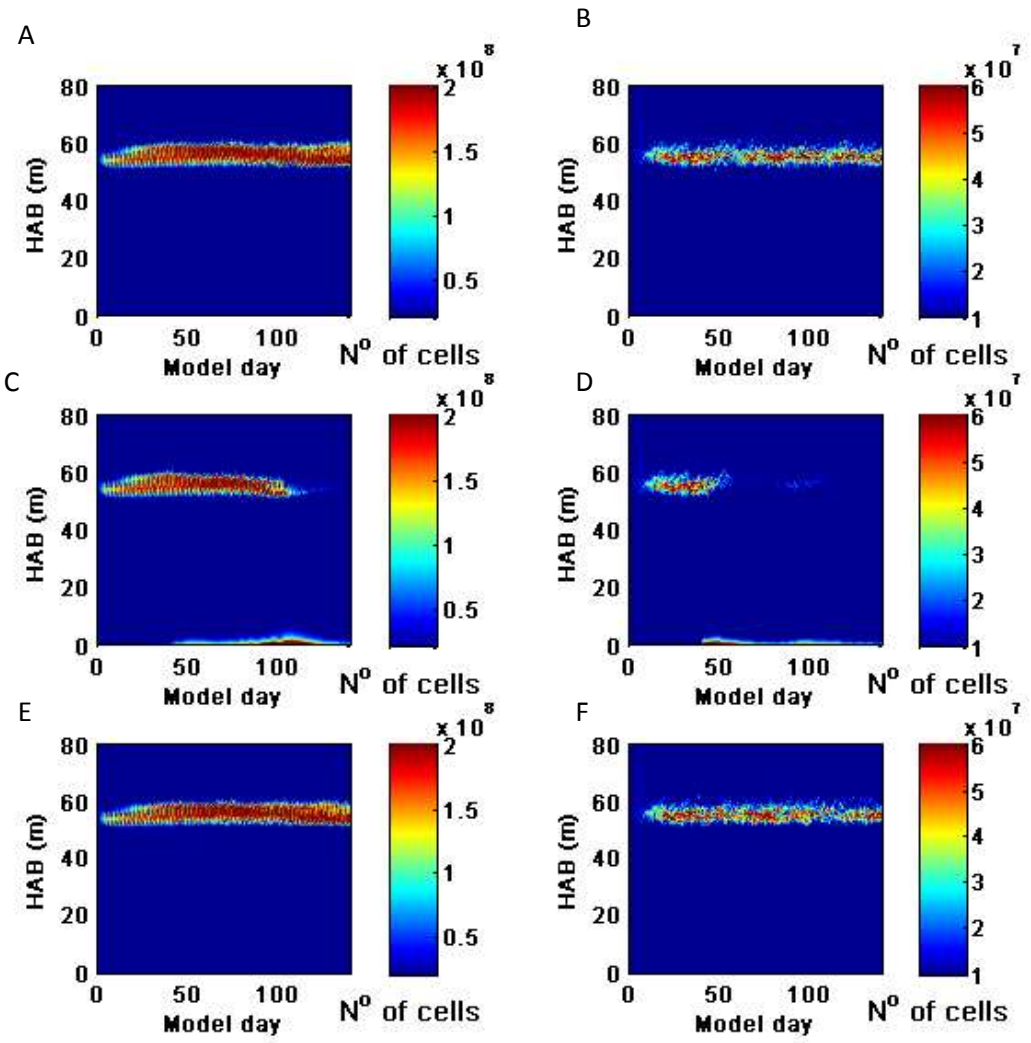

Figure 2.3: Number of cells and SCM formation of motile cells in a) Experiment 1, c) Experiment 2 (re-access from BML denied once cell is eroded after day 40) and e) Experiment 3 (re-access allowed but no N uptake below thermocline after day 40); and of non-motile, neutrally buoyant cells in b) Experiment 1, d) Experiment 2 and f) Experiment 3, over a 200 model day simulation.

Ross and Sharples (2008) found both the motile and non motile SCM to die out within 60 days when carrying out the exact experiment but with cell quota fractions f_1=0.7 and f_2=0.8. It is likely that the use of the optimum cell quota fractions for swimming behaviour allowed the motile SCM to be sustained against tidal erosion for almost twice as long.

Experiment 3

Uptake at or deeper than 50 m (z*) was prevented in Experiment 3 after day 40, but particle trajectories were not modified. Thus the SCM for both motile and non motile particles was allowed to develop with the same initial experimental conditions as Experiments 1 and 2. The SCM was maintained at a stable cell concentration of approximately 1×10^{8} cells m^{-3} for motile particles in the 200 day duration of the experiment (Fig. 2.3e), which was the same as that seen in the motile Experiment 1 (Fig. 2.3a). For the non motile particles, the SCM was maintained at a stable cell concentration of 1×10^{7} cells m^{-3} for the duration of the simulation, also the same as that observed in Experiment 1. Thus, preventing both motile and non motile particles from assimilating N in the BML did not influence SCM development or maintenance from that observed in the control (Experiment 1). In summary, the SCM formation in experiments 1, 2 and 3 for motile and non motile cells indicated that a stable SCM formed within 40 days of the model run time. Following this, in experiment 2, where reaccess to eroded cells was not allowed, the motile SCM was capable of sustaining its biomass against permanent tidal erosion for at least 40 days after a stable SCM formed. In the case of neutrally buoyant, non motile cells in experiment 2, the SCM was unable to sustain its biomass against permanent tidal erosion for longer than 20 days after a stable SCM was formed. This indicated that cell reaccess was important, in varying degrees, for both motile and non motile SCM maintenance. However, it was not clear from experiment 2 alone whether nutrient uptake below the thermocline played a role in the SCM maintenance together with cell reaccess. Experiment 3 then eliminated the option for motile and non motile cells of subthermocline nitrate uptake. The SCM was sustained in both the motile and non motile experiment 3 for the duration of the experiment at a concentration the same as that observed in the control experiment 1.

2.3.2 Particle trajectories

To ascertain how individual particles responded to the prevention of reaccess to the SCM and BML N assimilation, the analysis of 70 day individual particle trajectories and corresponding cellular N:C quotas for motile (Fig. 2.4) and non motile (Fig. 2.5) particles was carried out for each experiment. By tracking the

individual cell quota it is possible to gain an indication of the relationship between thermocline re-access and N and C assimilation.

Experiment 1

A typical particle trajectory for an eroded motile particle in Experiment 1 is shown in Fig. 2.4a. Motile particles in the thermocline displayed a vertical migration of approximately 10 m with a period of approximately 2 days for each up-down oscillation. With a swimming speed of 0.1 mm s^{-1} and 16 hours of daylight (and hence swimming light cue), each particle would have been capable of swimming approximately 5.7 m d^{-1}, and therefore it took almost 2 days (32 hours of daylight) for the appropriate assimilation of C to cause $Q < f_1 Q_{max}$ (Fig. 2.4a). The motile particle shown in Fig. 4a migrated upwards to approximately 60 m above bed to photosynthesise when it's cell quota exceeded 80% (f_2) of its maximum N:C storage quota (Q_{max}=0.28 mg N (mg C)$^{-1}$). The particle swam downwards to acquire nutrients to approximately 50 m above bed when its cell quota was below 75% (f_1) of Q_{max}. The particle shown evidently swam too deep on day 105 where it was subsequently eroded by tidal turbulence and became trapped within the BML (Fig. 2.4a). High intracellular N content meant that the cell quota remained high whilst the particle remained in the BML. On day 127 tidal turbulence pushed the particle into the base of the thermocline where *Pe*>>1 and motility could transport the particle further into the relatively quiescent thermocline.

Comparatively, non motile particles typically only regained access for very short periods, if ever (Fig. 2.5a). The non motile particle shown in Fig. 2.5a found itself within the thermocline where there were higher nutrient concentrations (Fig. 2.1a), and thus experienced an increase in its cell quota as a result of N assimilation in the thermocline. The subsequently nutrient replete particle evidently found itself too deep and became eroded on day 63 for >30 days. The non motile particle regained access to the very base of the thermocline on day 95, though it was subsequently eroded again shortly afterward.

Experiment 2

Permanently preventing reaccess resulted in the eventual mortality of eroded motile and non motile particles (Fig. 2.4b and Fig. 2.5b respectively). The motile

particle shown in Fig. 2.4b swam downwards on day 100 to assimilate N and became eroded into the BML whilst being nutrient replete. The cell quota of the particle remained high for the duration of the model simulation where cells were N replete together with intracellular C decreasing below C_{starve}. Similar behaviour was observed in non motile particles which became trapped in the BML when eroded and subsequently died (e.g. particle shown in Fig. 2.5b).

Experiment 3

When uptake below 50 m (z*) was prevented, the intracellular Q remained high in eroded motile particles regardless of N uptake being denied in the BML (e.g. Fig. 2.4c). Even when N starved for 10 days in the BML the motile particle was still able to survive when it gained reaccess to the base of the SCM. The behaviour of motile particles was unaffected by the inability to assimilate N in the BML (Fig. 2.4a and Fig. 2.4c).

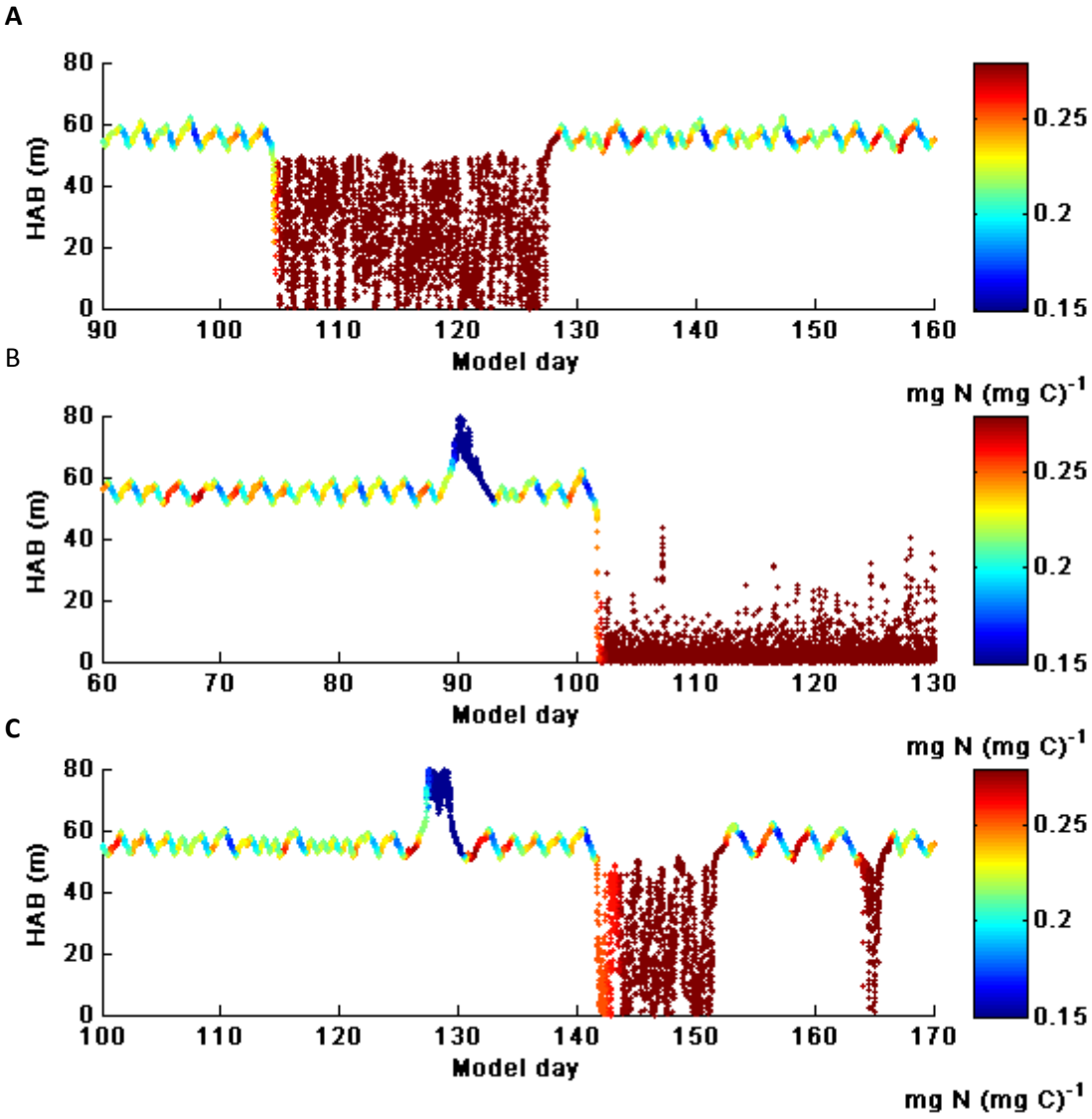

Figure 2.4: Motile individual particle tracks showing position and cell individual N:C quota every 10 minutes (70 day period shown) from one random particle in a) Experiment 1, b) Experiment 2, and c) Experiment 3.

The effect of N uptake in the BML on non-motile particles was slightly different to that observed for motile particles in Experiment 3. Analysis of the behaviour of one particular non-motile particle in Experiment 3 (Fig. 2.5c), shows that initially the particle had a high Q when eroded as a result of assimilating N at the base of the thermocline (day 88). The cell Q began to decrease (day 92 to 95) as a result of the eroded particle being pushed up via tidal turbulence shallow enough for a very small amount of C assimilation to occur, but still being below z* so prevented from to assimilate N. Once the nutrient deplete particle was mixed >50 m above bed it attempted to assimilate N, and thus the cell quota increased very slightly before it

was rapidly eroded (Fig. 2.5c; day 113). Although this eroded non-motile particle was unable to assimilate N in the BML where it remained for 30 days, it was able to survive by brief periods of turbulent reaccess to the thermocline. Thus, although the non motile particle quota behaviour in Experiments 1 and 3 differ, it is cell reaccess which determines the survival of non-motile cells and not N assimilation in the BML.

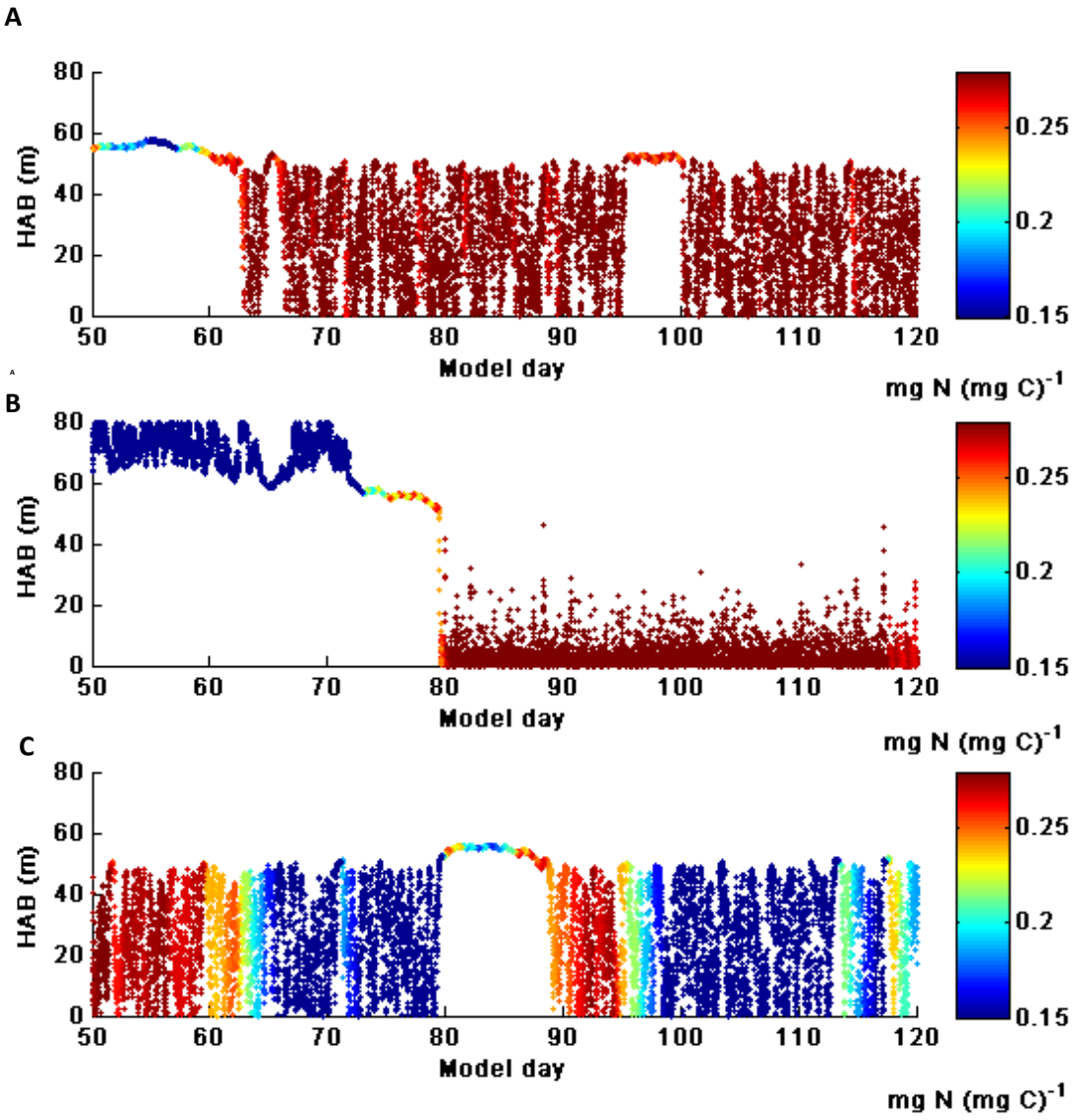

Figure 2.5: Non -motile individual particle tracks showing position and individual particle N:C quota every 10 minutes (random 70 day period shown) from one random particle in a) Experiment 1, b) Experiment 2, and c) Experiment 3.

2.3.3 Daily depth-integrated carbon

The daily total C gradually increased from the initial total intracellular value of 2 g C m^{-2} to a steady state of ~6 g C m^{-2} on day 40 in all experiments (Fig. 2.6). On model day 40, total cellular C decreased in for motile particles in Experiment 2 as a response to reaccess being prevented. The rate of decrease increased on day 100 where the motile particles were no longer able to sustain SCM biomass against tidal erosion. Comparatively, the cellular C of the non-motile particles in Experiment 2 decreased drastically on model day 40 as a response to the prevention of reaccess to the thermocline (Fig. 2.6b). This indicates that non-motile particles were unable to sustain biomass by growth only in the SCM once permanent erosion began, and died out quickly as a consequence of reaccess prevention.

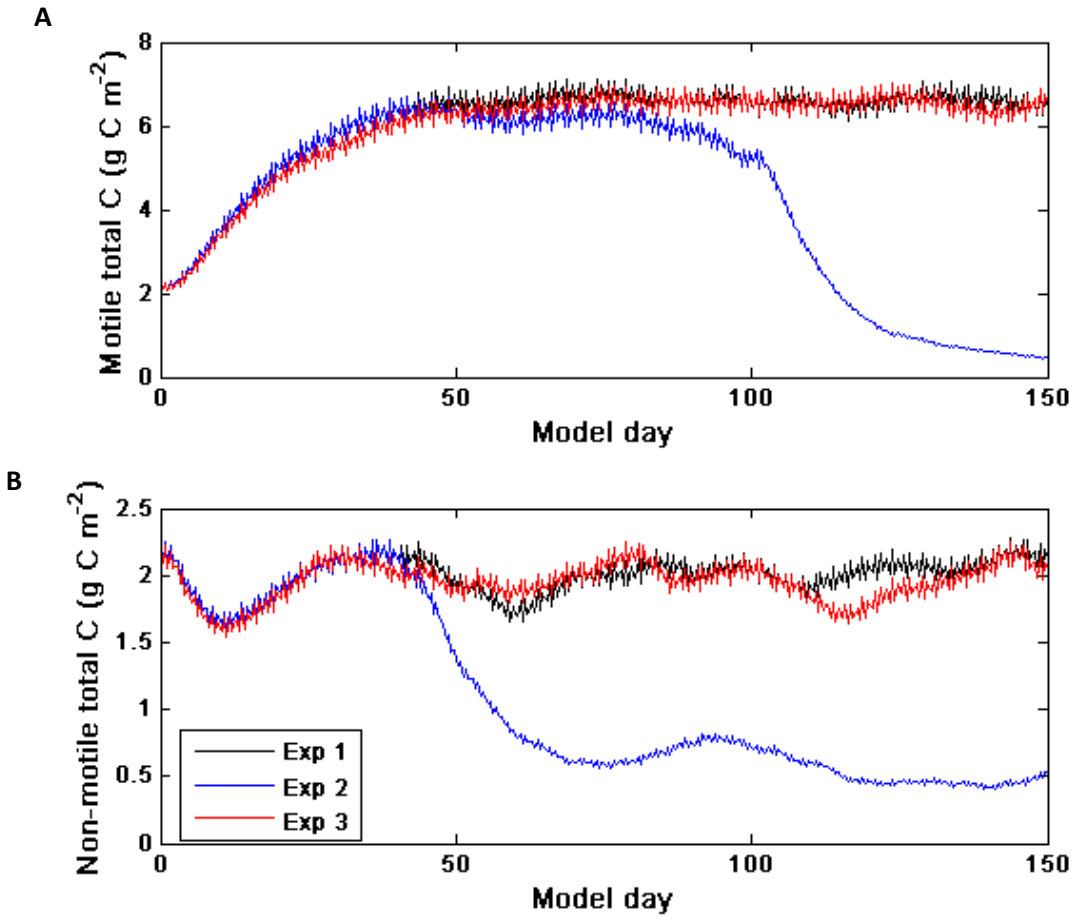

Figure 2.6: Daily depth integrated intracellular C for the initial 150 model days in a) the motile and b) non motile particles in Experiment 1 (black line), Experiment 2 (blue line) and Experiment 3 (red line). Data output for every 10 hour time step is shown.

When N uptake in the BML was switched off there was little effect on the motile daily total cellular C, other than a slight phase difference in small scale oscillations observed in Experiments 1 and 3 (Fig. 2.6a). The small diurnal oscillations (±0.5 g C) in total C occurred as a result of the daily light cycle and associated C assimilation whilst cells were photosynthesising. Evidently this daily C oscillation is larger in motile than non-motile particle experiments due to the swimming strategy of particles and 'swath' distribution at the SCM described previously.

2.4. Discussion

Various motile phytoplankton species are acknowledged to migrate deeper for nutrients (Eppley et al. 1968; Kiefer and Lasker, 1975; Heaney and Eppley, 1981), therefore investigating the role of deep nutrient uptake compared to uptake within the thermocline is important in the context of assessing the interpretation of measurements of diapycnal nutrient fluxes at the base of the shelf sea SCM. The swimming behaviour and nutrient assimilation of individual phytoplankton are properties that are difficult to measure experimentally and virtually impossible to measure in the real marine environment. Lagrangian particle tracking models are a useful tool that can be used to investigate how motility in individual cells plays a function in the existence of dense phytoplankton populations, such as the summer SCM. Here a documented Lagrangian model for the shelf sea environment, which describes turbulence and cell motility, has been implemented to investigate two main questions; for the maintenance of the SCM 1) what is the role of turbulent cell reaccess?, and 2) what is the role of nutrient uptake below the thermocline? Three simple experiments were set up to explore these questions.

Swimming by motile particles was only able to overcome turbulent mixing in a small region of the water column in the model (Fig. 2.1a). In Experiment 1 (control), motile particles which became eroded were usually able to gain reaccess to the SCM via tidal turbulence pushing them into the base of the relatively quiescent thermocline. A swim speed of 0.1 mm s^{-1} is representative of an intermediate swimming speed for dinoflagellates (Eppley et al., 1967; Kamykowski and McCollum, 1986), and gave a significant advantage to motile particles compared to non motile particles by allowing the motile particles to reach further up into the thermocline once turbulence had pushed them into the thermocline base. This

resulted in approximately 50% more cells at the motile SCM than at the non motile SCM in Experiment 1 (Fig. 2.3a and Fig 2.3b). However, non-motile particles were still able to maintain biomass in the SCM against tidal erosion, due to being periodically pushed into the base of the thermocline via tidal turbulence before being rapidly mixed out again (Fig. 2.5a). Turbulence evidently plays a role in transporting both motile and non-motile particles via both erosion and reaccess. When reaccess to thermocline by eroded particles was denied in Experiment 2 the motile SCM diminished within 110 days, and the non motile SCM diminished within 60 days (Fig. 2.3). Particles which became eroded were destined to perish in the BML, and as a result the total water column biomass decreased significantly in experiment 2 for both motile and non motile cells (Fig. 2.6). This result is similar to that presented in Ross & Sharples (2008), with the implication being that nutrient uptake within the BML might be important for sustaining the SCM. In Experiment 3, when uptake below the thermocline was prevented but particle trajectories were not modified, the concentration of cells at the SCM was unaffected in both motile and non-motile cells (Fig. 2.3d and Fig. 2.3e). Furthermore, the prevention of N assimilation below the thermocline in Experiment 3 was shown to have virtually no effect on the magnitude of total water column biomass of both motile and non-motile particles (Fig. 2.6).

A further point of interest is how phytoplankton motility may affect biogeochemical gradients, and thus the vertical flux of biological properties. The biological assimilation of nitrate determines the slope and position of the nitracline, and therefore the magnitude of the diapycnal flux of nitrate (Sharples et al. 2001a). Similarly, the depth where maximum C fixation occurs will affect the transport of POC and DOC throughout the water column. In Experiment 1 (control), for motile cells the peak in biomass was positioned at 56 m above the bed, which was slightly shallower than the peak in biomass for the non motile experiment 1 (55 m). This indicates that tidal turbulence may erode non-motile cells more easily than motile cells, as the biomass peak is closer to the bottom boundary generated mixing. Additionally, as indicated by experiment 1, non motile cells which are eroded are less likely than motile cells to reaccess the SCM. These eroded cells will be remineralised to inorganic nutrients in the BML, and therefore will be contributing to any vertical nitrate fluxes into the SCM (see Chapter 3 and 4). Thus the erosion of cells may also act as an additional nitrogen source in the BML.

In a typical temperate shelf sea environment the SCM is seen to persist throughout the summer period of ~120 days, and thus the SCM in Experiment 2 had a lifespan similar to that observed in the real environment. Thus, motile particles were able to sustain the SCM for a typical summer period without either BML nutrient transport into the SCM within the phytoplankton cells, or particle re-access to the thermocline. In stratified environments where reaccess to the thermocline by eroded motile cells is unlikely (i.e. $Pe<<1$), it could therefore be possible that motile cells are capable of conserving biomass at the SCM for a considerable period of time. Conversely, in Experiment 2 the non-motile SCM diminished within 60 days indicating that cell re-access is vital for non-motile cells living in the SCM and that ultimately, growth alone is unable to maintain the SCM against tidal erosion for non-motile cells. This would agree with observations of decreasing diatom abundance in the shelf sea SCM as summer progresses, and the SCM community becoming dominated by dinoflagellates by late summer (Holligan and Harbour, 1977). Ross and Sharples (2008) documented a similar experiment with this model, though both the motile and non-motile SCM diminished within 60 days in their simulation. The reason for the motile SCM surviving longer when reaccess was prevented in the experiment 2 compared to the results of Ross and Sharples (2008), is probably due to optimisation of the cell quota fractions, f_1 and f_2, which determine motile cell trajectories and the amount of C fixed. Realistically however, motile and non motile phytoplankton species have different physiological traits and there are trade-offs for motility (Litchman & Klausmeier, 2008). As previously mentioned, the photosynthetic and growth rates of motile phytoplankton are higher (Tang, 1995), and they are unable to internally store nutrients unlike non motile diatoms (Lomas & Glibert, 2000). Thus physiological benefits in non motile cells would additionally influence the formation and maintenance of the SCM. Additionally, the use of optimum cell quota fractions for swimming behaviour are meaningless for non motile cells, and only of use for motile cells in the experiments presented in this study for this particular model.

Although there are many different motile species of phytoplankton, we have identified an optimum cell quota fraction for swimming behaviour to produce maximum cell production and survival (Fig. 2.2). The optimum range we have found for parameters f_1 and f_2 indicate that a cell with the properties we have described will

be most successful when it's intracellular N:C stoichiometry is between 75% and 80% of its maximum storage quota. As we have acknowledged, this optimum range will vary for a given species depending its particular characteristics. However, the identification of these ideal fractions resulted in the motile SCM being sustained over a typical summer period despite permanent turbulent erosion of cells from the SCM. Therefore, the choice of these parameters to describe cell trajectories has important implications for the survival and growth of a particular species. Furthermore, the optimum f_1 and f_2 could change with changes in the environmental.

Tidal turbulence pushes cells into the base of the thermocline where motility can then play a role in transporting the cell further into the relatively quiescent, less turbulent thermocline and higher light levels (Fig. 2.1). Nutrient assimilation most likely takes place in the thermocline, thus it is the physical supply of nitrate to the thermocline that is a key measurement for understanding shelf sea summer production. BML uptake does not appear to be important in a tidally energetic shelf sea, though turbulent-driven re-access of biomass could play an important role in the maintenance of the SCM. This potentially contrasts markedly with a low-turbulence environment such as Monterey Bay where cellular transport of nutrients could well exceed the very weak diapycnal transport, and would be an interesting line of future work with the model. For a tidally energetic shelf sea, however, these results of these experiments indicate that a measure of the diapycnal nutrient flux represents a real limit on the rate of primary production within the summer SCM.

This study has used a documented Lagrangian model which explicitly describes turbulence and motility to explore whether the SCM was maintained by nitrate sourced below the thermocline by motile phytoplankton in a tidally turbulent shelf sea environment. The numerical experiments presented initially identified that phytoplankton motility and reaccess is important for sustaining the SCM over the duration of summer (~120 days) in experiment 2. The SCM was unable to sustain its biomass against permanent tidal erosion for the duration of summer, thus reaccess by motile cells helps to maintain the SCM in turbulent shelf seas. Experiment 3 went on to investigate whether eroded motile cells sourced nitrate below the thermocline and transported it to the SCM when migrating. In experiment 3 it was shown that nitrate uptake below the thermocline played no role in SCM maintenance, and thus it is the vertical flux of nitrate to the SCM that limits the production there. Additionally, the

experiments indicated that non motile cells which are eroded struggle to reaccess the SCM. These eroded cells are likely to be remineralised in the BML and thus contribute to the nitrate concentrations there, and consequently the vertical nitrate fluxes to the SCM. The findings in this chapter have suggested that nitrate sourced below the thermocline is irrelevant when considering the limit on new production at the SCM. The turbulent supply of nitrate to the SCM is therefore likely to be the primary nitrate source to the SCM, and therefore the focus of the remaining chapters in this thesis is to explore the vertical nitrate flux to the SCM via various physical mechanisms.

2.5 References

Broekhuizen, N. 1999. Simulating motile algae using a mixed Eularian-Lagrangian approach: does motility promote dinoflagellate persistence or co-existence with diatoms? J. Plank. Res. 21: 1191-1216.

Broekhuizen, N., J. Oldman, and J. Zeldis. 2003. Sub-grid-scale differences between individuals influence simulated phytoplankton production and biomass in a shelf sea system. Mar. Ecol. Progr. Ser. 252: 61-76.

Canuto, V. M., A. Howard, Y. Cheng, and M. S. Dubovikov. 2001. Ocean turbulence. Part 1. One-point closure model – momentum and heat vertical diffusivities. J. Phys. Oceanogr. 31: 1413-1426.

Cullen, J. J., and S. G. Horrigan. 1981. Effects of nitrate on the diurnal vertical migration, carbon to nitrogen ratio, and the photosynthetic capacity of the dinoflagellate *Gymnodinium-splendens.* Mar. Biol. 62 (2-3): 81-89.

Eppley, R. W., R. W. Holmes, and J. D. H. Strickland. 1967. Sinking rates of marine phytoplankton measured with a fluorometer. J. Exp. Biol. & Ecol. 1:191-208.

Eppley, R. W., O. Holm-Hansen, and J. Strickland. 1968. Some observations on the vertical migration of dinoflagellates. J. Phycology. 4: 333-340.

Eppley, R., and W. G. Harrison. Physiological ecology of *Gonyaulax polyedra*, a red water dinoflagellate in southern California. *In:* Proceedings of first international conference on toxic dinoflagellate blooms, 1974, pp 11-23. Ed. By V. R. LoCicero. Wakefield, Mass.: Massachusetts Technology Foundation. 1975.

Fraga, F., F. Perez, F. G. Figueiras, and A. F. Rios. Stoichiometric variations of N, P, C and O2 during *Gymnodinium catenatum* red tide and their interpretation. Mar. Ecol. Progr. Ser. 87: 123-134.

Geider, R. J., H. L. MacIntyre, and T. Kana. 1998. A dynamic regulatory model of phytoplanktonic acclimation to light, nutrients and temperature. Limnol. Oceanogr. 43(4): 679-674.

Heaney, S. I., and R. W. Eppley. 1981. Light, temperature and nitrogen as interacting factors affecting diel vertical migrations of dinoflagellates in culture. J. Plankt. Res. 3(2):331-344.

Hickman, A. E., P. M. Holligan, C. M. Moore, J. Sharples, V. Krivstov, and M. R. Palmer. 2009. Distribution and chromatic adaptation of phytoplankton within a shelf sea thermocline. Limnol. Oceanogr. 54: 525-536.

Hickman, A. E., C. M. Moore, J. Sharples, M. I. Lucas, G. H. Tilstone, V. Krivtsov, and P. Holligan. 2012. Primary production and nitrate uptake within the seasonal thermocline of a stratified shelf sea. Mar. Ecol. Progr. Ser. 463:39-57.

Holligan, P. M., and D. S. Harbour. 1977. The vertical distribution and succession of phytoplankton in the western English Channel in 1975 and 1976. J. Mar. Biol. Assoc. 57: 1075-1093.

Holling, C. S. 1959. Some characteristics of simple types of predation and parasitism. Can. Ent. 91: 395-398.

Hunter, J. R., P. D. Craig, and H. E. Phillips. 1993. On the use of random walk models with spatially variable diffusivity. J. Computat. Phys. 106: 366-376.

Inoue, T., and Y. Iseri. 2012. Diel vertical migration and nutrient transport of the dinoflagellate *Peridinium bipes f. occultatum* in a thermally stratified reservoir. Water. Sci. Technol. 66(6): 1212-1219.

Kamykowski, D., and A. S. McCollum. 1986. The temperature acclimatised swimming speed of selected marine dinoflagellates. J. Plankt. Res. 8(2):275-287.

Kamykowski, D., H. Yamazaki, and G. S. Janowitz. 1994. A Lagrangian model of phytoplankton photosynthetic response in the upper mixed layer. J. Plankt. Res. 16: 1059-1069.

Kamykowski, D., and H. Yamazaki. 1997. A study of metabolism-influenced orientation in the diel vertical migration of marine dinoflagellates. Limnol. Oceanogr. 42: 1189-1202.

Kiefer, D. A., and R. Lasker. 1975. Two blooms of *Gymnodinium splendens*, an unarmoured dinoflagellate. Fish. Bull. U. S. 73: 675-678.

Kitidis, V., N. J. Harman-Mountford, E. Litt, I. Brown, D. Cummings, S. Hartman, D. Hydes, J. R. Fishwick, C. Harris, V. Martinez-Vicente, E. M. S. Woodward, and T. J. Smyth . 2012. Seasonal dynamics of the carbonate system in the western English Channel. Cont. Sh. Res. 42:30-40.

Lomas, M., and P. Glibert. 2000. Comparisons of nitrate uptake, storage and reduction in marine diatoms and flagellates. J. Phycol. 36: 903-913.

Litchman, E., and C. A. Klausmeier. 2008. Trait-based community ecology of phytoplankton. Ann. Ecol. Evol. Sys. 39: 615-639.

Liu, G., G. S. Janowitz, and D. Kamykowski. 2001. A biophysical model of population dynamics of the autotrophic dinoflagellate *Gymnodinium breve.* Mar. Ecol. Progr. Ser. 210: 101-124.

MacIntyre, J., J. Cullen, and A. Cembella. 1997. Vertical migration, nutrition and toxicity of the dinoflagellate *Alexandrium tamarense.* Mar. Ecol. Progr. Ser. 148:201-216.

Rippeth, T. P., M. R. Palmer, J. H. Simpson, N. R. Fisher, and J. Sharples. 2005. Thermocline mixing in summer stratified continental shelf sea. Geophys. Res. Let. **32**:1-4., doi: 10.1029/2004GL022104.

Rippeth, T. P., P. J. Wiles, M. R. Palmer, J. Sharples and J. Tweddle. 2009. The diapcynal nutrient flux and shear-induced diapcynal mixing in the seasonally stratified western Irish Sea. Cont. Sh. Res. **29**:1580-1587.

Ross, O. N., and J. Sharples. 2004. Recipe for 1D Lagrangian particle tracking models in space-varying diffusivity. Limnol. Oceanogr: Methods. 2: 289-302.

Ross, O. N., and J. Sharples. 2007. Phytoplankton motility and the competition for nutrients in the thermocline. 347: 21-28.

Ross, O. N., and J. Sharples. 2008. Swimming for survival: A role of phytoplankton motility in a stratified turbulent environment. J. Mar. Sys. 70: 248-262.

Sharples, J., C.M. Moore, T. R. Rippeth, P. M. Holligan, D. J. Hydes, N. R. Fisher and J. Simpson. 2001a. Phytoplankton distribution and survival in the thermocline. Limnol. Oceanogr. **46**:486–496.

Sharples, J., O. N. Ross, B. E. Scott, S. P. R. Greenstreet, and H. Fraser. 2006. Inter-annual variability in the timing of stratification and the spring bloom in the north-western North Sea. Cont. Sh. Res. 26 (6): 733-751.

Sharples, J., J. F. Tweddle, J. A. M. Green, M. R. Palmer, Y. Kim, A. E. Hickman, P. M. Holligan, C. M. Moore, T. P. Rippeth, J. H. Simpson, and V. Krivstov. 2007. Spring-neap modulation of internal tide mixing and vertical nitrate fluxes at a shelf edge in summer. Limnol. Oceanogr. **52**:1735–1747, doi:10.4319/lo.2007.52.5.1735.

Smayda, T. J. 1997. Harmful algal blooms: their ecophysiology and general relevance to phytoplankton blooms in the sea. Limnol. Oceanogr. 42: 1137-1153.

Steinbuck, J., M. Stacey, M. A. McManus. O. M. Cheriton, and J. Ryan. 2009. Observations of turbulent mixing in a phytoplankton thin layer. Mar. Ecol. Progr. Ser. 378:55-69.

Stoecker, D. 1999. Mixotrophy among dinoflagellates. J. Eukaryotic Microbiol. 46: 397-401.

Tang, Y. 1995. The allometry of algal growth rates. J. Plankton. Res. 17: 1325-1335.

Visser, A. W. 1997. Using random walk models to simulate the vertical distribution of particles in a turbulent water column. Mar. Ecol. Pr. Ser. 158: 275-281.

Williams, C. A. J., J. Sharples, M. Green, C. Mahaffey, and T. P. Rippeth. (2013). The maintenance of the subsurface chlorophyll maximum in the western Irish Sea. Limnol. Oceanogr. Fluids & Environments.3: 61-73.

Woods, J., and J. Barkmann. 1994. Simulating plankton ecosystems by the Lagrangian ensemble method. Phil. Trans. Biol. Sci. 343:27-31.

Chapter 3

The maintenance of the subsurface chlorophyll maximum in the stratified western Irish Sea*

* Published in Limnology and Oceanography: Fluids and Environments.
Williams, C. A. J., J. Sharples, M. Green, C. Mahaffey, and T. P. Rippeth. 2013. The maintenance of the subsurface chlorophyll maximum in the stratified western Irish Sea.3:61-73

3.1 Introduction

Shelf seas are areas of high biological activity, covering less than 8% of the global ocean surface area but supporting 15-30% of all oceanic primary production (Wollast, 1998). In temperate shelf regions the onset of spring stratification leads to the development of the spring phytoplankton bloom, which rapidly draws down the nutrients in the new surface layer and typically results in nitrate limitation, with relatively low rates of phytoplankton growth sustained by regenerated forms of nitrogen (Pingree et al., 1976; Fasham et al., 1983). New primary production, utilising nitrate supplied from sub-thermocline waters, occurs within the subsurface chlorophyll maximum (SCM) (Hickman et al., 2012). Carbon (C) fixation within the SCM plays an important role in feeding the pelagic and benthic ecosystems during summer (Richardson et al., 2000). These regions have been implicated as substantial sinks for atmospheric carbon dioxide on account of the undersaturation of carbon dioxide at the sea surface (Thomas et al., 2004), the magnitude of undersaturation being related to production in the SCM (Kitidis et al., 2012).

The thermocline provides a physical barrier to the transfer of nutrients and phytoplankton between the surface (euphotic) layer, where light is abundant, and the dark but nutrient rich deeper water (Sharples et al., 2001a). Weak turbulence at the base of the thermocline drives a supply of nutrients from the nutrient replete bottom water into the euphotic zone. Nitrate concentrations in the surface water typically remain undetectable (<0.1 mmol m^{-3}), which indicates that (1) the phytoplankton population in the SCM are able to utilise the entire diapycnal nutrient flux, and (2) the rate of diapycnal nutrient supply into the thermocline provides a limit to the rate of new primary production in the SCM (Sharples et al., 2001a). The source of energy to drive the diapycnal nitrate flux can be local, such as episodic wind events (Sharples and Tett 1994; Rippeth 2005) or internal tides, generated locally at steep bathymetry (Garrett 2003). A significant flux of internal tidal energy can also arrive from the shelf slope (Inall et al., 2011), potentially generating large diapycnal nitrate fluxes (Sharples et al., 2007).

The stratified western Irish Sea (SWIS) provides a good location for examination of diapycnal nitrate fluxes as here water column structure and fluxes are dominated by vertical exchange (e.g., Simpson and Rippeth 1998) (Fig. 3.1). The region is stratified during summer months, and surrounded by a tidal mixing front separating it from the vertically-mixed Irish Sea (Simpson and Hunter 1974; Hill et al., 1994). The stratification occurs because of the

relatively weak tidal flows in the area being unable to dissipate the large buoyancy inputs by surface heating during spring and summer. The surrounding mixed water isolates the SWIS from the shelf edge, so that sources of energy for internal mixing must be local. In addition to energy inputs from episodic wind events (Rippeth et al., 2009), there is thought to be a quasi-continuous supply of mixing energy driven by the internal tide generated close to the Isle of Man (Fig. 3.1) and dissipating their energy over the entire SWIS gyre (Green et al., 2010). The internal tide provides energy fluxes of approximately 100 W m^{-1} (Green et al., 2010); this is quantitatively similar to the documented internal tide energy flux generated at the Celtic Sea shelf edge (approximately 100 to 150 W m^{-1}; Green et al., 2008; Inall et al., 2011). Within the SWIS horizontal gradients in water properties are weak so that the advection of nitrate is small compared to vertical turbulent fluxes.

In summer nitrate is generally depleted from surface waters by June and is the limiting nutrient in the SWIS (Slinn 1974; Gibson et al., 1997). Nitrate concentrations in the bottom mixed layer are typically less than 8 mmol m^{-3} in July, which are comparatively low in contrast to the Celtic Sea and areas closer to the shelf edge (Hydes et al., 2004). A SCM is typically observed to persist throughout the stratified period, with chlorophyll *a* (chl *a*) concentrations typically reaching 4 mg chl *a* m^{-3}, which is approximately a quarter of the chl *a* concentration observed in the same region during a spring bloom (Gowen and Bloomfield 1996; Gowen and Stewart, 2005). The region is important for the commercially-exploited *Nephrops norvegicus* (White et al., 1988), with the post-spring primary production within the SCM thought to be an important source of organic material for these benthic organisms (Trimmer et al., 1999).

The diapycnal nitrate flux has previously been estimated to be 1.5 ± 0.3 (mean $\pm$ SE) mmol m^{-2} d^{-1} in the SWIS, which is capable of supporting total new production over the summer similar in magnitude to the total production generated during the spring bloom (17 g C m^{-2}; Rippeth et al., 2009). This flux is comparable to estimates of nitrate fluxes calculated at the Celtic shelf edge during neap tides and in the western English Channel (1–2 mmol m^{-2} d^{-1}; Sharples et al., 2001b; Sharples et al., 2007). Gowen and Bloomfield (1996) estimate that total primary production in the western Irish Sea is ~140 g C m^{-2} between April to September, which is lower than summer integrated primary production observed in Irish Sea coastal waters (~194 g C m^{-2}; Gowen and Bloomfield 1996). In the SWIS the SCM is estimated to account for approximately 53% of the water column chl *a* standing stock (Gowen and Bloomfield 1996).

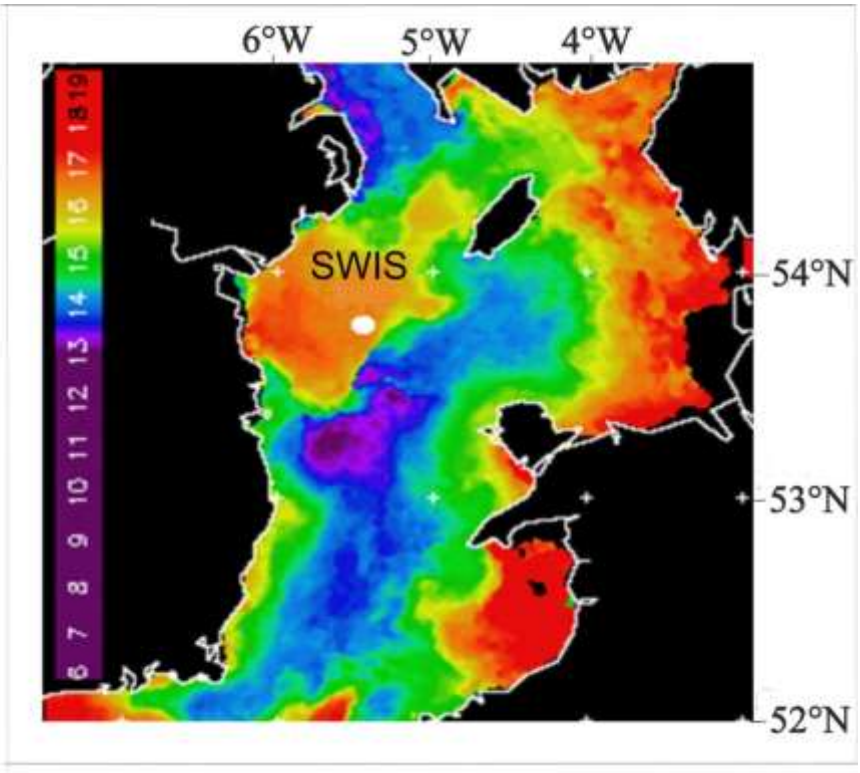

Figure 3.1: Sea surface contours of temperature (° C) in the Irish Sea taken from a composite of satellite data from 15 to 21 July 2005. The western Irish Sea gyre is clearly visible via the sea surface temperature and the stratified western Irish Sea (SWIS) station is marked by a white dot at the edge of the SWIS gyre. Image courtesy of Plymouth Marine Laboratory.

The purpose of the following study is to provide a robust lower limit of nutrient fluxes into the SCM in an isolated, relatively high energy shelf sea environment in comparison to nearby temperate shelf seas. We hypothesise that the documented energy flux for the internal tide in this region has a small contribution to the diapycnal nitrate flux, and thus on its own the internal tide is insufficient to sustain the documented summer primary production rates for the region. We, therefore, examine the lower limit to diapycnal nitrate fluxes in a region isolated from any significant influence of external sources of mixing energy and during a period of very low winds. This allows us to assess the potential new primary production supported by that flux compared with other measurements made in the SCM and with the production associated with the spring bloom.

3.2 Methods

Measurements were collected at the SWIS station located at 53° 43.00’ N, 5° 30.00’ W, during a research cruise in July 2006 on the RV *Prince Madog* (Fig. 3.1; See Simpson et al., 2009 and Green et al., 2010 for cruise details). The water depth is approximately 110 m, and the SWIS station is situated well within the stratified part of the Irish Sea, separated from the

well-mixed region by a tidal mixing front. The field campaign lasted 10 days; here we focus on 50 h of continuous measurements taken 2 days immediately before neap tides (July 16 – 18th). Measurements included profiles of turbulent energy dissipation rate (ε), temperature, chl *a* and nitrate.

3.2.1 *Chlorophyll a and inorganic nutrients*

Seawater samples were collected from 6 to 8 depths for determination of nitrate and chl *a* concentrations during 8 conductivity temperature depth (CTD) profiles over 50 h. Chl *a* was extracted from 1L of seawater filtered onto a Whatman glass fibre filter (GF/F) using acetone. Fluorescence was determined against a chl *a* standard using a Turner TD-700 fluorometer (Evans et al., 1987). To provide high resolution vertical profiles of chl *a*, the extracted chl *a* concentrations were used to calibrate a fluorescence sensor mounted on the CTD rosette frame. A regression of the extracted chl *a* concentrations against the fluorometer output (V) provided a calibration equation of chl $a_{calibrated}$ = 44.76V + 0.0529 mg m^{-3} (r^2 = 0.66, n = 28, $p < 0.001$). The root-mean-square scatter of the chl *a* samples from this regression was 0.34. Sharples et al., (2001a) suggested that much of this scatter was the result of attempting to sample thin layers (i.e., 1-3 m thick) of concentrated chl *a* with a standard CTD and bottle rosette system, where the Niskin bottles are approximately 1 m long and ~1 m above the fluorometer.

Concentrations of nitrate plus nitrite (herein nitrate, mmol m^{-3}) were determined using a LACHAT Instruments Quick-Chem 8000 auto analyser and standard colorimetric techniques (Hales et al., 2004; Papadimitriou et al., 2007) and analysed fresh onboard. The analytical limits of detection for nitrate were 0.1 mmol m^{-3}.

3.2.2 *Turbulence and water column physical structure*

A mooring at the SWIS station provided 8 days of continuous temperature and current measurements via the deployment of a thermistor chain with 22 VEMCO (Minilogger, VEMCO-AMIRIX, Canada) and SeaStar thermistors (Milli-T, Star-Oddi, Iceland), 6 of the thermistors were equipped with pressure sensors (Green et al., 2010). Sampling resolution was every 120 s with a vertical resolution between 2 to 10 m along the mooring line. A bed-frame mounted 300 kHz ADCP (Workhorse sentinel ADCP, Teledyne RDI, France) was deployed within 200 m of the thermistor mooring. The ADCP recorded current velocity every 2 s with a 2 m vertical bin size from 4.7 m above the bed to within 15 m of the surface. All

the data from both moorings were later interpolated to a common grid with 2 m vertical resolution and 2 min resolution in time (Green et al., 2010). The currents measured from the ADCP were used to calculate the barotropic (depth mean) current and the bulk shear (equation 3.1):

$$S^2 = \left(\frac{du}{dz}\right)^2 + \left(\frac{dv}{dz}\right)^2 \qquad [s^{-1}] \qquad [3.1]$$

where *du* and *dv* describe the difference in velocity between two layers for the *u* and *v* components of velocity respectively, *dz* is the vertical distance (m) between the two layers.

Vertical profiles of microstructure velocity shear and temperature were measured using a Fast Light Yo-yo (FLY) profiler (Dewey et al., 1987) for 50 h between 16th and 18th July 2006 (decimal day 196 -198), immediately before neap tides (for full details of the FLY instrumentation used see Simpson et al., 2009 and Green et al., 2010). The FLY profiler was allowed to fall freely through the water column to the seabed, providing measurements of turbulent dissipation to within 0.15 m of the seabed at a vertical resolution of 1.5 m. The data from the upper 5 m of each FLY profile may have been degraded by the presence of the ship's wake and the acceleration of the profiler, and were therefore removed during analysis. In the environment described here, 5 to 6 profiles could be obtained every 1 h. The microstructure shear and temperature vertical profiles were collected over the 50 h sampling campaign from the FLY shear profiler at ~1 cm vertical resolution. One ensemble of FLY dissipation data was made up of 5 to 6 consecutive vertical profiles. The profiles were averaged and calculated over 1.5 m depth bins. The microstructure shear was used to calculate the dissipation of turbulent kinetic energy, ε ($m^2 s^{-3}$) from:

$$\varepsilon = 7.5\upsilon\overline{\left(\frac{du}{dz}\right)^2} \qquad [m^2 s^{-3}] \qquad [3.2]$$

where υ is the kinematic viscosity of seawater, *du/dz* is the (small scale) vertical shear and the overbar denotes an average over 2 seconds of data. Hourly CTD casts provided independent temperature and conductivity measurements for calibration of FLY temperature and conductivity sensors.

Profiles of vertical eddy diffusivity, K_z, ($m^2 s^{-1}$), can be calculated from the profiles of the rate of dissipation of turbulent kinetic energy (ε [$m^2 s^{-3}$]) and the buoyancy frequency (N^2, [s^{-2}]) (e.g. Osborn 1980).

$$K_z = \Gamma \frac{\varepsilon}{N^2} \qquad [m^2 s^{-1}] \qquad [3.3]$$

where gamma (Γ) = 0.2 and represents the mixing efficiency (Osborn 1980). The mixing efficiency is defined as the ratio of potential energy gain to dissipation and is dependent on the shear, stratification and turbulence. Our assumption of a constant mixing efficiency assumes that the stratification, shear and turbulence are relatively stable which is unlikely to be the case. Density (ρ [$kg\ m^{-3}$]) and the rate of turbulent kinetic energy dissipation are both properties measured directly from the FLY profiler, and g is the acceleration due to gravity. The buoyancy frequency (N^2) within each 1 m bin is obtained via the vertical profile of density from the FLY profiler:

$$N^2 = \frac{-g}{\rho}\frac{\partial \rho}{\partial z} \qquad [s^{-2}] \qquad [3.4]$$

The vertical eddy diffusivity (Eq. 3.4) can be used to calculate the vertical flux (J) of a property, provided a reliable vertical gradient of that property is available. Thus for nitrate or chl *a* the vertical turbulent flux is:

$$J = -K_z \frac{\partial(nitrate\_or\_chla)}{\partial z} \qquad [\text{mmol or mg } m^{-2} s^{-1}] \qquad [3.5]$$

where *d(chl a)/dz* and *d(nitrate)/dz* are the vertical chl *a* and nitrate gradients (units of mg m^{-4} and mmol m^{-4} respectively).

In the western Irish Sea vertical variations in salinity are small and produce a density difference over the water column of less than 0.25 kg m^{-3}, while vertical temperature changes produce a density difference of more than 1 kg m^{-3} indicating that vertical stratification is controlled by temperature (Green et al., 2010). The correlation between nitrate and chl *a* with density or temperature within the thermocline was stronger than with depth, as the depth of the nitracline and SCM changes according to the vertical movement of isopycnals (Sharples et al., 2007). This has important implications for flux calculations, as such movements of the SCM and isopycnals means that selecting a single representative depth at which fluxes are calculated can lead to contamination of the turbulent diffusivity by high turbulence

immediately below the thermocline in the bottom tidally-mixed layer. Instead, fluxes need to be calculated across an isopycnal within the lower portion of the SCM (Gregg 1987). It is important to note that the nitrate-temperature relationship will be robust on relatively short timescales in comparison to the nutrient uptake rate of phytoplankton (Lucas et al., 2011). Here we are interested in calculating fluxes at the isopycnals marking the very base of the SCM and hence gaining an accurate value for the amount of nitrate being supplied to the SCM community and the amount of chl *a* being eroded into the bottom mixed layer. We used the chl *a* - density relationship for all CTD profiles to find the isopycnal marking the base of the SCM (Fig. 3.2).

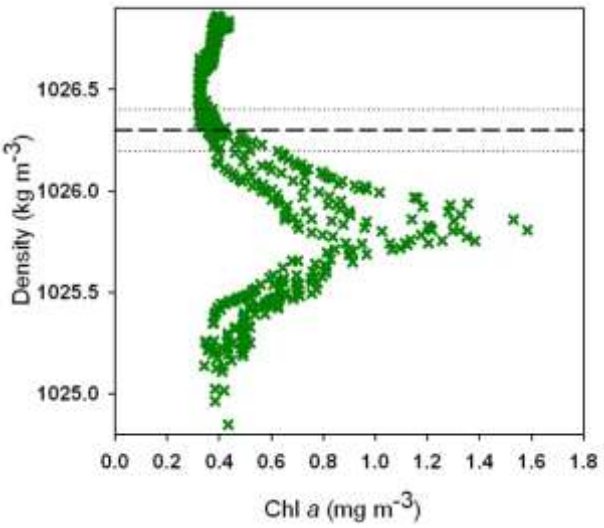

Figure 3.2: Density versus chl *a* measurements during the FLY sampling period. The dashed line marks the 1026.3 isopycnal (± 0.1 kg m^{-3} as marked by the dotted lines) which describes the density band marking the base of the SCM where fluxes were determined. Chl *a* concentrations were based on calibrated fluorescence values for each CTD cast during the FLY sampling campaign.

The vertical position of the SCM corresponds to the isopycnals between the 1025.4 kg m^{-3} and 1026.2 kg m^{-3}. This is equivalent to a width of more than 25 m. We associate the base of the SCM with the 1026.3 isopycnal (± 0.1 kg m^{-3}) (Fig. 3.2). As the FLY measures both density and TKE dissipation we were able to obtain TKE dissipation rates on isopycnals. Furthermore, the density-nitrate and chl *a* – density relationships were calculated centred on the 1026.3 (± 0.1 kg m^{-3}) isopycnal (Fig. 3.2). K_z measurements were also calculated from TKE dissipation across the same isopycnal band, where K_z was taken as an average over the

envelope of isopycnals used (1026.2 - 1026.4 kg m^{-3}). To calculate fluxes, a nitrate - density and chl *a* - density relationship was determined by collating all nitrate and chl *a* data in the base of the SCM (Fig. 3.3).

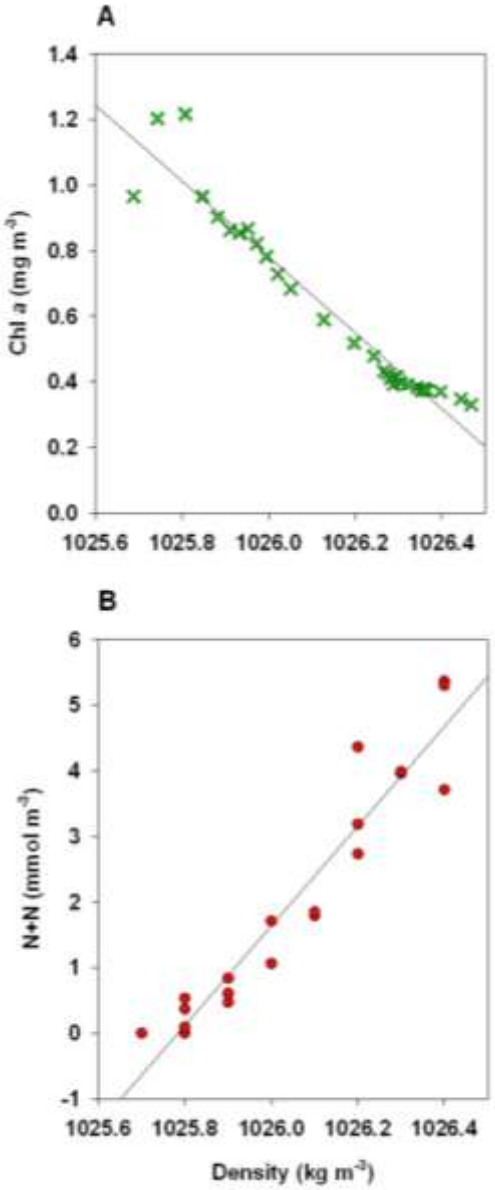

Figure 3.3: Relationship between (A) Chl *a* and (B) Nitrate and density for all measurements taken across the base of the subsurface chlorophyll maximum during the 50 hour FLY sampling campaign. The lines of best fit for each relationship provide regression lines where Chl *a* = (-1.16density) + 1186.6 mg m^{-3} (r^2 = 0.94) and nitrate = (7.60density) – 7791.80 mmol m^{-3} (r^2 = 0.92).

All chl *a*- and nitrate– density relationships were statistically significant. The r^2 values show strong correlation between density and nitrate ($r^2 = 0.92$) or chl *a* ($r^2 = 0.94$). The chl *a* gradient at the base of the SCM is negative, indicating that any chl *a* fluxes will be out of the SCM into the bottom boundary layer, i.e., loss of phytoplankton cells from the SCM.

Using the nitrate-density and chl a-density relationships (Fig. 3.3) has the advantage that the scalar gradients are calculated using FLY density measurements, thus co-locating in time and space the scalar gradients and the turbulent diffusivity. The nitrate (or chl *a*) flux calculation in Eq. 3.4 then simplifies to (Sharples et al., 2007):

$$J = m\frac{\Gamma\varepsilon\rho}{g} \qquad [\text{mmol m}^{-2}\text{ s}^{-1}] \qquad [3.6]$$

Here *m* is the slope of the density-nitrate (or chl *a* - density) linear regression as shown in Fig. 3.3. The mixing efficiency (Γ) is again taken as a constant of 0.2 (Osborn 1980).

Due to high temporal and spatial variability of turbulence during sampling, a Gaussian 'bootstrap' resampling method (Efron and Gong 1983) was used to calculate an average flux value with 95% confidence intervals from instantaneous fluxes into the base of the SCM over the 50 h sampling period.

3.3 Results

The thermocline thickness exceeded 20 m in all profiles (Fig. 3.4), with a density change of ~1 kg m^{-3}. This broad thermocline separated a ~20 m thick surface layer with weaker density structure from an approximately 60 m thick bottom mixed layer. The SCM was equally broad (10-20 m), though the vertical position of the chl *a* peak varied between 20 and 30 m depth between CTD casts. The subsurface chl *a* concentration at the peak ranged from 0.7 to 1.5 mg m^{-3}. Chl *a* concentrations were less than 0.5 mg m^{-3} in the upper 10 m of the water column during the duration of the FLY campaign. Nitrate concentrations were below the limits of detection in surface waters (0.1 mmol m^{-3}).

Turbulent energy dissipation (ε) varied by as much as 4 orders of magnitude through the water column (Fig. 3.5a). Enhanced turbulence was observed at the bed boundaries as previously noted in the region (Simpson et al., 2009, Green et al., 2010), and typical for tidally dominated shelf seas. Maximum dissipation observed at the bed extended upward with an increasing phase lag; this results from the maximum shear occurring later and with

decreasing intensity with increasing distance from the bed (Simpson et al., 2000). The mid-water dissipation rates ranged from 1×10^{-9} to 1×10^{-7} $m^2 s^{-3}$ and was dominated by short-lived turbulence events at the base of the thermocline (e.g., decimal day 196.5 in Fig. 3.5a). The lowest values of ε observed were within the thermocline and upper bottom mixed layer, between 20 and 60 m below the surface.

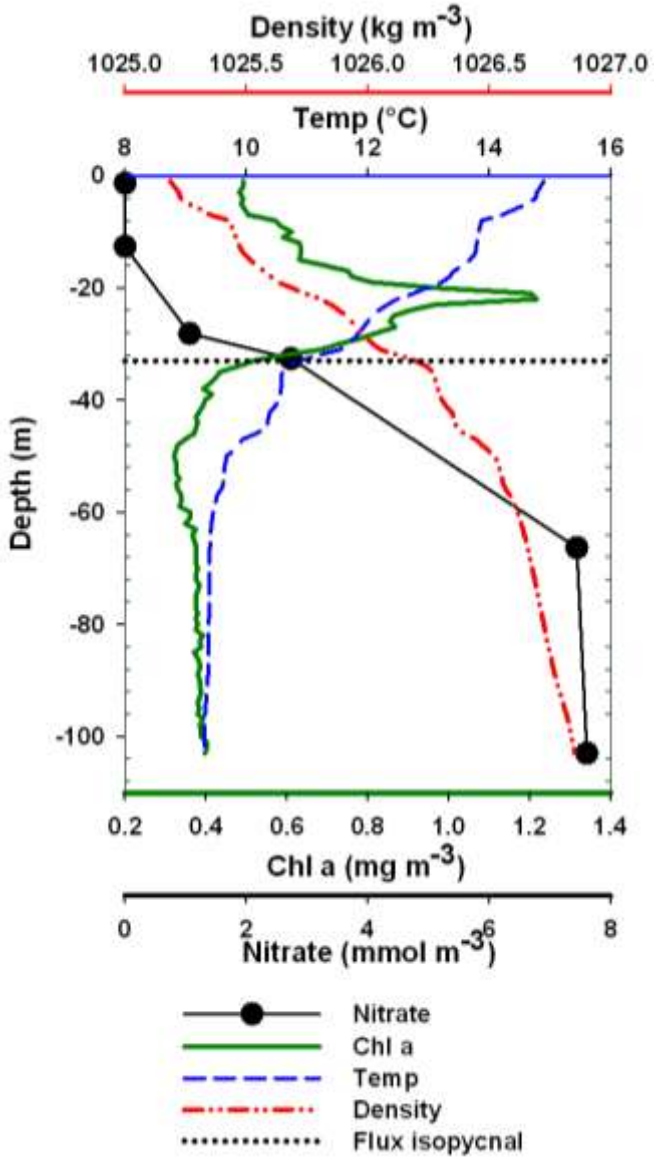

Figure 3.4: Typical profiles of Chlorophyll *a* and nitrate, temperature and density during the FLY sampling period for CTD 21 (day 196, 15 July 2006 23:16 local time). The 1026.3 isopycnal used to mark the base of the SCM where fluxes were determined is indicated by a dashed horizontal line.

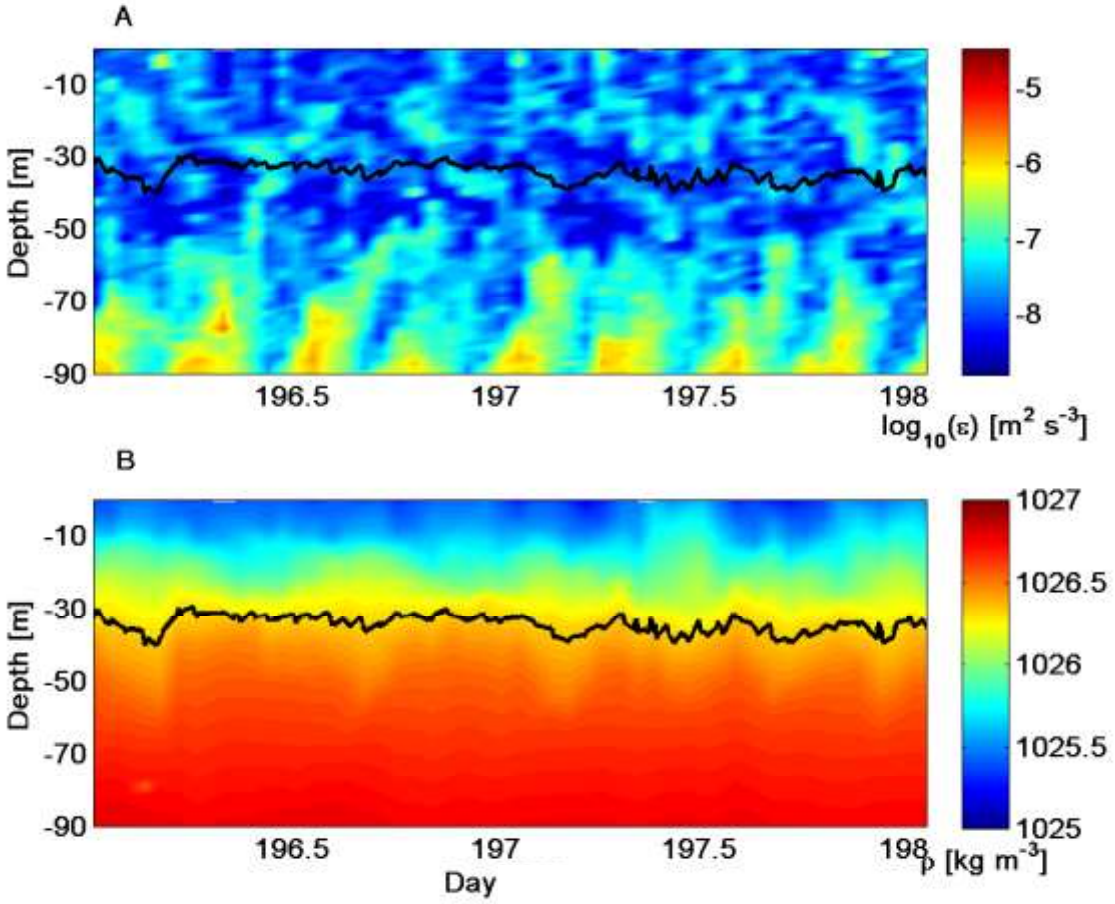

Figure 3.5: A 50 hour time series of (A) turbulent kinetic energy dissipation ($\log_{10}$ ε) and (B) density (ρ) measured from the FLY profiler at SWIS station in July 2006.The black line marks the 1026.3kg m^{-3} isopycnal used to determine diapycnal fluxes of nitrate and chlorophyll *a* and marks the base of the SCM.

In order to investigate the mechanisms contributing to the observed dissipation it is necessary to consider potential shear instabilities and the probability of mixing at the thermocline. The time-averaged vertical shear squared (S^2) was calculated for each depth bin (Eq. 3.1) using a bootstrap resampling method (Fig. 3.6a) over the 8 day period of ADCP measurements. S^2 was highest within thermocline, at a slightly shallower depth than our chosen isopycnals, which have an average S^2 value of 1.5 ± 0.06 x 10^{-4} s^{-2}. The 95% confidence intervals for S^2 (Fig. 3.6a) indicate that during our measurements there was relatively small variability of shear in the water column. There was a 180° phase shift between currents in the surface and bottom mixed layer consistent with the presence of baroclinic energy driven by a mode 1 internal tide (Green et al., 2010). Additionally the squared buoyancy frequency (N^2) was shown to have small variability throughout the water

column for the duration of our measurements and is not significantly different from S^2 within our selected isopycnals ($1.48 \pm 0.04 \times 10^{-4}$ s^{-2}). Shear instabilities occur when the gradient Richardson number (*Ri*) is 0.25, though the water column is said to be unstable when the *Ri* is less than 1 (Rippeth 2005; Thorpe and Liu 2009). Similar values for N^2 and S^2 would give a *Ri* of ~1 in the chosen isopycnal band implying that the flow is marginally stable. For the duration of our campaign *Ri* ranged between 0.45 and 2 within the selected isopycnals band but had a mean value of 1.1 (±0.03). The Ozmidov scale describes the overturning length scale of eddies. It is important to note that the ADCP bin size (2 m) is significantly larger than the Ozmidov scale of shear in the midwater column. Therefore the shear and thus *Ri* estimates provided here may have eliminated the detail in the small scale shear (<2 m) at the base of the thermocline.

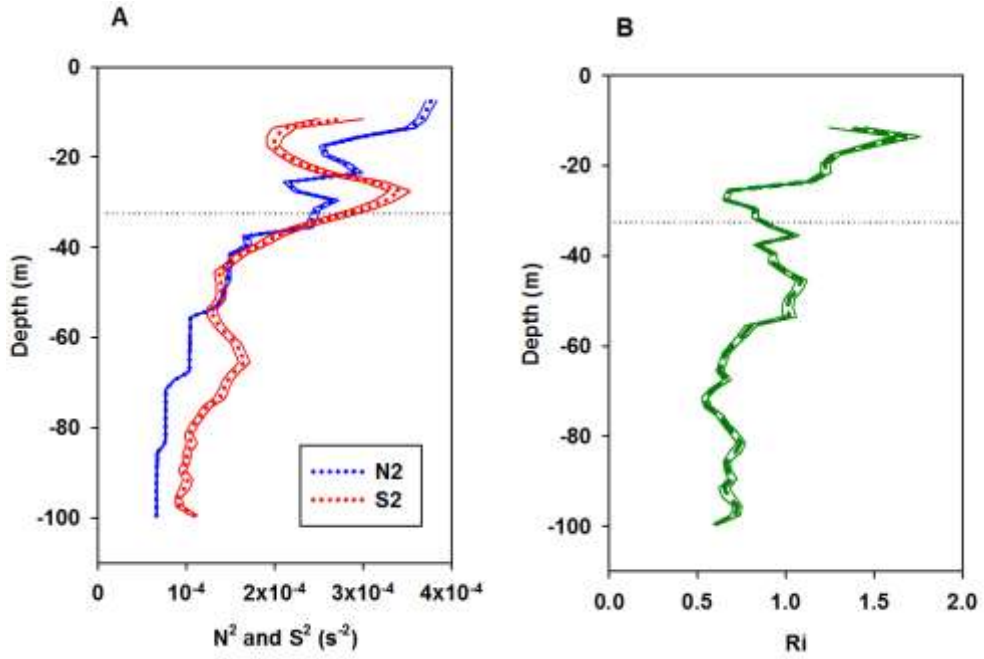

Figure 3.6: (A) The time-averaged vertical profiles of the shear squared, S^2 ($s^{-2:}$ red dashed line), and the buoyancy frequency N^2 (s^{-2}: blue dashed line) averaged using a bootstrap method over a 9 day period between day 192 and 201 at the SWIS mooring station. The solid lines bordering the average indicate the 95% confidence intervals for estimates. (B) The time-averaged gradient Richardson number (dashed green line) over day 192 to 201, calculated from the buoyancy frequency and shear squared terms, and averaged using a bootstrap resampling method. The solid lines bordering the average mark the 95% confidence limits. The dashed black horizontal line marks the approximate isopycnal depth where fluxes have been calculated.

Turbulent dissipation was patchy within the base of the SCM. The instantaneous nitrate fluxes experienced at the base of the SCM from single profiles ranged

from approximately 9×10^{-7} to 2×10^{-5} mmol m^{-2} s^{-1}. Chl *a* was eroded from the SCM via diapycnal mixing at a rate ranging between 1×10^{-8} to 3×10^{-6} mg chl *a* m^{-2} s^{-1}.

Chl *a* fluxes showed the same spikes as those shown by the nitrate fluxes (Fig. 3.7), largely because variability in scalar fluxes is dominated by the variability of the turbulence rather than changes to the scalar gradients. Table 3.1 summarises the daily chl *a* and nitrate fluxes at the base of SCM. These fluxes are converted into C units (mg C) in order to compare C transfer associated with phytoplankton cells being mixed out of the SCM (i.e., downward chl *a* fluxes) and new nitrate-driven production (i.e., fuelled by upward nitrate fluxes). In order to convert chl *a* flux into a C flux we assume a constant C:chl *a* of 40:1 for SCM phytoplankton (Holligan et al., 1984). The concentration of chlorophyll in phytoplankton cells may change according to where they are vertically in the water column and thus the light they experience. The carbon to chlorophyll ratio in phytoplankton changes with depth, however as we are focusing on the C:chl *a* ratio only at the SCM we may adopt a constant value that has been well used in the literature (e.g., Sharples et al. 2007). The Redfield ratio (Redfield 1958) was used to estimate nitrate-supported C fixation rates (units of mmol m^{-2} d^{-1}, or mg m^{-2} d^{-1} when multiplied by the molecular weight of C, 12). Whereas the C to nitrogen (N) ratio in phytoplankton can vary (Tett et al., 1985), we assume that the average C:N ratio is 6.6:1 for phytoplankton growth in response to a supply of nitrate (Geider and La Roche 2002).

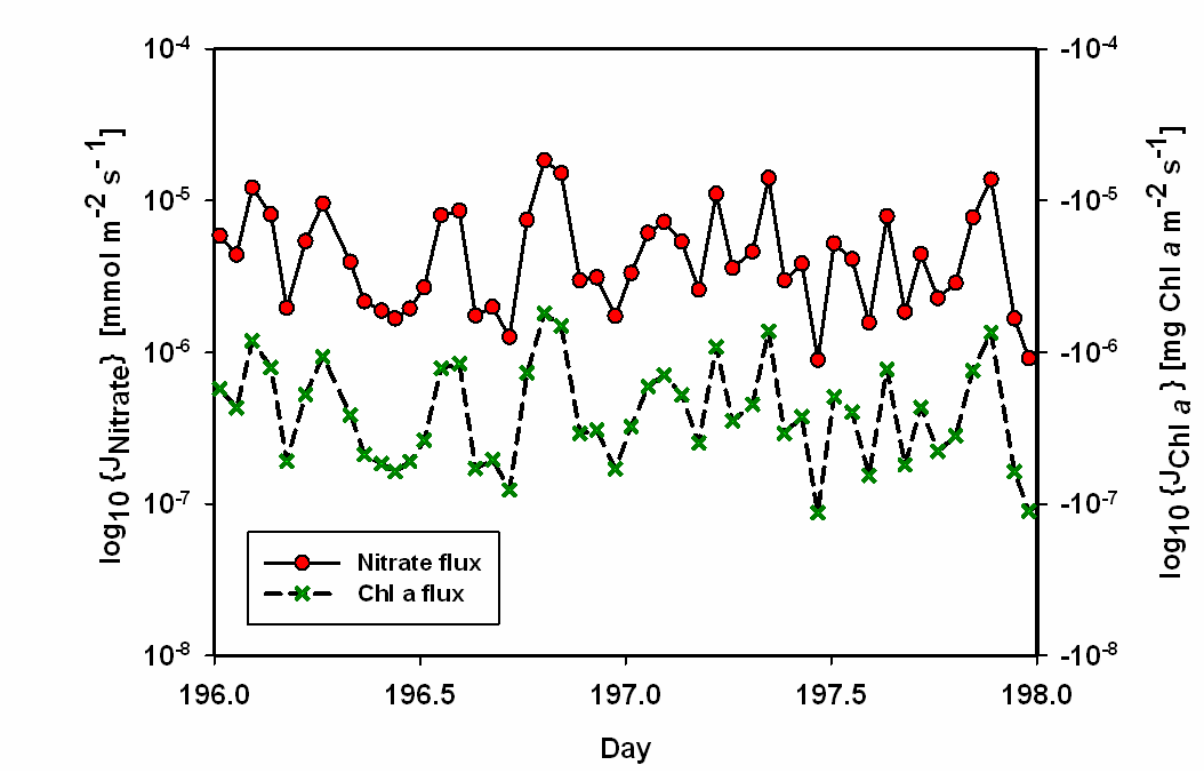

Figure 3.7: Variation in nitrate fluxes and chl *a* instantaneous fluxes through the base of SCM from the 50 hour sampling period. The values shown are the average fluxes (every 6 FLY profiles, i.e. hourly averages). The $\log_{10}$ nitrate fluxes shown are the nitrate flux into the base of the SCM, the chl *a* flux shown is the chl *a* flux out of the base of the SCM and hence is negative.

The net rates of C fixation reported in Table 3.1 represent the potential net organic C accumulation in the SCM as a result of the turbulent erosion of live cells and growth fuelled by diapycnal nitrate fluxes. The 95% confidence intervals (calculated using the bootstrap method) for nitrate and chl *a* fluxes had a small range (0.22 – 0.43 mmol m^{-2} d^{-1} and 0.036 – 0.072 mg chl *a* m^{-2} d^{-1}, respectively), indicating that we have calculated a backround estimate with low variability for diapycnal fluxes across the SCM and with little evidence of sporadic spikes for the period when we sampled compared to other studies (e.g., Sharples et al., 2007). The loss of C via erosion of live cells from the SCM was approximately 1.92 mg C m^{-2} d^{-1} (95% C.I =1.44 – 2.88 mg C m^{-2} d^{-1}); the potential C fixation that could be supported by the nitrate flux into the SCM was approximately 12 times more than this export via turbulent erosion (24.7 ± 1.3 mg C m^{-2} d^{-1}). It is important to note that the C loss estimate via turbulent erosion only accounts for the removal of intact cells containing chl *a* from the SCM and not the removal of dead cells.

Table 3.1: Daily nitrate and chl *a* daily fluxes and the corresponding estimates of nitrate-driven production, C export and net C gained per day. The values for the fluxes are calculated using the bootstrap sampling method, and the values given in brackets represent the 95% confidence interval. The net rates of C fixation reported represent the potential net organic C that could result from diapycnal fluxes.

Nitrate flux (mmol m^{-2} d^{-1})	**Nitrate driven production (mg C m^{-2} d^{-1})**	**Chl *a* flux (mg Chl *a* m^{-2} d^{-1})**	**C export (mg C m^{-2} d^{-1})**	**Potential net C accumulation (mg C m^{-2} d^{-1})**
0.31 (0.22 – 0.43)	24.7 (17.0 – 34.3)	-0.048 (-0.036– -0.072)	-1.92 (-1.44 – -2.88)	**22.8 (15.6 – 31.4)**

Table 3.2: Comparisons of documented turbulent kinetic energy dissipation (epsilon), daily nitrate fluxes and potential new nitrate driven production from various shelf seas in the North Atlantic Ocean.

Location	Epsilon observed in thermocline (m^2 s^{-3})	d(nitrate)/dρ (mmol m^{-4})	Daily $J_{Nitrate}$ into base (mmol m^2 d^{-1})	Nitrate driven production (mg C m^{-2} day^{-1})
SWIS present study	10^{-9} - 10^{-7}	7.6	0.2 – 0.4	15.8 – 34.1
SWIS (Rippeth et al. 2009)	10^{-8} - 10^{-7}	-	1.2 – 1.8	95 – 142.6
Celtic shelf edge (Sharples et al. 2007)	10^{-5} - 10^{-4}	10.4 - 11.2	1.3 – 9	103 – 712.8
Western English Channel (Sharples et al. 2001a)	10^{-8} - 10^{-5}	5.7	0.8 – 3.2	63- 253

3.4 Discussion

Observations of turbulence, nitrate and chl *a* in the seasonally stratified western Irish Sea during a period approaching neap tides indicate that background nitrate fluxes are the lowest observed in shelf seas to date (Table 3.2). We have shown that the mid-water turbulence in the SWIS supplies 0.22 - 0.43 mmol N m^{-2} d^{-1} to the SCM, and erodes phytoplankton from the base of SCM at a daily rate of 0.04 – 0.07 mg chl *a* m^{-2} d^{-1}. By

assuming the Redfield ratio and a fixed C to chl *a* ratio we have translated the nitrate flux and chl *a* erosion rate into units of C (Table 3.1). During the field campaign, nitrate was consistently below the limits of detection in the surface waters. This suggests that nitrate supplied to the euphotic zone via mid-water mixing is removed from the water column at the SCM, preventing transport into the surface layer. The concentrations of chl *a* observed at the SCM varied between 0.7 and1.5 mg chl *a* m^{-3}, and were consistently less than 0.5 mg chl *a* m^{-3} in the surface waters corresponding with the very low concentrations of nitrate observed here. The lowest levels of turbulence in the SWIS were observed within the thermocline and upper bottom mixed layer with rates of turbulent dissipation varying between 1×10^{-9} and 1×10^{-7} m^2 s^{-3}.

The SWIS has an internal tide energy flux of 100 W m^{-1} (Green et al., 2010), which is quantitatively similar to the internal tide energy flux documented at the Celtic Sea shelf edge (~139 W m^{-1}; Green et al., 2008). The nitrate flux we have observed in the SWIS however is much lower than that observed at the Celtic shelf edge during neaps (Table 3.2, 3.3 mmol m^{-2} d^{-1}; Sharples et al., 2007). This suggests that although the internal tide here is almost as energetic as that observed at the shelf edge, it propagates through the region conservatively, with low levels of dissipation and, therefore, mixing within the thermocline. A comprehensive study of the physical processes during this field campaign has been provided by Green et al., (2010), who highlight that there is no clear separation of the contribution to the mixing from each of these processes. The time-averaged Richardson number calculated at the base of the SCM was 1.1 ± 0.03, and was observed to occasionally approach the critical value of <1 for the duration of our sampling. This indicates that the base of the SCM was in a state of marginal stability (Fig. 3.6), similar results have also been have been reported for other seasonally stratified temperate shelf seas (van Haren et al., 1999; MacKinnon and Gregg 2003; Rippeth et al., 2005). In the SWIS it appears that the internal tide sets up a background state that on its own is insufficient to produce shear instabilities and significant mixing, but may be modified via the addition of shear from non-linear internal waves (NLIW) and wind-driven inertial oscillations. The addition of shear from these processes would most likely be enough to result in a *Ri* of ~ 0.25 and thus cause shear instabilities and intermittent mixing. We argue that internal tide energy fluxes are, therefore, not sufficient for estimating vertical mixing and the diapycnal fluxes of nutrients.

The estimate for the daily nitrate flux to the base of the SCM (0.31 ± 0.01 mmol m^{-2} d^{-1}) is approximately a fifth of the estimate given by Rippeth et al., (2009) in the same region

(1.5 ± 0.05 mmol m^{-2} d^{-1}; Table 3.2). The low range in the variability of the nitrate flux signal (see 95% C.I in Table 3.1) indicates that the SWIS data were background, not event driven fluxes. Rippeth et al., (2009) calculated the nitrate flux across the thermocline using a fixed depth and a fixed isotherm method, this latter method is similar to the method we have used to estimate the nitrate flux here. Both methods resulted in very similar flux estimates, which may suggest little vertical movement of isopycnals during their observations. By replicating the fixed depth method in our observations we estimate a mean nitrate flux of 1.3 ± 0.4 mmol m^{-2} d^{-1}. This is significantly higher than the nitrate flux we report across a fixed isopycnal. The higher flux results from episodic contamination of thermocline turbulence with high turbulence within the upper part of the tidally-mixed bottom layer (these high turbulence events are not relevant to the mixing of scalars through the base of the thermocline). The large discrepancy in flux estimates using the fixed depth and fixed isopycnal methods suggests that the vertical movement of isopycnals by the internal tide was significant during our observations. Additionally, the vertical eddy diffusivity (K_z) within the thermocline during our observations ($0.77 \pm 0.25 \times 10^{-5}$ m^2 s^{-1}) was significantly smaller than that reported by Rippeth et al., (2009) (1.7 ± 0.41 m^2 s^{-1}) for the period of flux calculations when intermittent shear spikes were observed. This highlights the variability of the SWIS in terms of intermittent mixing events.

The diapycnal nitrate flux has the potential to support 25 mg C m^{-2} d^{-1} of new production, which over a summer period of 120 days would result in 3 g C m^{-2} of new production in the SWIS. This potential daily production rate is relatively low compared to the Celtic Sea SCM where primary production estimates during summer range from 170 to 390 mg C m^{-2} d^{-1} (Hickman et al., 2012). Primary production estimates for the SWIS are sparse, the most comprehensive estimate taken from Gowen and Bloomfield (1996) suggests a primary production value between April and September of 140 g C m^{-2}, which is only slightly higher than the Celtic Sea (Hickman et al., 2012). By using the Redfield ratio (C:N =6.6), we can estimate the amount of nitrate required to drive the production estimated by Gowen and Bloomfield. We can assume (following Trimmer et al., 1999) that ~70% of this production is derived from the spring bloom (60 days), therefore primary production during summer (120 days) is responsible for the remaining 30% (42 mg C m^{-2}). The amount of nitrate required to fuel 42 mg C m^{-2} of new production is 530 mmol m^{-2}; our daily nitrate flux estimate extrapolated over the summer period of 120 days would provide 37.2 mmol m^{-2}. This would be 7% of the nitrate for summer production provided by the diapycnal nitrate flux. This could

also be interpreted as a *f* ratio (the ratio of total primary production fuelled by nitrate) of 0.07, which seems unlikely. Alternatively, a study by Trimmer et al., (1999) used chl *a* standing stock measurements to estimate total (new from nitrate and regenerated from recycled nitrogen) between February and July, giving a total annual production value of 44.8 g C m^{-2} y^{-1}. Again 30% (13.44 g C m^{-2}) of this total annual production occurs during summer. Approximately 170 mmol m^{-2} of nitrate is needed to drive summer production estimated by Trimmer et al., (1999). Extrapolating the nitrate flux, we find that the diapycnal nitrate flux in the SWIS provides 16 to 30% of the nitrate required for total primary production during summer. Primary production estimates provided by these studies suggest that our primary production rate is very low if extrapolated over the summer period. The implication is that the diapycnal flux driven new production does not integrate to the mean production over the summer. Instead, the wind and/or NLIW may be crucial in supporting phytoplankton populations during summer by increasing the average flux of nitrate substantially.

At the base of the SCM, the loss of C via erosion of the SCM is negligible compared to the possible nitrate driven production. The turbulent erosion of phytoplankton cells from the SCM via background mixing potentially exports almost 2 mg C m^{-2} d^{-1}. This corresponds to ~0.2 g C m^{-2} exported from the SCM during summer in the SWIS. C loss via erosion is ~7% of the potential nitrate driven production if we assume that all nitrate is assimilated by the phytoplankton population and converted into biomass at the Redfield ratio. It is important to note, however, that the C export value only accounts for the loss of live cells transported out of the SCM during mixing and does not consider loss by grazing, viral cell lysis or direct sinking of particles. Therefore, the remaining 93% of potential nitrate driven new production in the SCM must be removed via the various removal processes of dead cells that occur during periods of low wind and approaching neap tides. Event driven mixing, such as non-linear internal waves and/or wind, would result in enhanced chl *a* erosion from the SCM as well as increased nitrate fluxes. In order to accurately quantify C budgets in shelf seas the export of C to the deep water via turbulent erosion of live cells (at least 7%) should be taken into account as well as the other removal processes.

Significance to aquatic environments

Identifying and quantifying the supply pathways of nutrients to phytoplankton in stratified seas is vital to understand primary production and hence carbon (C) use in the ocean. Such pathways would include C export from the euphotic zone as well as the delivery

of nutrients. This study identified the physical processes that drive new production in an isolated, stratified oceanic area via physical and biogeochemical measurements and estimated the export of C via turbulence.

We found that although the stratified western Irish Sea (SWIS) has a significant internal tide (an internal wave caused by tides on the water surface), it propagates through the region causing only minor dissipation (energy loss to water motion) at the thermocline and hence contributes to relatively small nitrate fluxes into the surface waters. This quiescent, 'background' mixing driven by the internal tide is not sufficient to sustain the C fixation observed in the region and thus event-driven mixing, via the wind and/or non-linear internal waves, must be responsible for the maintenance of summer production in this ecologically important environment. The low level mixing indicates the thermocline is in a state of marginal stability meaning that shear from the wind or non-linear internal waves would likely 'tip the balance' and generate diapycnal mixing (i.e., mixing of nutrients through the thermocline).

In the past decade there has been an increased interest in climate change including increased winds in the North Atlantic. If maintenance of primary production in the subsurface chlorophyll maximum in temperate regions such as SWIS depends on event-driven large pulses of nutrients, then increased wind may enhance primary production during summer. This is contrary to the belief that increased winds are more likely to dampen production by deepening the euphotic zone and causing phytoplankton to experience a reduction in light (e.g., Ueyama & Monger, 2005).

3.5 References

Armstrong, R. A. 2006. Optimality based modeling of nitrogen allocation and photoacclimation in photosynthesis. Deep Sea Res. **53**: 513–531.

Carr, M. E., M. R. Lewis, and D. Kelley. 1995. A physical estimate of new production in the equatorial Pacific along 150°W. Limnol. Oceanogr. **40**: 138-147.

Dewey, R. K., W. R. Crawford, A. E. Gargett, and N. S. Oakey. 1987. A microstructure instrument for profiling oceanic turbulence in coastal bottom boundary layers. J. Atmos. Ocean. Technol. **4**: 288–297.

Efron, B., and G. Gong. 1983. A leisurely look at the bootstrap, the jackknife, and cross-validation. The Amer. Statist. **37**: 36–48.

Evans, C. A., J. E. O'Reilly, and J. P. Thomas. 1987. A handbook for the measurement of chlorophyll a and primary production. Vol 8: p 114, In: Biological investigations of marine Antarctic systems and stocks (BIOMASS). College Station, Texas A & M University, Texas.

Fasham, M. J. R., P. M. Holligan, and P. R. Pugh. 1983. The spatial and temporal development of the spring phytoplankton bloom in the Celtic Sea, April 1979. Progr. Oceanogr. **12**: 87–145.

Garrett, C. 2003. Internal tides and ocean mixing. Science. **301**: 1858–1859. *doi:* 10.1126/science.1090002.

Geider, R. J., and J. La Roche. 2002. Redfield revisited: variability of C:N:P in marine microalgae and its biochemical basis. Europ. J. Phycol. **37**: 1–17, doi: 10.1017/S0967026201003456.

Gibson, C. E., B .M. Stewart and R. J. Gowen. 1997. A synoptic study of nutrients in the north-west Irish Sea. Est. Coast. Shelf Sc. **45**: 27–38.

Gowen, R. J., and S. P. Bloomfield. 1996. Chlorophyll standing crop and phytoplankton production in the western Irish Sea during 1992 and 1993. J. Plank. Res. **18**: 1735–1751.

Gowen, R. J., and B. M. Stewart. 2005. The Irish Sea: Nutrient status and phytoplankton. J. Sea. Res. **54**: 36–50, doi:10.1016/j.seares.2005.02.003.

Green, J. A. M., J. H. Simpson, S. Legg, and M. R. Palmer. 2008. Internal waves, baroclinic energy fluxes, and mixing at the European shelf edge. Cont. Sh. Res. **28**: 937–950, doi: 10.1016/j.csr.2008.01.014.

Green, J. A. M., J. H. Simpson, S. A. Thorpe, and T. P. Rippeth. 2010. Observations of internal tidal waves in the seasonally stratified region of the western Irish Sea. Cont. Shelf Res. **30**: 214–225, doi:10.1016/j.csr.2009.11.004.

Gregg, M. C. 1987. Diapycnal mixing in the thermocline: A review. J. Geophys. Res. **92**: 5249-5286.

Hales, B., T. Takahashi, and A. Van Geen. 2004. High-frequency measurement of seawater chemistry: Flow-injection analysis of macronutrients. Limnol. Oceanogr. **2**: 91–101.

Hickman, A. E., C. M. Moore, J. Sharples, M. I. Lucas, G. H. Tilstone, V. Krivtsov, and P. Holligan. 2012. Primary production and nitrate uptake within the seasonal thermocline of a stratified shelf sea. Mar. Ecol. Progr. Ser. **463**: 39-57

Hill, A. E., R. Durazo, and D. A. Smeed. 1994. Observations of a cyclonic gyre in the western Irish Sea. Cont. Shelf Res. **14**: 479–490.

Holligan, P. M., P. J.Williams, D. Purdie, and R. P. Harris. 1984. Photosynthesis, respiration and nitrogen supply of plankton populations in stratified, frontal and tidally mixed shelf waters. Mar. Ecol. Progr. Ser. **17**: 201-213.

Hydes, D. J., R. J. Gowen, N. P. Holliday, T. Shammon, and D. Mills. 2004. External and internal control of winter concentrations of nutrients (N, P and Si) in north-west European shelf seas. Estuar. Coast. Shelf Sc. **59**: 151–161.

Inall, M., D. Aleynik, T. Boyd, M. Palmer, and J. Sharples. 2011. Internal tide coherence and decay over a wide shelf sea. Geophys. Res. Let. **38**: 1-6, doi:10.1029/2011GL049943.

Kitidis, V., N. J. Harman-Mountford, E. Litt, I. Brown, D. Cummings, S. Hartman, D. Hydes, J. R. Fishwick, C. Harris, V. Martinez-Vicente, E. M. S. Woodward, and T. J. Smyth . 2012. Seasonal dynamics of the carbonate system in the western English Channel. Cont. Sh. Res. **42**: 30-40.

Lucas, A. J., P. J. S. Franks, and C. L. Dupont. 2011. Horizontal internal-tide fluxes support elevated phytoplankton productivity over the inner continental shelf. Limnol. Oceanogr. [Fluids & Environ.] **1**: 56–74, doi: 10.1215/21573698-1258185.

Mackinnon, J., and M. C. Gregg. 2003. Mixing on the late-summer New England shelf – solibores, shear and stratification. J. Phys. Oceanogr. **33**: 1476-1492.

Osborn, T. 1980. Estimates of the local rate of vertical diffusion from dissipation measurements. J. Phys. Oceanogr. **10**: 83-89, doi: 10.1175/1520-0485(1980)010<0083:EOTLRO>2.0.CO.

Papadimitriou, S., D. N. Thomas, H. Kennedy, H. Kuosa, and G. S. Dieckmann. 2007. Biogeochemical composition of natural sea ice brines from the Weddell Sea during early austral summer. Limnol. Oceanogr. **52**: 1809-1823.

Pingree, R. D., P. M. Holligan, G. I. Mardell, and R. N. Head. 1976. The influence of physical stability on spring, summer and autumn phytoplankton blooms in the Celtic Sea. J. Mar. Biol. Ass. UK. **56**: 845–873.

Redfield, A. C. 1958. The biological control of chemical factors in the environment. Amer. Scientist. **46**: 205–221.

Richardson, K., A. W. Visser, and F. Pedersen. 2000. Subsurface phytoplankton blooms fuel pelagic production in the North Sea. J. Plankt. Res. **22**: 1663–1671.

Rippeth, T. R. 2005. Mixing in seasonally stratified shelf seas: a shifting paradigm. Phil. Trans. Royal Soc. **363**: 2837–2854.

Rippeth, T. P., M. R. Palmer, J. H. Simpson, N. R. Fisher, and J. Sharples. 2005. Thermocline mixing in summer stratified continental shelf sea. Geophys. Res. Let. **32**: 1-4., doi: 10.1029/2004GL022104.

Rippeth, T. P., P. J. Wiles, M. R. Palmer, J. Sharples, and J. Tweddle. 2009. The diapcynal nutrient flux and shear-induced diapcynal mixing in the seasonally stratified western Irish Sea. Cont. Sh. Res. **29**: 1580-1587.

Schafstall, J., M. Dengler, P. Brandt, and H. Bange. 2010. Tidal-induced mixing and diapycnal nutrient fluxes in the Mauritian upwelling region. J. Geophys. Res. **115**: C1004, doi:10.1029/2009JC005940.

Sharples, J., C.M. Moore, T. R. Rippeth, P. M. Holligan, D. J. Hydes, N. R. Fisher, and J. Simpson. 2001a. Phytoplankton distribution and survival in the thermocline. Limnol. Oceanogr. **46**: 486–496.

Sharples, J., C. Moore, and E. Abraham. 2001b. Internal tide dissipation, mixing, and vertical nitrate flux at the shelf edge of NE New Zealand. J. Geophys. Res. [Oceans]. **106:** 14069–14081, doi:10.1029/2000JC000604.

Sharples, J., J. F. Tweddle, J. A. M. Green, M. R. Palmer, Y. Kim, A. E. Hickman, P. M. Holligan, C. M. Moore, T. P. Rippeth, J. H. Simpson, and V. Krivstov. 2007. Spring-neap modulation of internal tide mixing and vertical nitrate fluxes at a shelf edge in summer. Limnol. Oceanogr. **52**: 1735–1747, doi:10.4319/lo.2007.52.5.1735.

Sharples, J., and P. Tett. 1994. Modelling the effect of physical variability on the midwater chlorophyll maximum. J. Mar. Res. **52**: 219-238.

Simpson, J. H., and J. R. Hunter. 1974. Fronts in the Irish Sea. Nature. **250**: 404–406.

Simpson, J. H., and T. P. Rippeth. 1998. Non-conservative nutrient flues from budgets in the Irish Sea. Est.Coast. Shelf Sea. Sc. **47**: 707-714.

Simpson, J. H., T. P. Rippeth, and A. R. Campbell. 2000. The phase lag of turbulent dissipation in tidal flow. pp55 -57. In: Interactions between estuaries, coastal seas and shelf seas. Ed. T. Yanagi. Terrapub. Tokyo.

Simpson, J. H., J. A. M. Green, T. P. Rippeth, T. R. Osborn, and W. A. M. Nimmo-Smith. 2009. The structure of dissipation in the western Irish Sea front. J. Mar. Sys. **77**: 428–440.

Slinn, D. J. 1974. Water circulation and nutrients in the North-west Irish Sea. Estuar. Coast. Mar. Sci. **2**: 1-25.

Tett, P., S. I. Heaney, and M. R. Droop. 1985. The Redfield ratio and phytoplankton growth rate. J. Mar. Biol. Assoc. U.K. **65**: 487–504.

Thomas, H., Y. Bozec, K. Elkalay, and H. J. W. de Baar. 2004. Enhanced open ocean storage of CO2 from shelf sea pumping. Science. **304**: 1005–1008, doi:10.1126/science.1095491.

Thorpe, S., and Z. Liu. 2009. Marginal Stability? J. Phys. Oceanog. **39**(9): 2373-2381.

Trimmer, M., R. J. Gowen, B. M. Stewart, and D. B. Nedwell. 1999. The spring bloom and its impact on benthic mineralisation rates in western Irish Sea sediments. Mar. Ecol. Progr. **185**: 37–46., doi: 10.3354/meps185037.

Ueyama, R., and B. C. Monger. 2005. Wind-induced modulation of seasonal phytoplankton blooms in the North Atlantic derived from satellite observations. Limnol. Oceanogr. 50(6):1820-1829.

van Haren, H., L. Mass, J. T. F. Zimmerman, H. Ridderinkhof, and H. Malschaert. 1999. Strong inertial currents and marginal internal wave stability in the central North Sea. Geophys. Res. Let. **26**: 2993–2996.

White, R. G., A. E. Hill, and D. A. Jones. 1988. Distribution of Nephrops norvegicus (L.) larvae in the western Irish Sea, an example of advective control on recruitment. J. Plank. Res. **10**: 735–747.

Wollast, R. 1998. Evaluation and comparison of the global carbon cycle in the coastal zone and in the open ocean. Vol 10, pp: 213-252. In: Brink, K. H., and Robinson, A. R. (Eds). The Sea, John Wiley and Sons, New York.

Chapter 4

Wind driven nutrient pulses to the subsurface chlorophyll maximum in seasonally stratified shelf seas[†]

*Published in Geophysical Research Letters.
Williams, C. A. J., J. Sharples, C. Mahaffey and T. P. Rippeth. *2013*. Wind driven nutrient pulses to the subsurface chlorophyll maximum in seasonally stratified shelf seas. Geophys. Res. Let. 40: 5467-5472

4.1 Introduction

Shelf seas are regions of high biological activity, disproportionately contributing 15-30% of the global oceanic primary production (Wollast, 1998) whilst occupying only 8% of the global ocean surface area. Temperate shelf seas have been implicated as substantial sinks for atmospheric carbon dioxide at the sea surface (Thomas et al., 2004; Jahnke, 2010). In these shelf seas annual primary production is partitioned approximately equally between the relatively short duration spring bloom and weaker but more sustained growth in the subsurface chlorophyll maximum (SCM) within the base of the seasonal thermocline through the summer (Hickman et al., 2012), with CO_2 drawdown being linked to the diapycnal flux of nutrient rich water to the SCM (Kitidis et al., 2012). This diapycnal nutrient flux from the bottom mixed layer (BML) to the SCM sets a limit on summer new production (e.g. Sharples et al., 2001). Observations of vertical nitrate fluxes in shelf seas have demonstrated typical background rates of 1 – 2 mmol m^{-2} d^{-1} (e.g. Sharples et al., 2001; Williams et al., 2013) which can be augmented significantly by topographically-driven internal waves (e.g. Sharples et al., 2007; Lucas et al., 2011; Tweddle et al., 2013). Shear and instabilities at the thermocline arising from wind-driven inertial oscillations potentially provide another mechanism for generating a vertical turbulent nitrate flux (Rippeth, 2005; Rippeth et al., 2005). These inertial oscillations are generated by a sudden change in wind forcing which causes the surface layer to oscillate horizontally over the bottom mixed layer at the inertial frequency (e.g. Pollard, 1980; Itsweire et al., 1989). However, current shear and mixing generated by this slab-like motion of the surface layer is thought to occur in short-lived spikes, when the wind and shear vectors are aligned (Burchard and Rippeth, 2009). Here we present observations of vertical turbulent nitrate fluxes during calm weather and during strong winds, demonstrating the large effect that winds can have on daily rates of nitrate supply to the SCM. We show that the increased nitrate flux is dominated by a few very short bursts of turbulence. Moreover, we use these observations to estimate the likely contribution that episodic wind events could have on the primary production in a temperate shelf system.

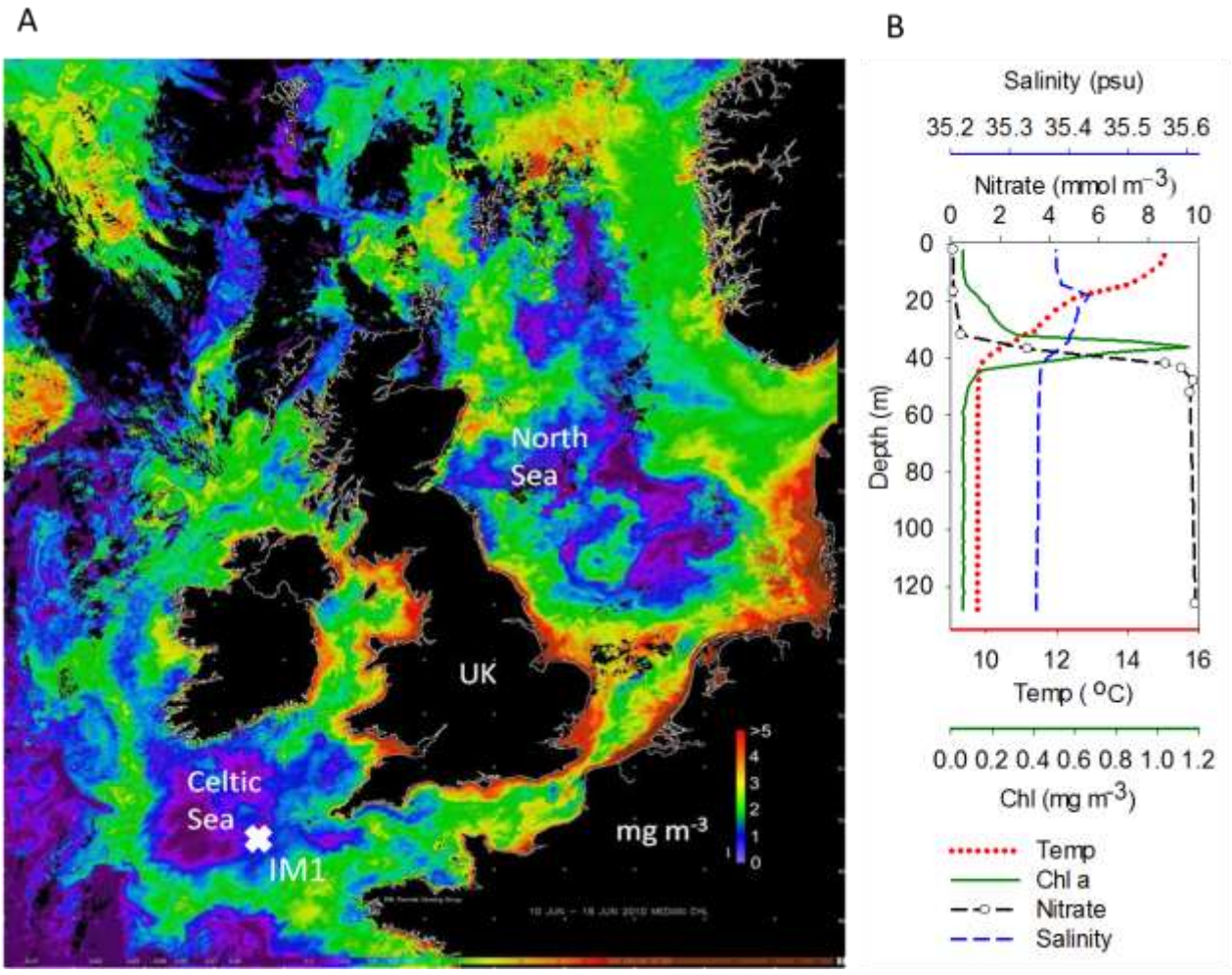

Figure 4.1: a) Sea surface chlorophyll composite from 10th-16th of June 2010 showing the Celtic Sea and sampling station IM1 (indicated by white cross; image courtesy of NEODAAS). b) Typical profile of nitrate (dashed line with open circle), chlorophyll *a* (green solid line), temperature (red dotted line) and salinity (blue dashed line) from CTD 007 (6th June 2010 at 02:31 hours), showing that the position of the subsurface chlorophyll maximum corresponds to the base of the thermocline and a sharp nitrate gradient.

4.2. Methods

Measurements were collected from the *RRS Discovery* (cruise D352) during neap tides at a station in the Celtic Sea located on the NW European shelf at station IM1 (Fig. 4.1; 49° 25' N, 08° 58' W). The sampling campaign, [decimal days 156 to 161 in 2010] consisted of measurements of vertical profiles of turbulent kinetic energy dissipation, water and wind velocity, inorganic nutrients and chlorophyll *a* (hereafter chl *a*).

4.2.1 Water column structure, chlorophyll *a* and inorganic nutrients

A rosette frame supporting a Seabird 911 conductivity, depth, temperature (CTD) instrument, a Chelsea Instruments Aquatracka MkIII fluorometer and 10 L Niskin bottles was used to collect vertical profiles (e.g. Fig. 4.1b) of salinity, temperature and chl *a* fluorescence and seawater samples. Seawater samples were analysed fresh within 2 hours of collection onboard the vessel for inorganic nutrients and extracted chl *a* concentrations. Inorganic nutrient concentrations were determined using a Bran and Luebbe QuAAtro 5-channel segmented flow nutrient analyser. Discrete measurements of chl *a* were determined by filtering 1 L of seawater onto a Whatman glass fibre filter (GF/F) and extracting with acetone. Fluorescence was determined against chl *a* using a Turner TD-700 fluorometer (Evans et al. 1987). The extracted chl *a* concentrations were used to calibrate the fluorescence sensor, with calibration having a root mean square deviation of ±0.1 mg m^{-3}.

4.2.2 Turbulence and vertical structure of the water column

Vertical profiles of velocity microstructure, temperature and salinity were collected over two sampling campaigns (days 156-158, and 160-161) using a Rockland Oceanographic VMP500 Velocity Microstructure Profiler. Profiles were taken continuously during each time series, with each down-up profile taking approximately 10 minutes. Interruptions to the time series occurred due to either ship repositioning or a CTD operation. The microstructure velocity shear measured from the VMP500 was used to calculate the dissipation of turbulent kinetic energy (TKE), ε, following Rippeth et al. (2003).

4.2.3 Meteorology and tidal currents

Meteorological and current data were collected from a mooring at the IM1 station. A surface toroid buoy was fitted with an Airmar PB200 meteorological sensor package, and recorded 10-minute averages of wind speed and direction which were used to calculate the wind stress at the sea surface. An upward-looking 150 kHz ADCP, attached to a frame on the seabed, measured components of velocity through the

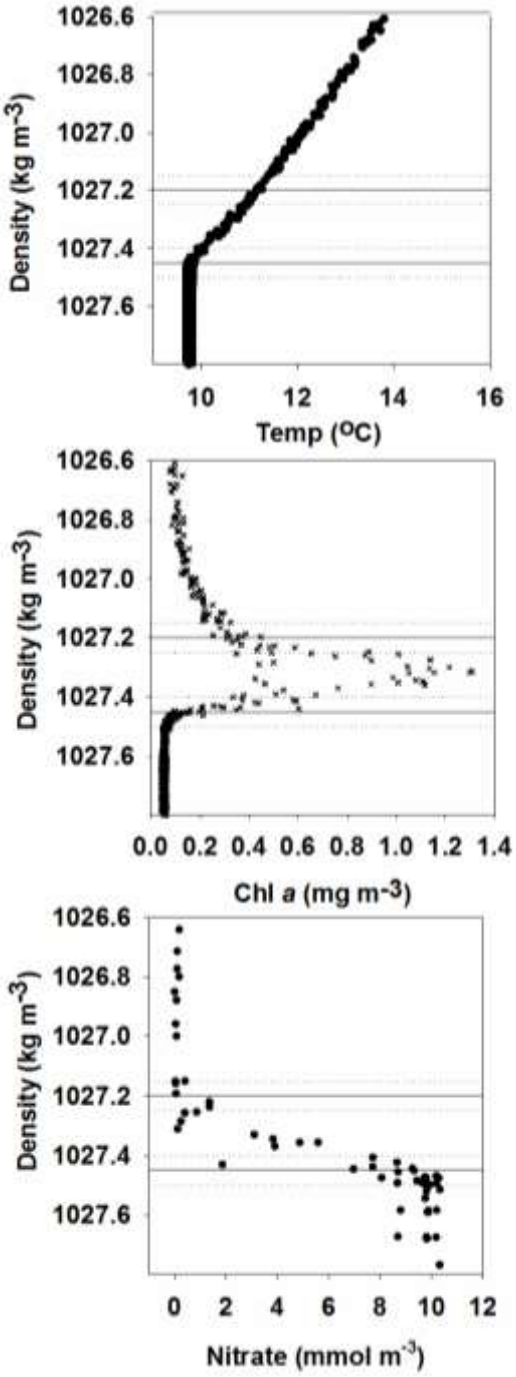

Figure 4.2: A) Chlorophyll *a* (mg m^{-3}) versus density (kg m^{-3}) measurements during the VMP sampling period. B) Temperature (°C) versus density (kg m^{-3}) measured from the CTD profiles during the VMP sampling campaign. C) Nitrate (mmol m^{-3}) concentration relative to density values (kg m^{-3}). The nitrate-density gradients at the top and base of the thermocline were 19.74 and 40.32 mmol m^{-4} respectively. The solid lines mark the 1027.2 (± 0.05) kg m^{-3} and 1027.45 (± 0.05) kg m^{-3} (marked by dotted lines isopycnals) which describes the density band marking the top and base of the SCM where fluxes were calculated over respectively.

water column at 2 m vertical resolution and averaged every 2 mins. The difference in velocity at each depth bin within the thermocline was used to calculate the mean interfacial shear squared term ($S^{2=}(du/dz)^2$; i.e., Eq. 1.4). The weather station on the surface buoy recorded 10-minute averages of wind speed and direction, which were used to calculate the wind stress at the sea surface.

4.2.4 Flux calculations

Nitrate fluxes were calculated from TKE dissipation and nitrate concentrations following Sharples et al. (2007), with means and 95% confidence intervals estimated using a Gaussian bootstrap resampling method (Efron and Gong, 1983). If the rate of the turbulent nitrate supply into the SCM is greater than the nitrate uptake rate by the SCM community, it may be possible that some nitrate from the BML is mixed through the thermocline and into the surface layer. Thus estimating the nitrate flux out of the upper thermocline and into the SML is also of interest, as it provides an indication of whether the rate of nitrate assimilation by phytoplankton in the SCM is sufficiently high to remove nitrate transported from the BML via turbulent mixing. In order to correctly identify the thermocline base and top accurately we calculated the fluxes across fixed isopycnals rather than fixed depths. The nitracline was defined as the nitrate gradient across the boundary of the SCM (Fig. 4.2a), which in turn was defined by specific isopycnals using all of the available density and chlorophyll measurements (Fig. 4.2b). This allowed us to gain a nitrate gradient across the region of the nitracline and SCM where we were interested in calculating fluxes across. The base of the nitracline was defined as the 1025.2 isopycnal (± 0.05) kg m^{-3} and the top of the nitracline as the 1025.45 (± 0.05) kg m^{-3} (Fig. 4.2a). The density-nitrate relationships at the top and base of the nitracline were calculated within these isopycnal bands (Fig. 4.2c) and were statistically robust (R^2=0.68 and 0.83 respectively, $p<0.0001$). The 'background' nitrate flux was estimated from the second VMP sampling campaign taken during low winds. The wind-driven nitrate flux is described in the results and was estimated over the initial 50 hour VMP sampling period during enhanced winds.

4.3. Results and discussion

4.3.1 Water column structure

The thermocline was typically 30 m thick in all profiles, and vertical salinity variations were small (<0.1 (PSS)) so that the density structure was driven primarily by temperature variations (Fig. 4.2a). The isopycnals encompassing the SCM covered a vertical range of up to 15 m (Fig. 4.2b). The thermocline consistently coincided with the SCM peak, the position of which varied vertically between depths of 35 to 50 m. An SCM was evident in all CTD casts before, during and after the wind mixing event. The concentration of the SCM peak varied considerably throughout all CTD profiles (0.4 – 1.4 mg m^{-3}), indicating either horizontal patches of chl *a*, or the turbulent erosion of phytoplankton from the SCM via vertical mixing. Surface chl *a* concentrations were consistently below 0.05 mg m^{-3} and nitrate concentrations were below the limit of detection (0.1 mmol m^{-3}). The bottom mixed layer was replete in inorganic nutrients; nitrate concentrations were relatively stable at a concentration of 9.5 – 10 mmol m^{-3} below the nitracline. The nitracline was observed to correspond with the SCM peak (Fig. 4.2).

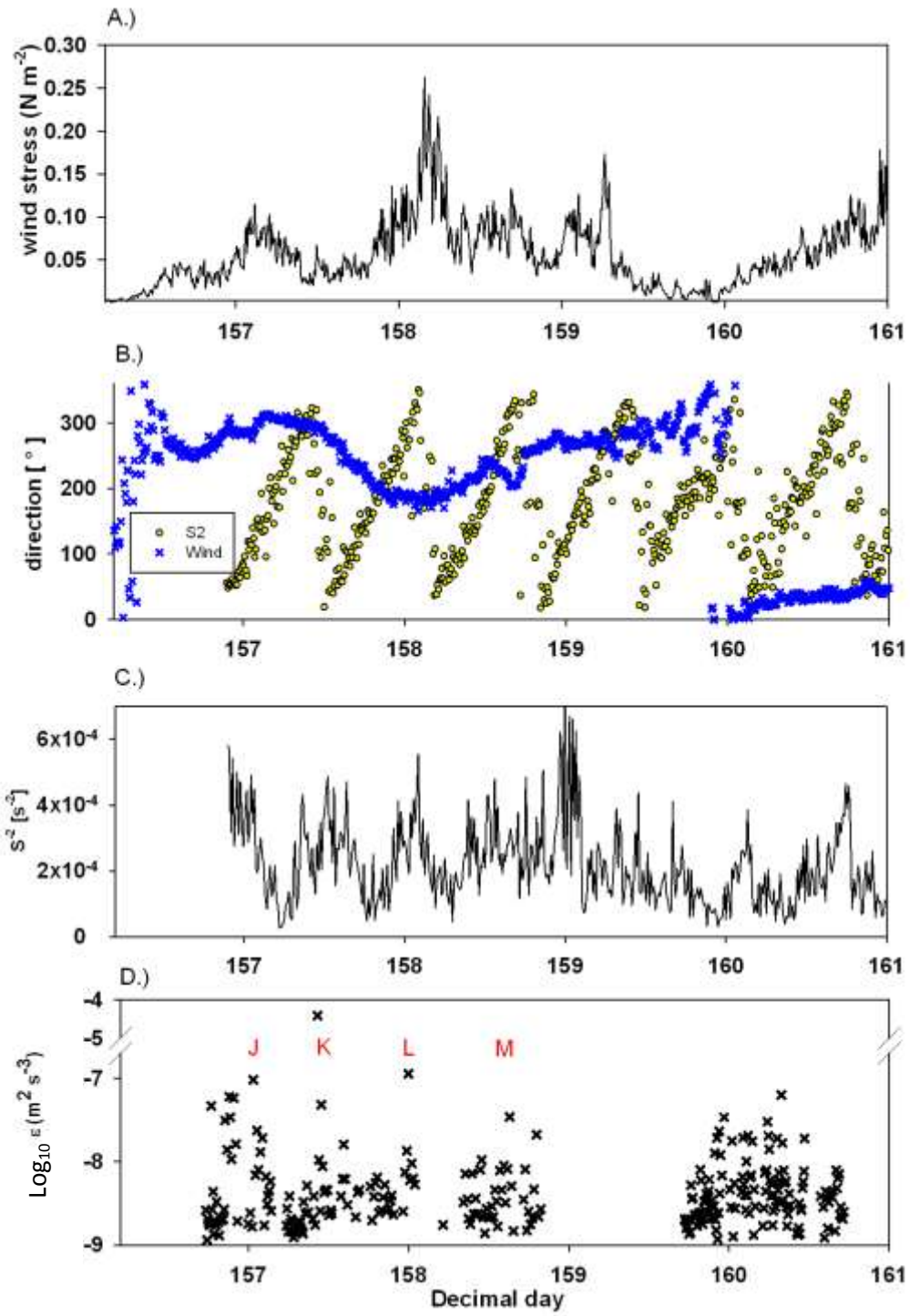

Figure 4.3: a) Wind stress calculated from the 10 minute time-averaged wind speed (m s^{-1}) measured from the Airmar PB200 weather station on the surface buoy at IM1. b) Direction (°) of the interfacial shear (10 minute smoothed) within the thermocline (dots) and the wind vector (crosses). c) Instantaneous $\log_{10}$ dissipation of turbulent kinetic energy, ε, within the thermocline (m^2 s^{-3}). All measurements were taken at station IM1 in the Celtic Sea (49° 25' N, 08° 58' W) during decimal days 156.8 – 160.8 (6^{th} – 8^{th} June) in 2010.

4.3.2 Wind driven mixing

Wind data from the IM1 mooring indicated a pronounced increase in wind stress from <0.05 N m^{-2} (wind velocity <5 m s^{-1}) on day 156 to 0.10 N m^{-2} (wind velocity = 8 m s^{-1}) on day 157, with a wind stress peak exceeding 0.25 N m^{-2} (wind velocity > 12 m s^{-1}) on day 158 (Fig. 4.3a). Shear magnitude (s^{-2}) at the base of the thermocline appeared to oscillate between 6 × 10^{-4} s^{-2} and <1 ×10^{-4} s^{-2} with a frequency of 12 to 15 hours (Fig. 4.3c). Intermittent spikes of high dissipation within the thermocline occurred during the initial VMP time series (days 156-158), and ranged between 1×10^{-7} to 1×10^{-5} m^2 s^{-3} (Fig. 4.3d), these spikes have been annotated as J, K, L and M on Fig. 3d. Dissipation within the thermocline was strongly intermittent, varying by more than 2 orders of magnitude (Fig. 4.3d). High frequency vertical oscillations of the isopycnals marking the thermocline were observed and may have been due to the presence of passing internal waves, which are generated at the shelf edge (Sharples et al., 2007), but have also been documented to propagate energy further onto the shelf (Inall et al., 2011). During the second VMP time series no clear separated spikes of dissipation from the background dissipation were observed and the wind stress increased linearly from 0 to 0.08 N m^{-2} (Fig. 4.3d). The dissipation of turbulent kinetic energy remained between 1×10^{-9} and 1×10^{-8} m^2 s^{-3} for the duration of the second VMP time series and corresponded to a period when the vertical oscillation of the thermocline was largest. The largest observed mixing event occurred on day 157.4 (event K), with a dissipation rate of 6×10^{-5} m^2 s^{-3}, more than two orders of magnitude larger than the other mixing events observed (J, L and M). Turbulent kinetic energy dissipation events corresponded with peaks in the shear magnitude (J, K, L, and M on Fig. 4.3d). Interestingly we failed to sample the strongest shear event (just after day 159.0). The largest mixing event observed (event K) could be interpreted as anomalous, however it appears consistent with measurements immediately before and after it and is made up of 7 individual dissipation values within the isopycnal band (0.5 m vertical range). Confidence in event K implies that large dissipation peaks are extremely short-lived and difficult to resolve, even with the continuously profiling VMP. It is therefore possible that we may have underestimated the magnitude of spikes in dissipation during event L and M. Following Burchard & Rippeth (2009), analysis of the shear and wind vectors demonstrated that the alignments of the wind and the

shear directions corresponded to spikes in diapycnal mixing across the thermocline during 3 of the 4 mixing events within the first VMP time series (K, L and M). Furthermore, the shear vector within the thermocline was seen to rotate in a clockwise direction at close to the inertial frequency following day 157 when the wind speed increased. Mixing events K and L, and L and M (Fig. 4.3d) were separated by a period of approximately 15 hours, corresponding to the local inertial frequency at this latitude (15.7 hours). There was a consistent lag in diapycnal mixing events, with peak mixing occurring approximately 1.5 to 3 hours after the initial shear-wind alignment. Shear production will have occurred throughout the shear-wind alignment, eventually resulting in shear instabilities and subsequent destruction of shear via turbulent dissipation and consequent mixing following the alignment. Several dissipation events occur at the beginning of the time series (event J) coinciding with a period of high shear. Current data before event J was unavailable, this enhanced shear and dissipation may have been the result of a wind-shear vector alignment that was not captured by the ADCP pre-day 157.

4.3.3 Nitrate fluxes

The daily background supply of nitrate to the base of the thermocline was calculated during the second VMP time series (day 160) as 1.3 (95% C.I =1.0 – 1.6) mmol m^{-2} d^{-1} which was consistent with the canonical nitrate flux estimates of 1-2 mmol m^{-2} d^{-1} for north-west European shelf seas (Sharples et al., 2001; 2007; Rippeth et al., 2009). Assuming the Redfield C:N ratio of 6.6 (Redfield, 1958), this flux is capable of supporting 105 mg C m^{-2} d^{-1} of new production (Table 4.1). Estimates of euphotic zone depth integrated total primary production from this period were between 174 and 386 mg C m^{-2} d^{-1} (Hickman et al., 2012). The background turbulent supply of nitrate was capable of supporting 27 to 60% of the total primary production observed in the euphotic zone, implying that the remaining production was regenerated. During enhanced winds, however, the mean nitrate flux into the base of the thermocline using a robust bootstrap resampling method increased almost 17-fold to 22 (2 to 81) mmol m^{-2} d^{-1}. The mean and 95% confidence limits used in this resampling technique highlight the variability of the system and take into account the occurrence of these intermittent mixing events. This flux would be capable of supporting 1735 (166 to 6404) mg C m^{-2} d^{-1} of new production. The wind-driven nitrate flux therefore provided between 500 (43 to

1659)% and 1000 (95 to 3680)% of the nitrogen needed to support the total PP that has been observed in the Celtic Sea, and thus the wind is an important, perhaps essential, supplier of nitrate to the SCM. If mixing events K, L and M are omitted from the flux calculation, the daily nitrate flux was 3 (2 to 4) mmol m^{-2} d^{-1}, which is of a similar magnitude to the canonical shelf sea nitrate flux estimates (e.g. Sharples et al., 2001; 2007; Rippeth et al., 2009; Williams et al., 2013), as well as our estimate during low wind and no enhanced dissipation events (Table 4.1). Thus high dissipation events induced by shear spikes drive the high nitrate flux which is only observed during the periods of high wind.

Only a small amount of the nitrate supplied from the BML appears to be either surplus to phytoplankton nitrogen requirements and/or is not assimilated quickly by phytoplankton in the SCM, and hence a small amount was able to reach the SML (0.3 mmol m^{-2} d^{-1}; Table 4.1). This indicates that potentially 500-1000% of the nitrate that is thought to be required for production may have been assimilated by phytoplankton within the SCM. The intermittent mix events were observed at the base of the thermocline, but not at the top into the nitrate deplete surface layer. However, the small increase in nitrate supplied to the SML during enhanced winds was equivalent to a 2-fold increase in new production (increased from 13 to 23.8 mg C m^{-2} d^{-1}; Table 4.1).

Table 4.1: Daily nitrate fluxes (mmol m^{-2} d^{-1}) into the top and base of the nitracline, during both low and enhanced winds (with and without spike J described in Figure 6). Daily nitrate fluxes have been converted into potential nitrate driven production using the Redfield ratio (mg C m^{-2} d^{-1}).

Flux	Top of thermocline	Base of thermocline
Daily background nitrate flux (mmol m^{-2} d^{-1})	0.2 (0.1– 0.2)	1.3 (1.0 - 1.6)
Background potential nitrate driven production (mg C m^{-2} d^{-1})	13 (10 -15)	105 (82 - 128)
Daily nitrate flux during enhanced winds (mmol m^{-2} d^{-1})	0.3 (0.2 - 0.6)	22 (2 - 81)
Potential nitrate driven production during enhanced winds (mg C m^{-2} d^{-1})	23.8 (12 - 48)	1735 (166 - 6404)

The increase in nitrate supplied to the surface during enhanced winds was not observed in the surface nitrate concentrations, which were consistently <0.1 mmol m^{-3} (BLD). It is likely that nitrate supplied to the surface layer from the thermocline would have been immediately removed via efficient nutrient uptake by small celled phytoplankton (Chisholm, 1992). Data from nutrient uptake experiments conducted on the same research cruise (C. Williams, unpublished data, 2013) indicates that the surface layer community were capable of assimilating up to 0.1 mmol m^{-3} h^{-1} of nitrate. Assuming an approximate 10 m thick surface layer, this is equivalent to a depth integrated uptake rate of approximately 1 mmol m^{-2} hr^{-1}, and thus any additional nitrate supplied via turbulent fluxes would not have been captured in our observations.

4.4. Summary

Shelf seas are an important global carbon sink, with primary production in the SCM thought to account for a significant fraction of the carbon fixation occurring there (Kitidis et al., 2012). In order for carbon fixation to be accurately predicted in shelf seas, biophysical models need to incorporate the effect of wind driven inertial oscillations which, as we have demonstrated, can potentially supply large, intermittent fluxes of nutrients into the euphotic zone. Additionally, these large, intermittent mixing events are likely to erode and export carbon from the SCM, removing particulate organic carbon from the euphotic zone and transporting it to the BML. The importance of high temporal resolution sampling of turbulence in order to fully capture and quantify the importance of these short-lived wind-driven mixing events is clear. It is possible that some excess nitrate supplied to the base of the thermocline may reach the nitrate limited surface community, though the evidence suggests that this may be assimilated on a faster timescale than the traditional sampling resolution of nutrients.

The overall contribution of wind-driven mixing events to annual carbon fixation in the Celtic Sea can be estimated by approximating how often this mixing mechanism might occur through a typical stratified season. Using wind data from 10

successive summers in the Irish Sea, Sherwin (1987) estimated that wind-driven inertial oscillations may occur every 2 weeks during the summer period (120 days). This is equivalent to ~9 wind-driven inertial events occurring every summer, with each event potentially supplying 22 (2 to 81) mmol m^{-2} d^{-1} of nitrate to the SCM. The total supply of nitrate to the SCM during summer via wind-driven inertial oscillations would therefore be 197 (19 to 728) mmol m^{-2} y^{-1}, with the potential to support 15 (1.5 to 58) g C m^{-2} y^{-1} of new production annually in the SCM respectively. Measurements of the depth integrated daily total PP from the Celtic Sea (Hickman et al., 2012) equate to an annual summer total PP estimate of 21 to 46 g C m^{-2} y^{-1}. Therefore, we can estimate that between approximately 33% and 71% of the total summer primary production in the euphotic zone is supported by wind-driven fluxes of nitrate from the BML into the base of the thermocline. However, there are uncertainties on the values reported in this study – for example, there is increasing evidence to suggest that a considerable proportion of PP is shunted into the dissolved organic carbon (DOC) pool (see Chapter 5). The PP values extrapolated here are based on measurements of the particulate organic carbon (POC) pool only, and therefore may be underestimates of shelf sea PP (i.e., >> 21 to 46 g C m^{-2} y^{-1} from Hickman et al., 2012). This would mean that our estimates of the contribution to shelf sea PP (15 g C m^{-2} y^{-1}) from the wind-driven nitrate flux may be an overestimate. Though based on the estimates of PP we have and the observations available, this finding implies that between one and two thirds of the summer PP could be unaccounted for in models which do not simulate inertially-generated shear spikes correctly, either due to insufficiently resolved wind forcing or poor parameterisation of thermocline mixing. At present there are no shelf sea models which can accurately predict inertially-generated shear spikes and consequential mixing, thus it is likely that PP resulting from wind-driven oscillations is unaccounted for in models. In order for PP in shelf seas to be accurately quantified in models these inertially-driven shear spikes, and the resulting short lived mixing events, need to be represented in models.

The findings here have shown that the SCM is likely to be dependent on wind for the nitrate supply which sustains it. The frequency of wind events is determined by the position of the Jet Stream, and as the climate changes the position of the storm track is expected to change (Hu and Wu, 2004). Thus the frequency and intensity of

storms over the North Atlantic may change, and it is possible that these future potential changes may result in an increase in intermittent inertial mixing events. We have demonstrated that wind-driven inertial oscillations are an important mixing mechanism that need to be considered in order to gain accurate global carbon fixation estimates.

Between 16 and 30% of global PP occurs on the shelf (Wollast, 1998), half of the PP on the shelf occurs at the SCM (Hickman et al., 2012). This means that between 8 and 15% of the global PP occurs at the SCM. In this study we suggest that between one and two thirds of PP at the SCM is supported by short-lived, wind-driven mixing events. Therefore, though this is a rough estimate with uncertainties that we have mentioned, we approximate that this would equate to between 2 and 10% of the global PP being supported by wind-driven pulses of nitrate to the SCM in shelf seas.

4.5 References

Burchard, H., and T. P. Rippeth. 2009. Generation of bulk shear spikes in shallow stratified tidal seas. Amer. Met. Soc. **29**:969-985, doi: 10.1175/2008JPO4074.1

Chisholm, S. W. 1992. Phytoplankton size. In: Falkowski, P. G., Woodhead, A. D. (Eds.), Primary productivity and biogeochemical cycles in the sea. Plenum press, New York, pp. 213-237

Efron, B., and G. Gong. 1983. A leisurely look at the bootstrap, the jackknife, and cross-validation. The Amer. Statist. 37: 36 – 48.

Evans, C. A., J. E. O'Reilly, and J. P. Thomas. 1987. A handbook for the measurement of chlorophyll *a* and primary production. Vol 8: p 114, In: Biological investigations of marine Antarctic systems and stocks (BIOMASS).

Hickman, A. E., C. M. Moore, J. Sharples, M. I. Lucas, G. H. Tilstone, V. Krivtsov, and P. Holligan. 2012. Primary production and nitrate uptake within the seasonal thermocline of a stratified shelf sea. Mar. Ecol. Progr. Ser. **463**:39-57.

Hu, Z. Z., and Z. H.Wu. 2004. The intensification and shift of the annual North Atlantic Oscillation in a global warming scenario simulation. Tellus A 56:112–124

Inall, M. E., D. Aleynik, T. Boyd, M. Palmer, & J. Sharples. 2011. Internal tide coherence and decay over a wide shelf sea. Geophys. Res. Let. **38**, L23607, DOI:0.1029/2011GL049943.

Jahnke, R. A. 2010. Global Synthesis, p. 597-615. *In* K. K. Liu, L. Atkinson, R. A. Quinones and L. Talaue-McManus [eds.], Carbon and Nutrient Fluxes in Continental Margins: A Global Synthesis. Springer-Verlag.

Kitidis, V., N. J. Harman-Mountford, E. Litt, I. Brown, D. Cummings, S. Hartman, D. Hydes, J. R. Fishwick, C. Harris, V. Martinez-Vicente, E. M. S. Woodward, and T. J. Smyth . 2012. Seasonal dynamics of the carbonate system in the western English Channel. Cont. Sh. Res. **42**:30-40.

Lucas, A. J., P. J. S. Franks, and C. L. Dupont. 2011. Horizontal internal-tide fluxes support elevated phytoplankton productivity over the inner continental shelf. Limnol. Oceanogr. [Fluids & Environ.] **1**: 56–74, doi: 10.1215/21573698-1258185.

Itsweire, E. C., and K. N. Hellend. 1989. Spectra and energy transfer in stably stratified turbulence. J. Flu. Mechan. **207**:419-452.

Pollard, R. T. 1980. Properties of near-surface inertial oscillations. Amer. Met. Soc. **10**:385-398.

Redfield, A. C. 1958. The biological control of chemical factors in the environment. Amer. Scientist. **46**:205–221.

Rippeth, T. R. 2005. Mixing in seasonally stratified shelf seas: a shifting paradigm. Phil. Trans. Royal Soc. **363**:2837–2854.

Rippeth, T. R., J. H. Simpson, E. Williams, and M. E. Inall. 2003. Measurements of the rates of production and dissipation of turbulent kinetic energy in an energetic tidal flow: red wharf bay revisited. J. Phys. Oceanog. **33(9)**:1889-1901.

Rippeth, T. P., M. R. Palmer, J. H. Simpson, N. R. Fisher, and J. Sharples. 2005. Thermocline mixing in summer stratified continental shelf sea. Geophys. Res. Let. **32**:1-4., doi: 10.1029/2004GL022104.

Rippeth, T. P., P. J. Wiles, M. R. Palmer, J. Sharples and J. Tweddle. 2009. The diapcynal nutrient flux and shear-induced diapcynal mixing in the seasonally stratified western Irish Sea. Cont. Sh. Res. **29**:1580-1587.

Sharples, J., C.M. Moore, T. R. Rippeth, P. M. Holligan, D. J. Hydes, N. R. Fisher and J. Simpson. 2001. Phytoplankton distribution and survival in the thermocline. Limnol. Oceanogr. **46**:486–496.

Sharples, J., J. F. Tweddle, J. A. M. Green, M. R. Palmer, Y. Kim, A. E. Hickman, P. M. Holligan, C. M. Moore, T. P. Rippeth, J. H. Simpson, and V. Krivstov. 2007. Spring-neap modulation of internal tide mixing and vertical nitrate fluxes at a shelf edge in summer. Limnol. Oceanogr. **52**:1735–1747, doi:10.4319/lo.2007.52.5.1735.

Sherwin, T. J. 1987. Inertial oscillations in the Irish Sea. Cont. Sh. Res. **7**:191-213.

Thomas, H., Y. Bozec, K. Elkalay, and H. J. W. de Baar. 2004. Enhanced open ocean storage of CO2 from shelf sea pumping. Science. **304**:1005–1008, doi:10.1126/science.1095491.

Tweddle, J. F., J. Sharples, M. R. Palmer, K. Davidson, and S. McNeil. (in press). Enhanced nutrient fluxes at the shelf sea seasonal thermocline caused by stratified flow over a bank. Progr. Oceanogr.

Williams, C. A. J., J. Sharples, M. Green, C. Mahaffey, and T. P. Rippeth. (2013). The maintenance of the subsurface chlorophyll maximum in the western Irish Sea. Limnol. Oceanogr. Fluids & Environments. **3**: 61–73.

Wollast, R. 1998. Evaluation and comparison of the global carbon cycle in the coastal zone and in the open ocean. Vol 10, pp213-252. In: Brink, K. H., and Robinson, A. R. (Eds). The Sea, John Wiley and Sons, New York.

Chapter 5

Impact of diapycnal mixing on primary and secondary production in the stratified shelf sea: an experimental approach[3]

[3] Submitted as a manuscript to Marine Ecology Progress Series. C. A. J. Williams, A. Panton, L. Abram, C. Davis, J. Sharples, and C. Mahaffey. (submitted). Impact of diapycnal mixing on primary and secondary production in the stratified shelf sea: an experimental approach. Mar. Ecol. Pr. Ser.

5.1 Introduction

Despite occupying only 9% of the global ocean surface area, shelf seas are responsible for 15 to 30% of global oceanic primary production (Wollast, 1998, Simpson and Sharples, 2012), and thus are disproportionally important in the global ocean carbon cycle. In temperate regions specifically, shelf seas have been implicated as substantial sinks for atmospheric carbon dioxide via the 'continental shelf pump' (Thomas et al., 2004; Jahnke, 2010). Temperate shelf seas undergo seasonal vertical stratification when the input of solar energy from the sun prevails over mixing energy from the wind and tides (Simpson and Hunter, 1974). At the onset of thermal stratification, phytoplankton which inhabit the surface layer are supplied with ample nutrients in a stable, well-lit region of the water column causing the onset of the phytoplankton spring bloom and rapid depletion of nutrients in the surface layer (Pingree and Pennyquick, 1975). The thermocline acts as a physical barrier between the surface and bottom mixed layer (SML and BML respectively, Sharples et al. 2001). Subsequently, a peak in phytoplankton biomass and chlorophyll is observed at the base of the thermocline, where there is sufficient light and a turbulent supply of nutrient replete BML water (Sharples et al. 2001). This subsurface chlorophyll maximum (SCM) is a well-documented feature in temperate shelf seas, and the plankton community that thrive there differ significantly from the mostly small-celled phytoplankton that are found in the nutrient depleted SML (Sharples et al. 2007; Hickman et al. 2009).

In temperate shelf seas the annual primary production is partitioned approximately equally between the relatively short-lived spring bloom and weaker but sustained growth in the SCM within the base of the seasonal thermocline through the summer (Hickman et al., 2012). The physical supply of nitrate to the subsurface chlorophyll maximum (SCM) sustains the summer primary production (Sharples et al., 2007; Rippeth et al., 2009; Williams et al., 2013). The background flux of nitrate into the SCM driven by tidal turbulence is 1-2 mmol m^{-2} d^{-1} (Sharples et al., 2007; Rippeth et al., 2009). However, observations from the stratified Western Irish Sea indicate that these background fluxes are insufficient to support the observed productivity (Williams et al., 2013). Wind-driven inertial oscillations have been identified as important mechanisms for enhancing diapycnal fluxes of nutrients by causing large-scale, intermittent pulses of nutrient rich bottom mixed layer (BML)

water to the SCM. Wind-driven mixing events may supply up to 81 mmol m^{-2} d^{-1} of nitrate to the community at the base of the SCM (Williams et al., 2013). Observations indicate that these wind-driven mixing events do not penetrate into the SML and thus do not supply nutrients to the phytoplankton living in the nutrient-deplete SML. Instead, it is presumed that the nutrients are rapidly assimilated by phytoplankton living in the SCM. Assuming a C:N ratio of 6.6:1 (Redfield, 1958), these short-lived pulses supplied by wind events have been estimated to support up to two-thirds of the shelf sea summer production (Williams et al., 2013).

While there have been direct observations of the impact of wind events on plankton communities in coastal seas (Nielsen and Kiorboe, 1990), as well as experiments conducted in the Celtic sea to investigate the response of mixing events on primary and secondary production (Davidson et al., 2013), both studies focused their observations on the nutrient-deplete SML communities rather than the SCM. However, wind-driven inertial oscillations are unlikely to mix water from the BML through the SCM and into the SML (Williams et al., 2013), and thus the SCM is more likely to receive water from the BML via this mechanism. Thus there is currently no verification of the above estimate of potential wind-driven production in the SCM. Here we use an experimental approach to simulate an episodic mixing event that supplies water from the BML into the SCM (amended) and removal of diapycnal mixing (unamended). The aim of the experiment was to investigate the response of the plankton community in terms of rate of nutrient drawdown, primary and secondary production and phytoplankton species succession. The results present the first experimental investigation into the response of the shelf sea SCM to diapycnal fluxes.

5.2 Methods

5.2.1 Experimental design

Experiments were conducted on 6th of June 2010 (CTD8) during a 23 day cruise to the Celtic Sea on the RRS Discovery (D352). Seawater was collected from the subsurface chlorophyll maximum (SCM, 37 m) and the bottom mixed layer (BML, 70 m, Fig. 5.1). An experiment was setup on 6th June to investigate the effect of a one-off large scale mixing event (amended) and the impact of isolating the SCM from background mixing (unamended). The amended incubations were prepared by

adding 1 L of unfiltered seawater from the BML to 9 L of seawater from the SCM into pre-cleaned polycarbonate carboys (10% vol:vol). For these amended incubations 10 carboys were prepared, where 3 carboys were sacrificed for measurements at the start (T-zero) and end (T-final) of the incubation, and 2 carboys were sacrificed for measurements at each time point at 24 h (T=24 h) and 48 h (T=48 h) after the start of the incubation. The unamended incubation consisted of incubating 10 L of seawater from the SCM. In unamended incubations, measurements at T-zero were taken directly from three separate CTD Niskin bottles, and 5 carboys were prepared with 10 L of SCM water; 3 carboys were sacrificed for measurements at T-final and 1 carboy was sacrificed at each time point at T=24 h and T=48 h. All carboys were incubated in on-deck incubators adjusted to the light level at the SCM (4% surface irradiance) and the temperature was maintained using surface seawater from the ship's underway flow system. At T-zero and time points at 24, 48 and 96 h, samples were collected for the following parameters: (a) inorganic and organic nutrients, (b) particulate organic carbon and nitrogen, (c) chlorophyll *a* (herein chl *a*), (d) rates of primary production, (e) bacterial production and respiration, and (f) phytoplankton enumeration and identification. All sample and incubation bottles were acid-washed, triple rinsed with DIW and triple rinsed with sample water prior to sample collection. Measurements for various parameters were made by the following PhD students:

Table 5.1: List of measurements taken and scientific personnel responsible for collecting them in the experiments.

Measurement	Person responsible
Nutrients, phytoplankton identification and enumeration	Charlotte Williams
Rates of primary production, bacterial production, chlorophyll *a*, DOC and DON	Anouska Panton
POC and PON	Lucy Abram

Previous findings show that the background turbulent mixing supplies 1-2 mmol m^{-2} d^{-1} of nitrate into the SCM (Sharples et al., 2001a; 2001b; 2007; Rippeth et al., 2009). A true control incubation would require the addition of BML water of the order of 5-10 ml per day, or setup of a continuous culture-type incubation where water is added and removed to maintain the nutrient concentration at that observed at the SCM. Both options were not viable during this investigation.

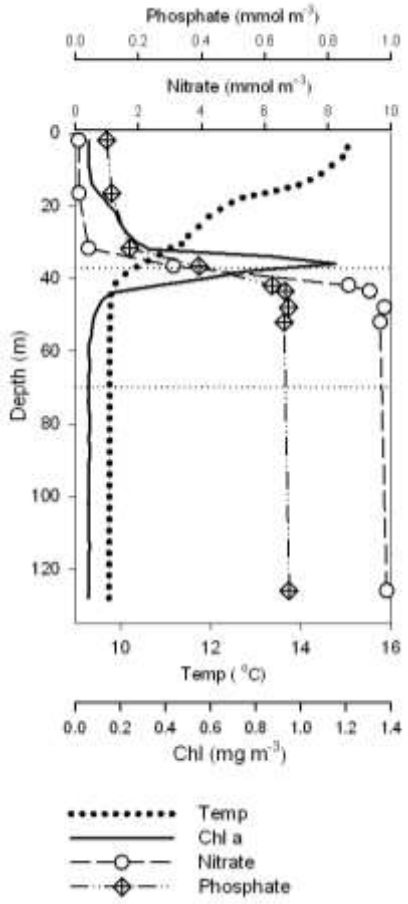

Figure 5.1: Vertical profile of temperature (^{o}C, dotted line), chlorophyll *a* (mg m^{-3}, solid line), nitrate (mmol m^{-3}, open circle) and phosphate (mmol m^{-3}, crossed diamond) from the CTD cast used for the experimental incubations (CTD 8, 6th June 2010). Horizontal dotted lines indicate the depth horizon of the subsurface chlorophyll maximum (SCM, 37 m) and the bottom mixed layer (BML, 70 m).

5.2.2 Dissolved inorganic nutrients

Unfiltered samples for determination of dissolved inorganic nutrient concentrations were collected directly into high density polyethylene (HDPE) bottles and analysed immediately. Nutrient concentrations, specifically nitrate plus nitrite (herein nitrate), silicate and phosphate were determined using a Bran and Luebbe

QuAAtro 5-channel segmented flow nutrient analyser using standard colorimetric techniques. Limits of detection were 0.1 mmol m^{-3} for nitrate and silicate and 0.05 mmol m^{-3} for phosphate. Precision of analysis for each nutrient analysed was ± 0.02 mmol m^{-3} for nitrate and phosphate and ± 0.06 mmol m^{-3} for silicate.

Table 5.2: Parameters at the start of the experiments (T-zero) in the unamended and amended incubations. Standard error is reported as well as the statistical significance from t-test (0<0.05) between the unamended and amended conditions at the 95% confidence interval.

	Unamended (SCM initial concentration)	**Amended (initial concentration)**	**Statistically different (t-test, p<0.05)**
Nitrate (mmol m^{-3})	**5.12 ±0.48**	**5.40 ±0.47**	**No**
Phosphate (mmol m^{-3})	**0.45 ±0.00**	**0.48 ±0.02**	**No**
Silicate (mmol m^{-3})	**3.20 ±0.02**	**3.20 ±0.02**	**No**
Chl *a* (mg m^{-3})	**1.41**	**1.38 ±0.16**	**No**
Primary production (mg C m^{-2} d^{-1})	**10.12 ±1.48**	**8.14 ±0.69**	**No**
Bacterial production (mg C m^{-2} d^{-1})	**0.55 ±0.01**	**1.38 ±0.06**	**Yes**
Bacterial respiration * (mg C m^{-2} d^{-1})	**1.99 ±0.26**	**4.45 ±0.72**	**Yes**
DOC (mmol m^{-3})	**95.63 ±2.36**	**82.44 ±9.27**	**No**
DON (mmol m^{-3})	**4.44 ±0.4**	**4.80 ±0.4**	**No**
Ciliates (cells L^{-1})	**60 ±33**	**60 ±33**	**No**
Dinoflagellates (cells L^{-1})	**23960 ±4000**	**22904 ±1886**	**No**
Diatoms (cells L^{-1})	**1000 ±3000**	**1067 ±66**	**No**
Flagellates (cells L^{-1})	**6.1 ±0.8e6**	**1.1 ±3.5e6**	**No**

5.2.3 Dissolved organic nutrients

Samples for dissolved organic nutrient analysis were filtered through a pre-combusted (450°C for 4 hours) glass fibre filter (GF/F) using a glass filter rig under low vacuum (< 10 mm Hg). The filtrate was collected and stored in 22 ml pre-combusted vials with Teflon lined lids and preserved with 20 µl of 50 % (v/v) hydrochloric acid. The concentration of dissolved organic carbon (DOC) and total dissolved nitrogen (TDN) were determined simultaneously by high temperature catalytic oxidation (Badr et al. 2003). Calibration was performed using a mixed potassium hydrogen phthalate/glycine standard and tested using Certified Reference Materials from the Hansell laboratory, Miami. Dissolved organic nitrogen (DON) concentrations were calculated by subtracting nitrate concentrations from the TDN concentration (ammonium data was not available). The limits of detection for DOC and TDN were 3.4 mmol m^{-3} and 1.8 mmol m^{-3} respectively, with a precision better than 2.5%.

5.2.4 Particulate organic matter

For determination of particulate organic nitrogen (PON) and particulate organic carbon (POC), 1 L of seawater was filtered through a pre-combusted GF/F. Filters were wrapped in combusted aluminium foil, stored at -80^{o}C and freeze dried prior to analysis. Total nitrogen (TN) and total organic carbon (TOC) concentrations were determined using a Carlo Erba Instruments NC2500 elemental analyser.

5.2.5 Size fractionated chlorophyll *a*

1 L of seawater was filtered sequentially through a 10, 2, and 0.2 µm polycarbonate filter under low vacuum pressure (< 10 mmHg). Filters were placed in capped glass test tubes and 5 ml of 90% acetone was immediately added. Test tubes were stored in the dark at 4°C for 24 h to allow chlorophyll to be extracted from the filter. The filter was removed and fluorescence was determined using a Turner TD700 fluorometer and chlorophyll *a* (chl *a*) concentration calculated relative to a chl *a* standard of the 0.2-2, 2-10 and > 10 µm size fractions.

5.2.6 Phytoplankton community structure

Phytoplankton were identified and enumerated using a Carl Zeiss inverted light microscope following the settling method outlined by Utermohl (1931). 100 ml of seawater was preserved with acid Lugol's solution (2% vol:vol) and stored in the dark. 10 ml or 50 ml of sample was settled for 24 hours before enumeration of flagellates, dinoflagellates, ciliates, diatoms and any zooplankton present took place. Organisms were identified down to species level where possible according to Tomas (1997). Cell counts were converted to number of cells per litre and were grouped into functional groups for the purpose of this study.

5.2.7 ^{14}C size-fractionated primary production

The rate of primary production (PP_{POC}, mg C m^{-3} d^{-1}) was measured using the ^{14}C method (Steeman Nielsen, 1952). Five 100 ml samples per incubation carboy were dispensed into clean 125 ml polycarbonate bottles. A stock of $NaH^{14}CO_3$ (Perkin Elmer, UK) was prepared daily in freshly filtered seawater and 12 μCi $NaH^{14}CO_3$ was added to each bottle. Three samples were incubated from dawn to dusk (approximately 16 hours) in on-deck incubators described above. One sample was stored in the dark and one filtered immediately thus acting as controls, with the dark sample used to correct for carbon uptake in the dark. Once the incubation was complete, the specific activity of three samples was tested by adding 200 μl of sample seawater into a scintillation vial containing 0.5 ml β- phenethylamine before filtering the remaining sample sequentially through 10, 2 and 0.2 μm polycarbonate filters. Filters were fumed with 1 ml of 10 % HCl for 24 h in the fume hood before adding 5 ml Ultima Gold scintillation cocktail. Activity was determined using a Perkin Elmer Tricarb 3100TR scintillation counter using internal quench standards. The rate of PP_{POC} for each size fraction (0.2-2, 2-10 and > 10 μm, mg C m^{-3} d^{-1}) was calculated by dividing the particulate uptake of ^{14}C (corrected for uptake in the dark) by the specific activity of the sample. This value was subsequently multiplied by the concentration of bicarbonate in seawater (24000 mg m^{-3}) and the $^{14}C/^{12}C$ isotopic uptake correction factor of 1.05 (Carrillo and Karl, 1999).

5.2.8 Bacterial production and respiration

Bacterial production (BP; mg C m^{-3} d^{-1}) was measured using the ^{3}H-leucine method (Chin-Leo and Kirchman, 1988). 10 ml of seawater was dispensed in triplicate into 30 ml polycarbonate bottles and spiked with 10 nM (final concentration) leucine prepared as 1 part ^{3}H-leucine (specific activity 50 Ci $mmol^{-1}$; Perkin Elmer UK) and 9 parts L-leucine (both prepared in deionised Milli-Q water). Samples were incubated in dark bags for 2 h in on-deck incubators. For controls incubations, ice-cold trichloracetic acid (TCA: 5% (vol:vol) was added to one sample containing ^{3}H-leucine and incubated alongside samples. At the end of the incubations, ice-cold TCA (5% vol:vol) was added to each sample bottle, which was subsequently filtered through 0.2 µm cellulose nitrate filters. Filters were twice rinsed with 1 ml 80% (vol:vol) ethanol before being dissolved with 1 ml ethyl acetate (Wicks and Robarts 1988). Activity of samples was measured using a scintillation counter as above. The rate of bacterial production (mg C m^{-3} d^{-1}) was calculated from the leucine incorporation rate using a conversion factor of 3.1 kg C mol Leu^{-1} (Simon and Azam, 1989). Bacterial respiration (BR) was estimated from a documented BP relationship (Eq. 5.1; Robinson, 2008).

$$BR = 3.69 \times BP^{0.58} \quad [5.1]$$

The bacterial carbon demand (BCD) was calculated using the BP and BR rate measurements and represents the total amount of C required by bacteria for growth and respiration (Eq.5. 2):

$$BCD = BP + BR \quad [5.2]$$

5.2.9 Dissolved fraction of primary production (PP_{DOC})

It is important to note that the ^{14}C bicarbonate derived PP (section 5.2.5) represents the net rather than gross C fixed, and does not account for loss of DOC via cell exudation and leakage. Using the change in DOC concentration during the incubation and the BCD (section 5.2.8), the rate of gross DOC exudation was estimated accounting for that used by BCD (Eq. 5.3). Addition of the PP_{POC} to PP_{DOC} represents the gross rate of primary production.

$$PP_{DOC} = \frac{\delta DOC}{\delta t} + BCD \quad [5.3]$$

5.3. Results

5.3.1 Initial conditions and experimental amendments

Seawater was collected just below the peak of the SCM, which coincided with the nitracline (Fig. 5.1). Nitrate, phosphate and silicate concentrations at this depth were 5.12, 0.45 and 3.2 mmol m^{-3}, respectively (Table 5.1). Chl *a* concentrations were 1.4 mg m^{-3} and rates of primary and bacterial production were 10.12 (±1.48) and 0.55 (±0.01) mg C m^{-2} d^{-1}, respectively. The 0.2-2 μm and > 10 μm size fraction represented 72% and 2% of the ambient chl *a* concentration in the SCM. The phytoplankton community was dominated by small (< 50 μm) dinoflagellates, mostly *Gymnodium sp.* and *Gyrodinium sp.*, as well as small (< 2 μm) flagellates. Diatoms, specifically the pennates *Nitzschia sp*. and *Navicula sp*., were also present at the SCM.

Nitrate, silicate and phosphate concentrations in the BML water were 9.62, 3.96 and 0.65 mmol m^{-3}, respectively. After the addition of unfiltered BML water (10% vol:vol) to the SCM water, representing the amended incubation, nutrient concentrations did not increase significantly according to a statistical t-test ($p<0.05$, Table 5.1) and therefore our amended incubations were not considered to be nutrient addition incubations. The SCM total chl *a* was diluted by 2% in the amended incubations (from 1.41 mg m^{-3} to 1.38 mg m^{-3}) via the addition of low chl *a* water from the BML (0.14 mg m^{-3}). However, we observed an initial change in the rate measurements which were disproportionate to the 10% vol:vol addition. This included a small decrease in the rate of primary production (from 10.12 ±1.48 to 8.14 ±0.69 mg C m^{-2} d^{-1}), and a 150% increase in rate of bacterial production (0.55 ±0.01 to 1.38 ±0.06 mg C m^{-2} d^{-1}). The community structure at the SCM was not significantly altered in the amended incubations (Table 5.1). The pennate diatom *Thalassiosira nitzschiodes*, was the only species that was exclusively observed in the BML and hence added to amended incubations. Cell counts from the BML addition water indicated very low cell numbers, though a low concentration of diatoms and dinoflagellates were present (10^2 cells L^{-1}).

5.3.2. Dissolved inorganic and organic nutrients

In the amended and unamended incubations, nitrate and phosphate concentrations decreased from ~ 5 and ~ 0.4 mmol m^{-3} respectively, to below limits of detection (BLD) within the 96 h incubation period (Fig. 5.2a). Silicate concentrations decreased by almost 23% in both amended (from 3.2 to 2.6 mmol m^{-3}) and unamended (from 3.2 to 2.5 mmol m^{-3}) incubations, indicative of growth of diatoms and/or silicoflagellates in the both incubations. DOC concentrations increased significantly by 21% (from 82.4 ± 9.27 mmol m^{-3} to 98.6 ± 2.06 mmol m^{-3}; $P<0.05$) in the amended incubation, although remained relatively constant over the 96 h incubation in the unamended incubation if we take into account the error associated with measurements (from 95.6 ±2.3 mmol m^{-3} to 92.0 ±1.6 mmol m^{-3}). However, a 45% decrease in DOC was observed within the initial 48 hours of the unamended incubation (from 95.6 ±2.3 mmol m^{-3} to 88.8 mmol m^{-3}; Fig. 5.2b). DON concentrations increased by 10% (from 4.8 ±0.4 to 5.3 ±0.1 mmol m^{-3}) in the amended incubation (Fig. 5.2c), and consequently the DOC:DON ratio increased from 17 to 19. In the unamended incubation DON increased by 33% over the entire incubation (4.38 ±0.4 mmol m^{-3} to 5.84 ±0.02 mmol m^{-3}; Fig. 5.2c) decreasing the DOC:DON ratio from 22 to 16, which is within the range of that previously observed in temperate shelf seas (e.g., Suratman et al., 2009; Davidson et al., 2013).

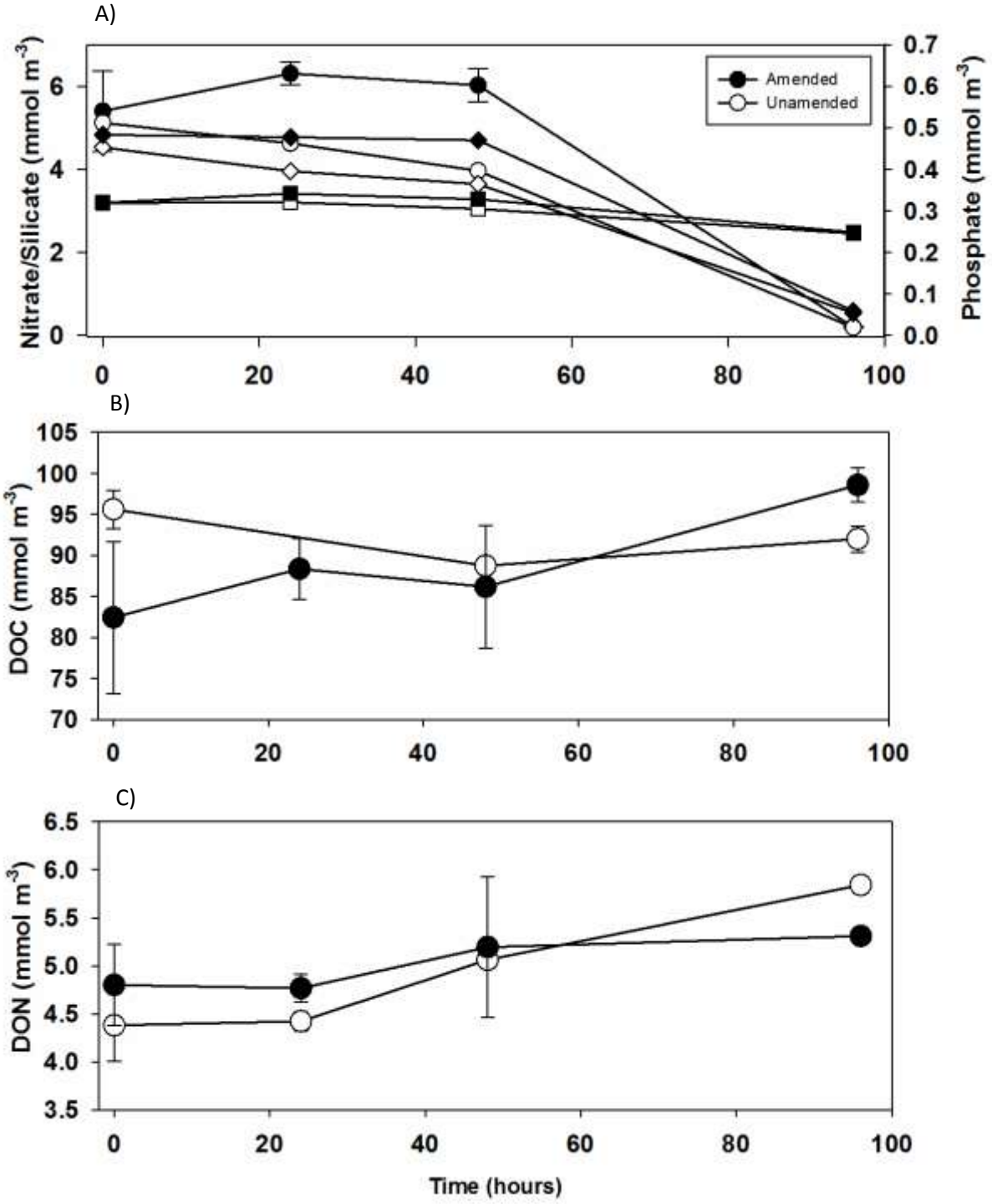

Figure 5.2: a) Inorganic nitrate (circles), phosphate (diamonds), and silicate (squares) and dissolved organic (c) carbon and (d) nitrogen for amended (open) and unamended (closed) incubations at 0, 24, 48 and 96 hours. Concentrations are in mmol m^{-3}. Error bars indicate the standard error from the mean concentration measured from duplicates of incubations where possible.

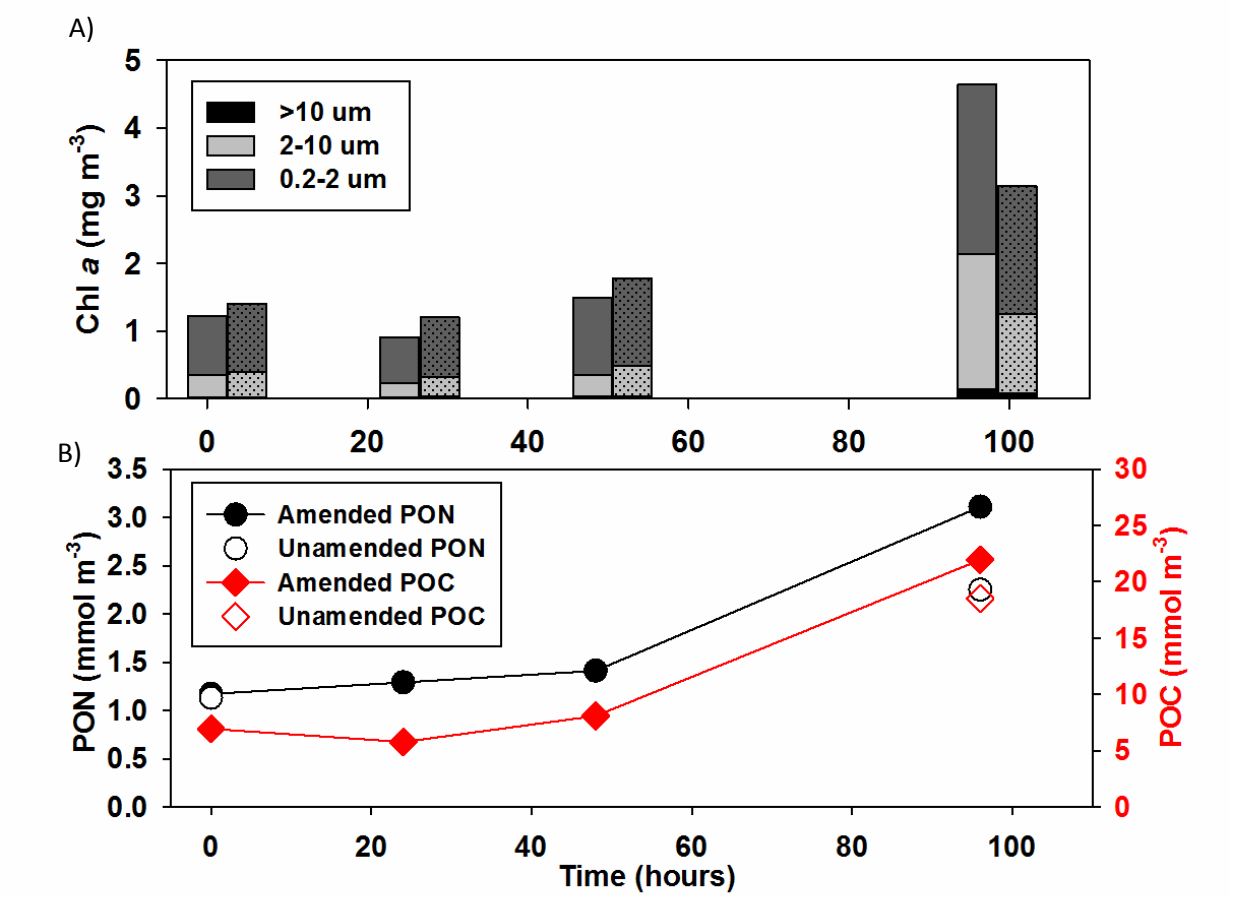

Figure 5.3: a) Size fractionated chlorophyll *a* concentrations as measured at 0, 24, 48 and 96 hours in the amended (block colour) and un-amended (spotted) incubations. The chl *a* concentrations are given for the smallest (0.2 to 2 µm; dark grey), medium (2 to 10 µm; light grey), and largest (>10 µm; black) size fractions. b) Particulate organic nitrogen (circles on black line) and carbon (diamonds on red line) for amended (open) and unamended (closed) incubations.

5.3.3. Biomass: particulate organic matter and chlorophyll

In the amended incubation, total chl *a* (i.e. the sum of all size fractions) increased > 3-fold during the 96 h incubation (1.4 mg m^{-3} to 4.7 mg m^{-3}), compared to the >2-fold increase observed in the unamended incubation (1.4 mg m^{-3} to 3.1 mg m^{-3}). The chl *a* in the 2-10 µm size fraction, which was mostly composed of small flagellates and dinoflagellates (e.g. *Gyrodinium sp*. and *Gymnodinium sp*.), increased by > 6-fold in the amended incubation. In the unamended incubations, the 2-10 µm size fraction of chl *a* concentrations increased by >3-fold (from 0.37 mg m^{-3} to 1.18 mg m^{-3}). The chl *a* associated with the >10 µm size fraction increased by >5-fold during the 96 h amended incubation despite only contributing 3% to total chl *a* at T-

final. In the unamended incubation the largest increase in chl *a* was observed in >10 µm size fraction, which increased >4-fold, though again this size fraction only contributed <3% to total chl *a* at T-final in the unamended incubation. Comparatively, the 0.2-2 µm size fraction increased by just <3-fold in the amended incubation and by <2-fold in the unamended incubation. However, this size fraction contributed 54% and 60% to the total chl *a* at T-final in the amended and unamended incubations respectively.

During the 96 h incubation, POC and PON concentrations increased by 3-fold (from 6.9 mmol m^{-3} to 21.9 mmol m^{-3} and 1.2 mmol m^{-3} to 3.1 mmol m^{-3} respectively) in the amended incubation, which resulted in an increase in the POC:PON ratio from 5.9 to 7.1 (Fig. 5.3b and 5.3c). In the unamended incubation, the PON concentration doubled in 96 h from 1.1 mmol m^{-3} to 2.3 mmol m^{-3}. POC increased by almost 3-fold from 6.9 to 18.5 mmol m^{-3} (Fig. 5.3b and 5.3a), resulting in the POC:PON ratio increasing from 6.1 to 8.2 in the unamended incubation.

5.3.4. Rates of primary production, bacterial production and bacterial respiration

Rates of total PP_{POC} increased by almost 6-fold from 8.14 mg C m^{-3} d^{-1} to 45.3 mg C m^{-3} d^{-1} over the course of the amended incubation (Fig. 5.4a). The 2-10 µm size fraction contributed 75% to total PP_{POC} at T_{final} and increased 9-fold (from 3.7 mg C m^{-3} d^{-1} to 34.0 mg C m^{-3} d^{-1}). The largest increase in the rate of PP_{POC} in the amended incubation was observed in the > 10 µm size fraction, which increased by almost 12-fold (from 0.23 mg C m^{-3} d^{-1} to 2.70 mg C m^{-3} d^{-1}) despite only contributing 6% of total PP_{POC}. This was larger than the increase observed in the unamended incubation. The total rate of PP_{POC} in the unamended incubation increased by 3-fold. The 2-10 µm size category contributed 81 % to total PP_{POC} at T-final, and increased by >3-fold over the unamended incubation (from 6.9 to 22.7 mg C m^{-3} d^{-1}; Fig. 5.4a). PP_{POC} associated with the 0.2-2 µm size fraction increased by 5.5-fold in the initial 48 hours of the incubation (from 2.9 to 15.8 mg C m^{-3} d^{-1}), but decreased to 4.1 mg C m^{-3} d^{-1} at T-final, contributing 16% to total PP_{POC} in the unamended incubation. Although the > 10 µm size fraction contributed only 3% to the total PP_{POC} at T_{final} in the unamended incubations, PP_{POC} associated with this size fraction increased by 6-fold within the initial 48 hours of incubation (from 0.29 to 1.71 mg C m^{-3} d^{-1}) and 4-fold in 96 h (0.29 to 1.09 mg C m^{-3} d^{-1}; Fig. 5.4a).

Bacterial activity and BCD increased over the course of the amended incubation (Fig. 5.4b and 5.4c). BP increased > 5-fold and the estimated BR increased by 3-fold

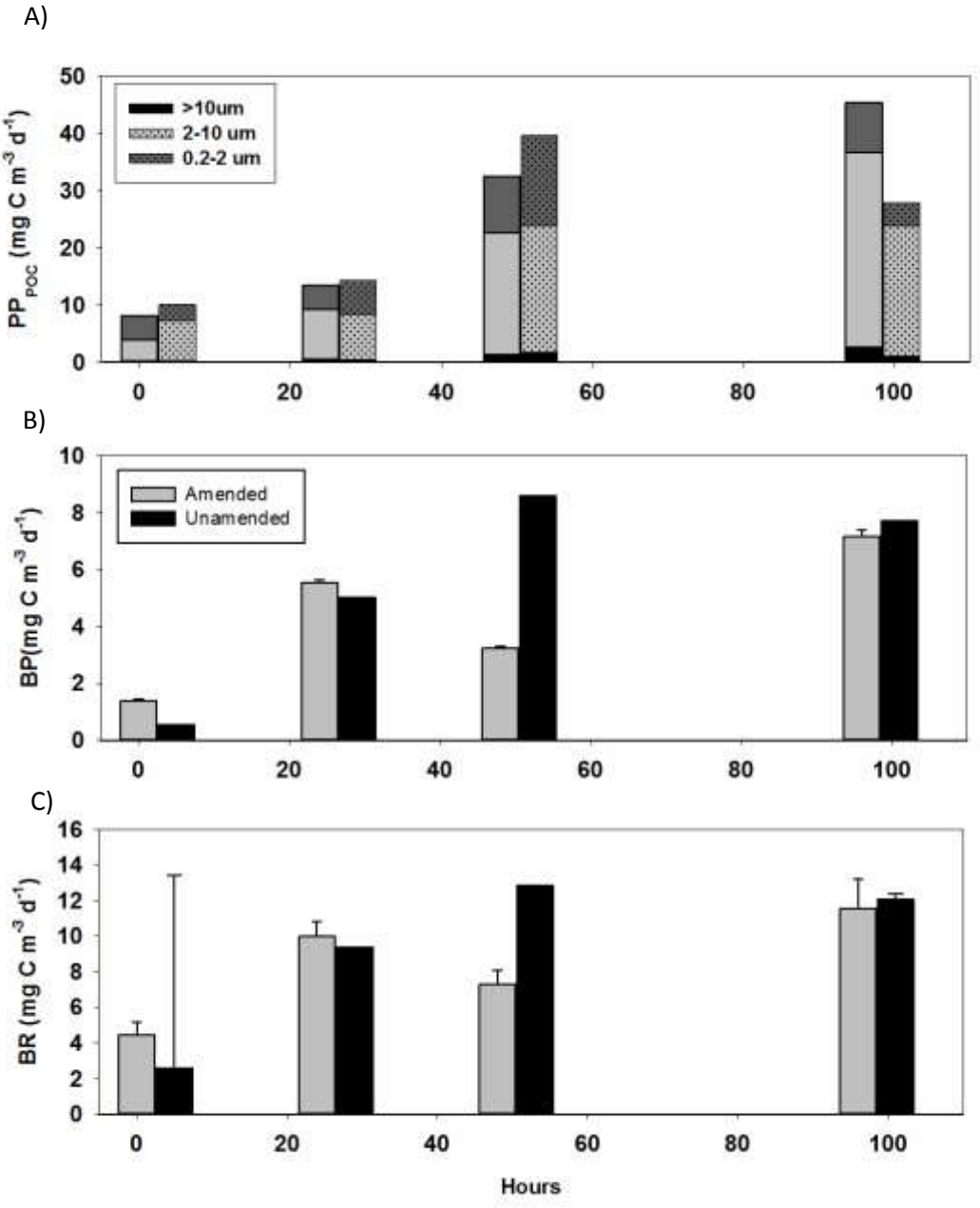

Fig 5.4: Rate measurements at 0, 24, 48 and 96 hours of a) size fractionated particulate primary (PP_{POC}) production from ^{14}C measurements from the amended (i.e. BML water addition; block colour bars) and unamended (spotted bars) incubations; and (b) bacterial production (BP), and (c) bacterial respiration (BR) for the amended (grey) and unamended (black) incubations.

over the entire amended incubation. The total cumulative BP was 18.2 ± 0.5 mg and BR was 34.7 ± 2.4 mg, and thus bacterial activity equated to a BCD of 52.9 ± 2.9 mg C m^{-3} d^{-1}.

Bacterial activity also increased over the course of the unamended incubation, BP increased >14-fold (0.55 mg C m^{-3} d^{-1} to 7.7 mg C m^{-3} d^{-1}), resulting in an associated 5-fold increase in the BR estimate. The total cumulative BP was 25.9 (±0.6) mg C m^{-3}, and the inferred BR was estimated as 42.1 (±4.8) mg C m^{-3}, giving a total BCD of 67.9 (±5.4) mg C m^{-3}, which is greater than that observed in the amended incubation. The amount of biomass synthesised relative to total C required for growth and respiration can be estimated via the bacterial growth efficiency (BGE=BP/BCD). In the amended incubations, the BGE was 34 ± 0.2% which is within the average of the documented estimated range for the ocean (1% to 67% range from oligotrophic to coastal waters respectively; del Giorgio & Cole, 1998). This BGE is lower than that observed in the unamended incubation (38 ± 0.1%), thus indicating a smaller amount of C being fixed into bacterial biomass relative to the total BCD in the amended incubation.

5.3.5. Carbon budget

The total nitrate assimilated during 96 h in the amended incubation was 5.2 (± 0.47) mmol m^{-3}, which using the Redfield C:N ratio is equivalent to 412 (± 39.6) mg C fixed into organic C via PP (Fig. 5.5; box 1). The ^{14}C method used to measure PP_{POC} measures new and regenerated production, and resulted in a cumulative total PP_{POC} estimate of 145 (±21.9) mg C fixed over the course of the incubation (Fig. 5.5; box 2). Evidently, there is a difference of 367 (±45.3) mg C between the potential nitrate driven production and the observed total PP_{POC}. As previously stated, estimates of PP using the ^{14}C technique represent net rather than gross PP due to the exudation of DOC. During the amended incubation, we observed an increase in DOC of 194 (± 17) mg C (Fig. 5.5; box 4). However, the increase in DOC concentrations represents the net increase, as some fraction of DOC exuded is assimilated by bacteria via BP and BR; the total represented by the BCD (BCD; Fig. 5.5; boxes 5, 6 and 7). The total cumulative BCD in the amended incubation was 53 (±2.87) mg C (Fig. 5.5; box 7). Accounting for the PP_{POC} (145 ± 22 mg C), net DOC increase

(194±17 mg C) and BCD (53 ±2.87 mg C) (Fig. 5.5; sum of box 2, 4 and 7), we estimate that the gross rate of primary production was 392 (±42) mg C. According to a statistical t-test ($p<0.05$), this is statistically similar to the estimate of C fixed from the observed nitrate uptake (412 ± 39.6 mg C m^{-2} d^{-1}), and means we can account for 95% (±10%) of the estimated C fixed from nitrate assimilation. The results imply that almost two-thirds of the C fixed in the amended incubation was exuded as DOC, and almost one third of the DOC exuded was used by bacterial to meet the BCD (Fig. 5.5).

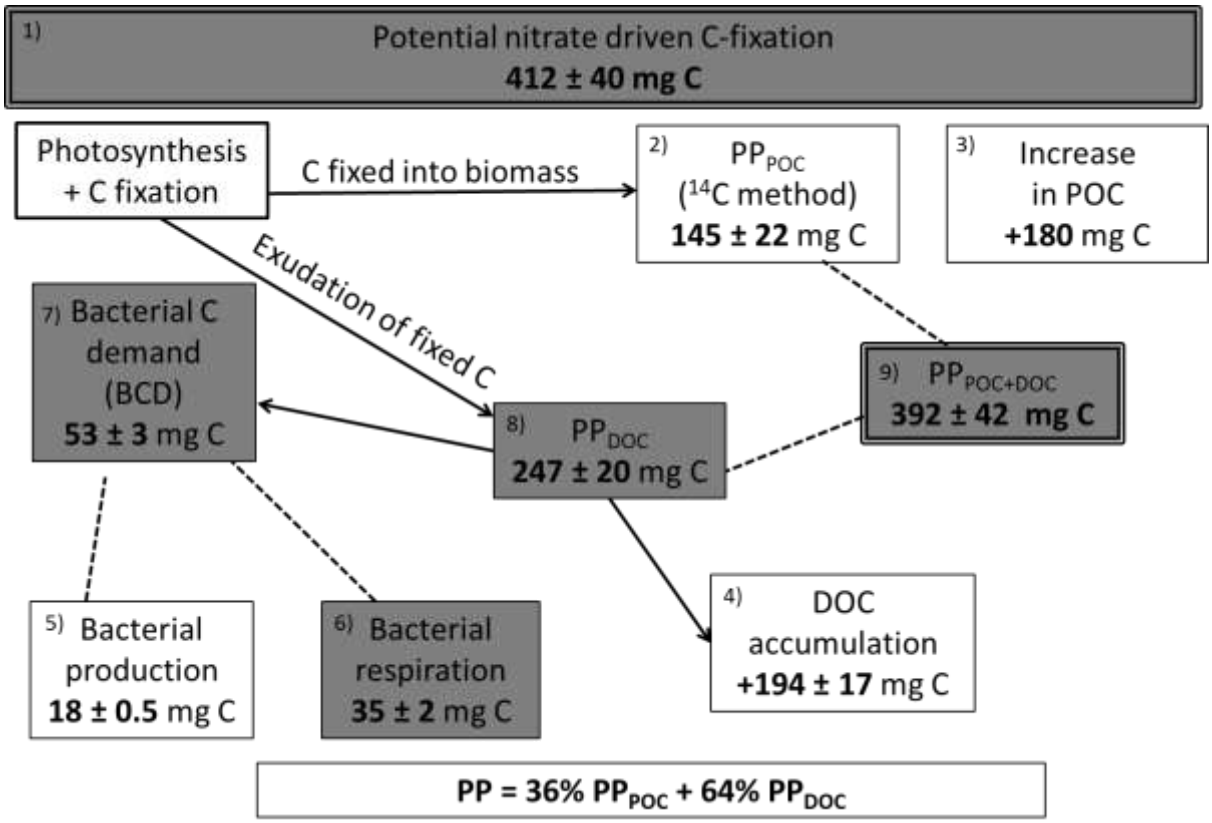

Figure 5.5: Total carbon partitioning over the course of 96 hour amended (10% vol:vol addition of BML water) incubation, where white boxes indicate measured variables and shaded boxes indicate estimates of C partitioning as described in text. Changes to the total carbon pool via primary production and bacteria activity rate measurements has been calculated as a cumulative amount of C over the 96 hour incubation (mg). Changes to measured particulate and dissolved organic C concentrations were taken as a net change from t-zero to t-final. Error bars are provided where possible. Numbered boxes are referred to in text.

Using a similar approach for the unamended incubation (Fig. 5.6), the total nitrate drawdown over the course of the experiment was 5.2 mmol m^{-3}, and the

estimated C fixed from the total nitrate assimilation via the Redfield ratio was 405.7 (±38.3) mg C (Fig. 5.6; box 1). However, the cumulative PP_{POC} measured using the ^{14}C method was 106.8 (±7.3) mg C (Fig. 5.6; box 2), leaving a difference of 298.9 (±45.6) mg C. As mentioned, PP_{DOC} was not directly measured in the incubations (Fig. 5.6; box 8), but DOC concentrations and the BCD were measured (Fig. 5.6; boxes 5, 6 and 7). In the unamended incubation, there was a small but insignificant decrease in DOC of 43.3 ±7.8 mg C in 96 h (Fig. 5.2c). The cumulative BCD in the unamended incubation (68 ± 6 mg C) was higher than the BCD observed in the amended incubation (53 ± 3 mg C). In the unamended incubation, the BCD exceeded or was equal to the rate of organic C production, which perhaps explains why we observed no increase in the DOC concentrations in the unamended incubation. Taking into account the net DOC change and the elevated BCD over the course of the unamended incubation we estimate a cumulative PP_{DOC} of 25±14 mg C (Fig. 5.6; box 8). Combining our cumulative PP_{POC} measurement and PP_{DOC} estimate we can account for 132±21 mg C being fixed ($PP_{POC+DOC}$), which was 32% (±5%) of estimated C fixed from the observed nitrate assimilation. Therefore, we were unable to account for approximately 274±43.7 mg (or 68%) of the C that was fixed, based on the conversion of nitrate uptake to C uptake via the Redfield ratio in the unamended incubation.

Considering the organic nutrient stoichiometry of the dissolved we found that the dissolved organic C:N ratio was initially high at 22 compared to Redfield stoichiometry but decreased to 16 in the unamended incubation. Comparatively, in the amended incubation the dissolved organic C:N ratio increased from 17 to 19. Although these ratios in both the unamended and amended incubation were still high relative to Redfield C:N stoichiometry. The particulate organic pool remained relatively close to Redfield stoichiometry in both the amended and unamended incubations though increased slightly over the course of the experiment. The amended POC:PON increased from 5.9 to 7.1, and the unamended increased from 6.1 to 8.2.

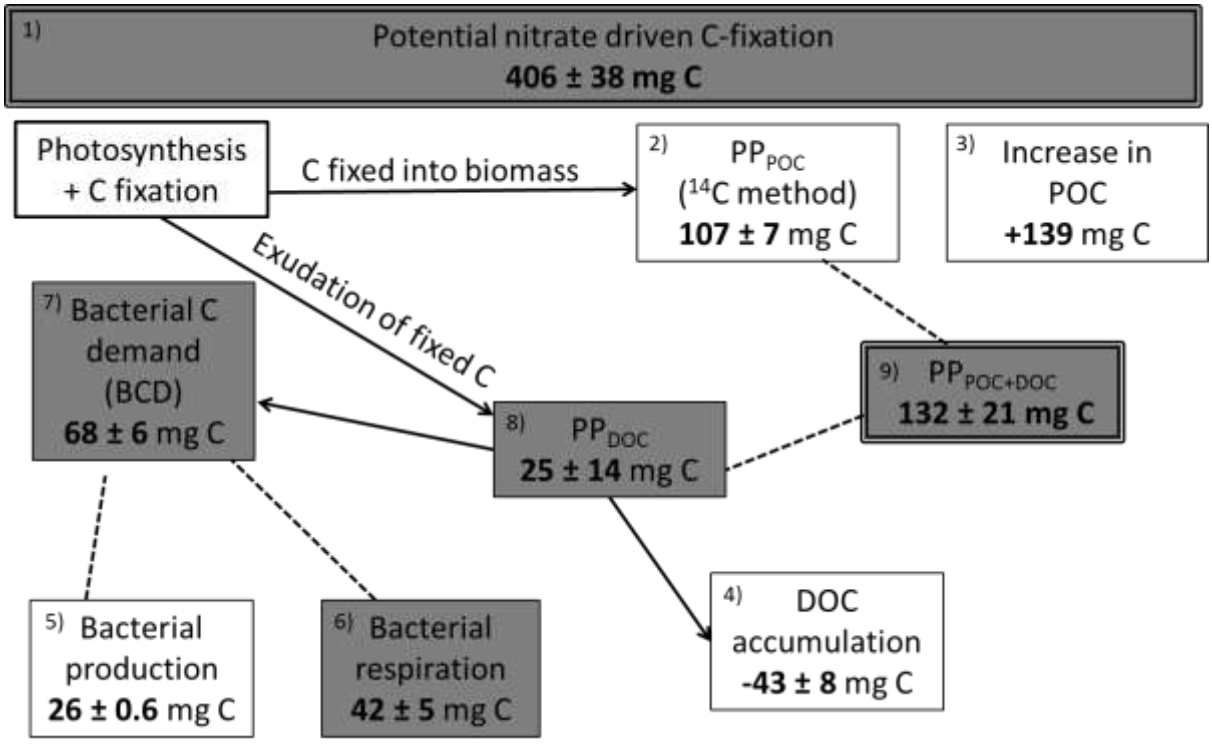

Figure 5.6: Total carbon partitioning over the course of 96 hour unamended incubation, where white boxes indicate measured variables and shaded boxes indicate estimates of C partitioning as described in text. Changes to the total carbon pool via primary production and bacteria activity rate measurements has been calculated as a cumulative amount of C over the 96 hour incubation (mg). Changes to measured particulate and dissolved organic C concentrations were taken as a net change from t-zero to t-final. Error bars are provided where possible and numbered boxes are referred to in text.

5.3.6. Community structure

Overall, changes in the abundance of phytoplankton and community structure were similar in the amended and unamended incubations (Fig. 5.7a). Diatom species, which mostly consisted of pennate *Nitzschia sp*. and *Navicula sp*., increased 10-fold during the unamended incubation (from 1000 cells L^{-1} to >10000 cells L^{-1}), but by 45-fold in the amended

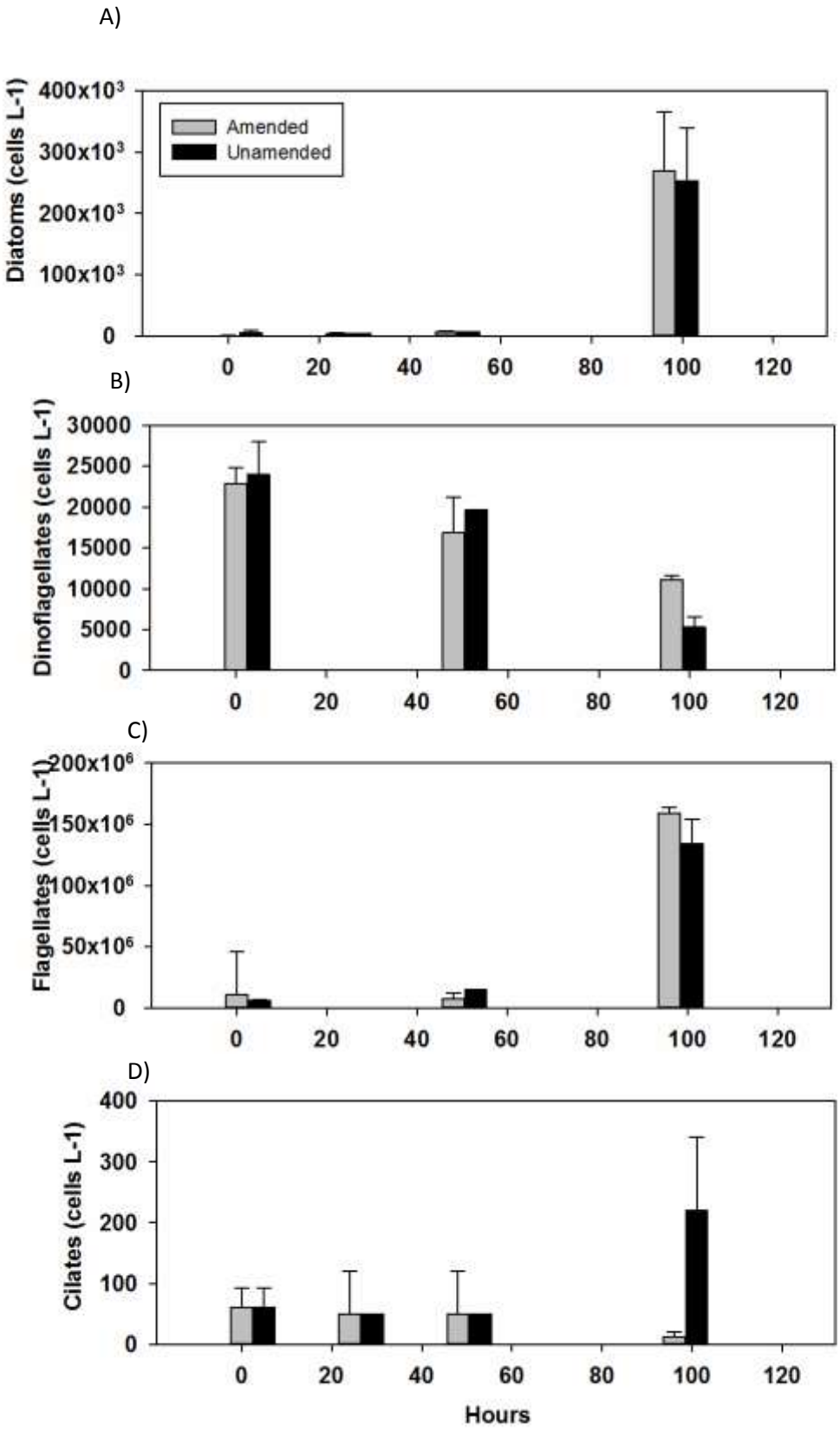

Figure 5.7: Phytoplankton community composition counted via light microscopy and sorted into functional groups of (a) diatoms, (b) dinoflagellates, (c) flagellates and (d) ciliates for the amended (grey) and unamended (black) incubations.

incubation (5200 cells L^{-1} to 238200 cells L^{-1}) (Fig. 5.7a). Almost 80% of the observed increase in diatoms in both incubations occurred 48 h after the start of the incubations. A small number of centric diatoms were also present in both amended and unamended incubations (*Lauderia sp*. and *Guinardia sp*.), although these contributed to less than 10% of the total diatoms counted. These diatoms were relatively small (10 µm to 30 µm). Dinoflagellates decreased by 50% (from 22500 to 10000 cells L^{-1}) and 80% (from 23960 cells L^{-1} to 5270 cells L^{-1}; Fig. 5.7b) in the amended and unamended incubations respectively. These were mostly comprised of *Gyrodinium* sp. and *Gymnodinium* sp., which have been documented as being mixotrophic and hence capable of both photosynthesis and phagotrophy, i.e., consumption of organic C (Stoecker, 1999). The abundance of small flagellates (1-2 µm) increased by more than 10-fold (1×10^7 cells L^{-1} to $>2\times10^8$ cells L^{-1}), and by 22-fold (from 1×10^7 cells L^{-1} to 1×10^8 cells L^{-1}) over the course of the amended and unamended incubations respectively. The only difference observed in the community between the amended and unamended incubations were the abundance of ciliates. Small mixotrophic ciliate species (20 µm; *Mesodinium* sp., *Strobilidium* sp. and *Strombidium* sp.) decreased by 80% (from 60 cells L^{-1} to 10 cells L^{-1}) during the amended incubation, though were observed to increase by 300% (from 60 cells L^{-1} to 220 cells L^{-1}) in the unamended incubation. These changes were observed after 48 h from the start of incubation time. However, it is important to note that the errors associated with enumerating mesozooplankton in the relatively small volumes of sample were large (Fig. 5.7d).

5.4. Discussion

5.4.1. Experiment set up and design

Based on estimates of diapycnal nitrate fluxes and assuming Redfield stoichiometry, wind-driven intermittent pulses of nutrients have been estimated to support between 33 and 71% of new production during summer in stratified shelf seas (Williams et al., 2013). However, there have been no direct studies to verify this estimate or to study the response of the phytoplankton in terms of nutrient drawdown, primary and secondary production and species succession to inputs of nutrient-rich water from the BML during such mixing events. Here we investigated the response of the plankton community from SCM to 1) a wind-driven mixing event

into the base of the thermocline (amended), and 2) isolation from any diapycnal fluxes (unamended), using a series of on-deck incubations conducted for 96 h. Assuming the nitrate concentration in the BML and SCM were approximately 10 mmol m^{-3} and 5 mmol m^{-3}, respectively (Fig. 5.1, see section 3.1), the 10% vol:vol addition in a volume of 10 L is equivalent to a 200 mmol m^{-2} d^{-1} flux of nitrate into the SCM. The conservative wind-driven nitrate flux to the base of the SCM has been estimated to be up to 81 mmol m^{-2} d^{-1}, although this is potentially an order of magnitude higher due to the under sampling of these short-lived events (Williams et al., 2013). Therefore, the amount of BML water that was added to the amended incubation here is representative of the SCM response to the upper limit of the wind-driven flux.

5.4.2. Biological C budget

Assuming Redfield stoichiometry, the observed nitrate drawdown would be expected to fuel approximately 400 mg C uptake in the amended and unamended incubations (412 ±40 mg C and 406 ±38mg C respectively). However, measurements of PP_{POC} represented only 35% and 26% of that predicted from nitrate assimilation in the amended and unamended incubations respectively. In both amended and unamended incubations, nitrate was drawn down to BLD in 96 h (Fig. 5.2a). An increase in POC was observed in both the amended (180 mg C) and the unamended (139 mg C) incubations respectively, and was of a similar magnitude (Fig. 5.5 and Fig. 5.6; box 3). This can be attributed to the increased PP_{POC} rates of 6-fold and 3-fold over the course of the amended and unamended incubations respectively. A certain proportion of C fixation via PP is leaked and/or exuded by phytoplankton and thus enters the DOC pool. Previous studies estimate that between 20% (Maranon et al., 2005) and 50% (Karl et al., 1998) of C fixed is exuded as DOC. However, grazing by zooplankton and viral/bacterial lysis of cells can result in up to 100% of photosynthetically fixed C being shunted into the dissolved pool where it is then available to fuel bacterial growth and respiration (Nagata, 2000). In the amended incubation, the cumulative BCD and increase in DOC were 53 ± 3 mg C and 194 ±17 mg C respectively (Fig. 5.5; boxes 7 and 4). By taking into account the observed DOC increase and as well as the DOC used to meet the BCD, we estimate the cumulative PP_{DOC} to be 247 ±22 mg C (Fig. 5.5; box 8). This means that 65% of the potential gross C fixed ($PP_{POC+DOC}$) was exuded as DOC, and more than

one third of the PP_{DOC} was consumed by bacteria (BCD). Thus, the gross amount of C fixed relative to nitrate drawdown could be accounted for in the amended incubation if we consider the partitioning of C into both dissolved and particulate pools.

In contrast, cumulative BCD was higher in the unamended (68 ±6 mg C; Fig. 5.6; box 7) than in the amended incubation, and DOC decreased (43 ±8 mg C) during the unamended incubation (Fig. 5.6; box 4). We can account for 132 ±21 mg C being fixed (PP_{POC} + PP_{DOC}) in the unamended incubation, but this is only 32% of the estimated nitrate driven C fixation, which leaves 274±59 mg C unaccounted for. In the unamended incubation there was a small but insignificant decrease in DOC implying that the BCD was equivalent to, or exceeded, DOC production. These observations suggest that the unamended system became net heterotrophic, as the amount of C consumed by bacteria was greater than the amount of organic C produced by autotrophs.

Despite partitioning of C between dissolved and particulate pools being different in the amended and unamended incubations, the change in community structure was similar (Fig. 5.7). Diatoms and flagellates, which were considered as mostly autotrophic species, increased following 48 h of incubation (Fig. 5.7a and 5.7c). Dinoflagellates decreased in both incubations. The only disparity between community changes in the amended and unamended incubations were the abundance of ciliates, which increased 4-fold in the unamended incubation but decreased to undetectable numbers in the amended incubation.

5.4.3. Explanation for differences between amended and unamended incubations

The initial conditions and outcomes of the amended and unamended incubations were relatively similar in terms of inorganic nutrient assimilation and community composition. However, there were 3 key differences between the incubations. There was good agreement between nitrate-driven C fixation and gross primary production in the amended but not unamended incubation. The response of bacteria differed between incubations and the abundance and growth of ciliates differed between incubations. The reason for the differences observed between incubations may have been due to a number of factors: 1) the community composition of water collected

from the BML, 2) difference in plankton C acquisition strategies, and 3) non-Redfieldian nitrate uptake. Here we will discuss these factors individually.

Community composition of BML addition water

The rates of bacterial activity were increased above the ambient SCM rates via the addition of BML water in the amended incubations. BP and BR were increased in the amended incubation by 150% and 45% 2 h after the addition of BML water in the amended incubation. Although there are no concurrent bacterial counts for this data set, a recent study in the Celtic Sea observed a higher abundance of bacteria above the thermocline than below (Davidson et al., 2013). This implies that bacterial abundance may have been diluted by the addition of water from the BML in the amended incubation. Instead, an increase in BP may have occurred in response to bacterial from the BML having access to more labile DOM in the waters collected from the SCM. An increase in BP has been observed previously via the addition of BML water to SML water (Davidson et al., 2013). Therefore the bacterial community in the amended incubation may have been different to that present in the unamended incubation. The utilisation of fresh organic matter in the amended incubation by bacterial from the BML may have resulted in the cycling of organic to inorganic nutrients, which are then available to autotrophs. Indeed, the ability of mesopelagic bacteria to assimilate dissolved organic matter more rapidly than surface dwelling bacterial communities has been observed in incubations conducted in the Sargasso Sea, where bacterial added to the mesopelagic zone remineralised DON faster than the surface bacterial community (Letscher et al 2012). This suggests that the bacterial communities differ between the SCM and BML in shelf seas but there is no evidence to support this. Additionally, the size and abundance of grazers may have differed between the amended and unamended incubations, which would have also influenced C budgets (see section 5.3.2).

Plankton C acquisition

The disparity between ciliate abundance in the amended and unamended incubations may have resulted from the addition of grazers (e.g., zooplankton) from water collected from the BML in the amended incubation. By isolating the SCM community from diapycnal fluxes of BML water in the unamended incubation, it is also possible that we excluded grazers and thus removed grazing pressure on the

ciliate community in the SCM allowing the abundance of ciliates to increase. Some species of ciliates, specifically *Mesodinium sp*., *Strombidium sp.* and *Strobilidium sp.* that were observed in both incubations have been reported to be mixotrophic plankton (e.g. Montagnes, 1996), and therefore capable of both photosynthesis and phagotrophy via consumption of organic C. Autotrophic phytoplankton with more efficient nutrient uptake strategies would likely outcompeted ciliates for inorganic nutrients in the unamended incubation. However, in the absence of grazing pressure, the ciliates may have been able to utilise their mixotrophic feeding strategy to consume organic C, which was being made readily available by autotrophic carbon fixation in the unamended incubation. Thus ciliate abundance may have been able to increase in the unamended via the absence of grazers and the ability to switch feeding strategies to heterotrophy, which would not have been accounted for in the bacterial production measurements.

We were unable to account for the potential nitrate driven C fixation in the unamended incubation. The combined BCD and the potential consumption of organic C by mixotrophic ciliates may have removed a significant amount of C from the DOC pool. The measurements of organic N can be used to investigate how the stoichiometry of the dissolved and particulate organic pools changed over the course of the experiments, and may help explain the observed unaccounted for C in our unamended C budget. The particulate organic pool remained relatively close to Redfield stoichiometry in both the amended and unamended incubations though increased slightly over the course of the experiment. The amended POC:PON increased from 5.9 to 7.1, and the unamended increased from 6.1 to 8.2. This suggests that the community in the incubations were acquiring C and N into their biomass relatively close to Redfield on average, though it should be noted that the POC and PON measurements incorporate ‘dead’ particulate matter also and does not measure phytoplankton biomass exclusively.

The dissolved organic C:N ratio decreased from 22 to 16 in the unamended incubation, but increased from 17 to 19 in the amended incubation. Although these ratios in both the unamended and amended incubation were still high relative to Redfield C:N stoichiometry, the change in C:N ratios over the course of the experiment suggest an accumulation of DOC relative to DON in the amended incubation. Conversely, in the unamended incubation, the decrease in the dissolved

organic C:N ratio may suggest that DOC was being consumed by mixotrophic ciliates over the course of the experiment. Grazing by ciliates alone may have consumed 67% (274±59 mg C) of the potential nitrate driven PP (406±38 mg C) in the unamended incubation.

The results from the unamended incubation highlight the importance of diapycnal fluxes to the SCM to maintain autotrophy, even over relatively short periods of time (i.e. 96 h). In the absence of the diapycnal supply of water from the BML, the system can rapidly switch to heterotrophy as we have observed in the unamended incubation.

Non-Redfieldian nitrate uptake

The potential primary production from the wind-driven nitrate flux was estimated in this study using the Redfield C:N ratio of 6.6:1, as in previous studies (Sharples et al., 2001a; 2001b; Rippeth et al., 2009). The adherence to Redfield stoichiometry may not have applied in this environment for a number of reasons. Previous observations have shown that excess nitrate may be assimilated by the SCM community in thermocline phytoplankton communities in summer (Hickman et al., 2012), although a considerable excess of nitrate uptake would be needed to explain the drawdown of almost 5 mmol m^{-3} and only 32% of the anticipated associated $PP_{POC+DOC}$ being observed in the unamended incubation. Furthermore, it is widely recognized that the internal nutrient stoichiometry of phytoplankton can vary considerably with species from the canonical Redfield ratio (Tett et al., 1985; Arrigo, 2005). In order to explain the observed nitrate drawdown and carbon accumulation in the unamended experiment by non-Redfieldian nitrate uptake, the community would have to drawdown nutrients at a C:N ratio of 2.1, which is much lower than the canonical Redfield ratio. However, another explanation is that there are differential timescales for C and N turnover, as well as the extrapolation of daily rate measurements for a total C fixation, which mean we may indeed underestimate PP in the incubations.

5.4.4 Conclusions and wider implications

The SCM community at the base of the thermocline (which are the realistically most likely to experience a wind-driven diapycnal flux) were not nutrient limited as they receive a constant supply of nutrient rich BML water (Sharples et al. 2001a). The experiment here therefore was not a nutrient addition experiment, but rather an investigation into the response of autotrophs and bacteria to the addition of water from the BML.

By simulating a large diapycnal flux of BML water into the SCM, the gross C fixed, was equal to the estimated C fixed via nitrate assimilation. While there was a significant increase in bacterial activity, the incubation remained autotrophic, that is, the amount of carbon produced by autotrophs was greater than that consumed by heterotrophs. By shutting the SCM off from diapycnal fluxes as we have in the unamended incubation, the gross C fixed did not equal the estimated C fixed via nitrate assimilation. In the unamended incubation the missing carbon (274 mg C) could not be allocated for and thus it is possible that we observed what could be described as a potentially heterotrophic response, i.e., the BCD and any heterotrophic consumption of C (including that by mixotrophic ciliates), was equal to or greater than carbon produced by autotrophs. The results from these incubations therefore highlight the importance of background nutrient fluxes in maintaining autotrophy in the SCM of shelf seas.

Most studies estimate the primary production generated from a nitrate flux by multiplying the flux by the C:N ratio of 6.6. Although this may be appropriate to estimate the total carbon fixed, we have shown that up to 60% of gross C fixed may be exuded as DOC. Though this proportion is high, some studies have suggested that up to 100% of photosynthetically fixed C is partitioned into the DOC pool (Nagata, 2000) and thus it is becoming increasingly apparent that the dissolved pool may account for a considerable proportion of fixed C in shelf seas.

A major implication of this study is that the majority of primary production supported by wind driven mixing events is shunted into the DOC pool and therefore not accounted for using the traditional C14 primary production methods. In Chapter 4, the wind driven nitrate flux was estimated to provide between one and two thirds of the annual shelf sea PP. However this estimate was based on

the extrapolation of C14 PP measurements of the particulate organic carbon (POC) pool only and did not take into account PP_{DOC}, therefore this may be an underestimate of shelf sea PP. The annual PP in the Celtic Sea is estimated between 21 to 46 g C m^{-2} y^{-1} (Hickman et al., 2012), the experiments presented here indicate that up to 60% of PP is shunted into the DOC pool and thus not measured. Therefore, the above estimate of annual PP would represent a mere 40% of the PP in shelf seas, thus the total PP in shelf seas accounting for the additional 60% (30 - 69 g C m^{-2} y^{-1}) not accounted for in the DOC pool would be more like ~51 – 115 g C m^{-2} y^{-1}. This updated $PP_{POC+DOC}$ estimate would also mean that the contribution of the wind-driven nitrate flux to annual shelf sea PP (15 g C m^{-2} y^{-1}) would be closer to 13-30% than up to ~70% as presented in Chapter 4.

The results presented here also indicate that more than one third of PP_{DOC} may be used by bacteria to meet their carbon demand. This has important implications for carbon export from shelf seas, whether carbon is exported to sediments off of the shelf in particulate form, physically exchanged in water containing DOC, or respired to CO_2. It has been suggested that dissolved organic nutrient pools rich in C may export organic C more efficiently off of the shelf into the deep ocean than particle export (Hopkinson et al. 2002, Hopkinson and Vallino, 2005; Lonberg et al. 2012). DOC is widely acknowledged as an important C pool in the open ocean (Karl et al. 1998), however we theorise that in the shelf sea SCM the exudation of DOC may account for a significant fraction of fixed C in response to diapycnal fluxes. Additionally, shelf seas are highly productive and responsible for up to 90% of the global fish catch. Thus the microbial loop may also be important in supplying C to the higher trophic levels in via grazers of bacteria (e.g., some ciliates such as Strombidium spp.).

The fate of organic matter in the ocean is vital to consider in order to understand the role of the ocean in climate change. Atmospheric CO_2 is fixed by primary producers in the upper ocean and transported to the deep ocean via the biological pump (see Chapter 1). The C fixed into phytoplankton biomass is then transported into the deep ocean by either sinking marine snow or as DOC. It is assumed that this organic material is remineralised in deep waters which is eventually ventilated at the sea surface via the thermohaline circulation. However, it is possible that some forms of DOC may act as long term C storage in the ocean

(Jiao et al., 2010). A large proportion of DOC is termed as recalcitrant (Jiao et al., 2010), and is capable of being stored for thousands of years in the deep ocean. Thus if a large proportion of the primary production in the shelf sea enters the DOC pool and is exported off of the shelf via the physical mechanisms mentioned above, it is possible that these regions also provide long term C export into the deep ocean exterior via the continental shelf sea pump (Chapter 1).

Thus the role of the microbial loop and DOC pools in the dynamic shelf sea environment, where time scales and residence times are relatively short, may be an extremely important process to consider when assessing the impact of physical mixing mechanisms on the global C budget.

5.5 References

Arrigo, K. R. 2005. Marine microorganisms and global nutrient cycles. Nature. **437**: 349-355.

Badr, E. A., E. P . Achterberg, A. D. Tappin, S. Hill, and C. B. Braungardt. 2003. Determination of dissolved organic nitrogen in natural waters using high-temperature catalytic oxidation. Trends in Analyt. Chem. **22:** 819-827.

Carrillo, C. J., and D. M. Karl. 1999. Dissolved inorganic carbon pool dynamics in northern Gerlache Strait, Antarctica. J. Geophys. Res. **104**: 15873-15884.

Chavez, F. P., and R. T. Barber. 1987. An estimate of new production in the equatorial Pacific. Deep Sea Res. **34**: 1229-1243.

Chin-Leo, G., and D. L. Kirchman. 1988. Estimating bacterial production in marine waters from the simultaneous incorporation of thymidine and leucine. Appl. Hydrobio. Beih. **31**: 19-26.

Davidson, K., L. C. Gilpin, R. Pete, D. Brennan, S. McNeill, G. Moschonas, and J. Sharples. 2013. Phytoplankton and bacterial distribution and productivity on and around Jones Bank in the Celtic sea.*in press*.

Dugdale, R. C., and J. J. Goering. 1967. Uptake of new and regenerated nitrogen in primary productivity. Limnol. Oceanogr. **12**:196-206.

Gieskes, W. W., G. W. Kraay, and M. A. Baars. 1979. Current 14C methods for measuring primary production: Gross underestimates in oceanic waters. Neth. J. Sea. Res. **13**: 58-78.

Hickman, A. E., C. M. Moore, J. Sharples, M. I. Lucas, G. H. Tilstone, V. Kristsov, and P. M Holligan. 2012. Primary production and nitrate uptake in the seasonal thermocline of a stratified shelf sea. Mar. Ecol. Prog. Ser. **463**: 39-57.

Hopkinson, C. S., and J. J. Vallino. 2005. Efficient export of carbon to the deep ocean through dissolved organic matter. Nature **433**: 142-145

Hopkinson, C. S., J. J. Vallino, and A. Nolin. 2002. Decomposition of dissolved organic matter from the continental margin. Deep-Sea Res. II **49**: 4461-4478

Jiao, N., G. Herndl, D. A. Hansell, R. Benner, G. Kattner, S. W. Wilhelm, D. L. Kirchman, M. G. Weinbauer, T. Luo, F. Chen, and F. Azam. 2010. Microbial production of recalcitrant dissolved organic matter: long-term carbon storage in the global ocean. Nature reviews Microbiol. 8:593-599.

Karl, D. M. D. V. Hebel, K. Bjorkman, and R. M. Letelier. 1998. The role of dissolved organic matter release in the productivity of the oligotrophic North Pacific Ocean. Limnol. Oceanogr. **43**: 1270-1286.

Karl, D. M., and J. E. Dore. 2001. Microbial ecology at sea: Sampling, subsampling and incubation considerations. In: J. H. Paul (ed.), Methods in Microbiology, vol. **30**: pp 13-39.

Kitidis, V., N. J. Harman-Mountford, E. Litt, I. Brown, D. Cummings, S. Hartman, D. Hydes, J. R. Fishwick, C. Harris, V. Martinez-Vicente, E. M. S. Woodward, and T. J. Smyth . 2012. Seasonal dynamics of the carbonate system in the western English Channel. Cont. Sh. Res. **42**:30-40.

Lonberg, C., and X. A. Alvarez-Salgado. 2011. Recycling versus export of bioavailable dissolved organic matter in the coast ocean and efficiency of the continental shelf pump. Global. Biogeochem. Cyc. 26 (3).

Mahaffey, C., K. Bjorkman, and D. M. Karl. 2012. Phytoplankton response to deep seawater nutrient addition in the North Pacific Subtropical Gyre. Mar. Ecol. Prog. Ser. **460**: 13-34.

Maranon, E., P. Cermeño, V. Pérez. 2005. Continuity in the photosynthetic production of dissolved organic carbon from eutrophic to oligotrophic waters. Marine Ecology Progress Series. **299:** 7-17.

Maruyama, S., T. Yabuki, T. Sato, K. Tsubaki, A. Komiya, M. Watanabe, H. Kawamura, and K. Tsukamoto. 2011. Evidences of increasing primary production in the ocean by Stommel's perpetual salt fountain. Deep Sea Res. **58**: 567-574.

Mills, M. M., C. Ridame, M. Davey, J. La Roche, R. J. Geider. 2004. Iron and phosphorus co-limit nitrogen fixation in the eastern tropical North Atlantic. Nature **429**:292−294.

Nagata T (2000) Production mechanisms of dissolved organic matter. In: Kirchman DL (ed.),
Microbial Ecology of the Oceans, 1st edn. Wiley-Liss, pp 121-152

Montangnes, D. J. S. 1996. Growth responses of planktonic ciliates in the genera *Strobilidium* and *Strombidium*. Mar. Eco. Prog. Ser. **130:** 241-254.

Redfield, A. C. 1958. The biological control of chemical factors in the environment. Amer. Scientist. **46**:205–221.

Rippeth, T. P., P. J. Wiles, M. R. Palmer, J. Sharples, and J. Tweddle. 2009. The diapycnal nutrient flux and shear-induced diapcynal mixing in the seasonally stratified western Irish Sea. Cont. Sh. Res. **29**:1580-1587.

Robinson, C. Heterotrophic bacterial respiration. In: Kirchman DL (ed.), *Microbial Ecology of the Oceans*, 2nd edn. John Wiley and Sons, pp 299-327

Rynearson, R., R. Lampitt, N. Poulton, K. Richardson, M Sieracki, and M. Perry. 2008. Return from the depths: examination of diatom resting cysts from the North Atlantic Bloom Experiment. Amer. Geophys. Union Fall meeting. Abstract no. OS31A-1254. AGU, San Francisco, CA

Simon, M., and F. Azam. 1989. Protein content and protein synthesis rates of planktonic marine bacteria. Mar. Ecol. Prog. Ser. **51**: 201-213

Simpson, J. H., W. R. Crawford, T. P. Rippeth, A. R. Campbell, and J. V. S. Cheok. 1996. The vertical structure of turbulent dissipation in shelf seas. J. Phys. Oceanogr. 26: 1579-1590.

Sharples, J., C.M. Moore, T. R. Rippeth, P. M. Holligan, D. J. Hydes, N. R. Fisher and J. Oceanogr. **46**:486–496. Simpson. 2001a. Phytoplankton distribution and survival in the thermocline. Limnol.

Sharples, J., C. Moore, and E. Abraham. 2001b. Internal tide dissipation, mixing, and vertical nitrate flux at the shelf edge of NE New Zealand. J. Geophys. Res. [Oceans]. **106:**14069–14081, doi:10.1029/2000JC000604.

Sharples, J., J. F. Tweddle, J. A. M. Green, M. R. Palmer, Y. Kim, A. E. Hickman, P. M. Holligan, C. M. Moore, T. P. Rippeth, J. H. Simpson, and V. Krivstov. 2007. Spring-neap modulation of internal tide mixing and vertical nitrate fluxes at a shelf edge in summer. Limnol. Oceanogr. **52**:1735–1747, doi:10.4319/lo.2007.52.5.1735.

Steeman Nielsen, E. 1952. The use of radioactive carbon (14C) for measuring organic production in the sea . J. Conseil, Conseil Perm. Intern. Exploration. Mer. **18:** 117-140.

Suratman, S., K. Weston, T. Jickells, and L. Fernand. 2009. Spatial and seasonal changes of dissolved and particulate organic C in the North Sea. Hydrobiologia. 628: 13-25

Tett, P., S. I. Heaney, and M. R. Droop. 1985. The Redfield ratio and phytoplankton growth rate. J. Mar. Biol. Assoc. U.K. **65:** 487 – 504.

Thomas, H., Y. Bozec, K. Elkalay, and H. J. W. de Baar. 2004. Enhanced open ocean storage of CO2 from shelf sea pumping. Science. **304**: 1005 – 1008, doi:10.1126/science.1095491.

Tomas, C. R .1997. Identifying marine phytoplankton. Academic Press, San Diego.

Utermöhl, H. 1931. Neue Wege in der quantitativen Erfassung des Planktons. (Mit besonderer Berücksichtigung des Ultraplanktons). *Verh. Int. Verein. Theor. Angew. Limnol.* **5**: 567–596

Wicks, R. J., and R. D. Robarts. 1988. Ethanol extraction requirement for purification of protein labelled with [^{3}H]leucine in aquatic bacterial production studies. Appl. Environ. Microbiol. **54**: 3191-3193.

Wilkerson, F. P., and R. C. Dugdale. 1992. The use of large shipboard barrels and drifters to study the effects of coastal upwelling on phytoplankton nutrient dynamics. Limnol. Oceanogr. **32**: 368-382.

Williams, C. A. J., J. Sharples, M. Green, C. Mahaffey, and T. P. Rippeth. 2013. The maintenance of the subsurface chlorophyll maximum in the western Irish Sea. **3**: 61-73.

Williams, C. A. J., J. Sharples, C. Mahaffey, and T. P. Rippeth. (accepted). The wind driven pulses of nutrients to phytoplankton in stratified shelf seas. Geophy. Res. Let.

Wollast, R. 1998. Evaluation and comparison of the global carbon cycle in the coastal zone and in the open ocean. In: Brink, K. H., Robinson, A. R. (Eds). The Sea, Vol 10. John Wiley and Sons, New York, 213 – 252.

6. Synthesis

6. Synthesis

Shelf seas are believed to play an important role in the oceanic export of carbon (C), with much recent scientific focus being placed on the 'continental shelf pump' (Tsunogai et al., 1999). Though the solubility pump dominates the flux of CO_2 between the atmosphere and the ocean (Canadell et al. 2007), the biological pump involves the assimilation of inorganic C. This not only supports higher trophic levels, but C can be buried and stored in sediments as particulate organic carbon (POC) (Muller-Karger et al., 2005), and transported off the shelf as organic C to the adjacent deep ocean interior (Tsunogai et al., 1999). Shelf seas are estimated to have an average C fixation rate per unit area a factor of ~2.5 greater than in the open ocean (Simpson and Sharples, 2012), and may transport POC to the seabed >3 times more efficiently than in the open ocean (Jahnke, 2010), where it can then be transported across the shelf edge to the adjacent shelf slope and deep ocean via circulation mechanisms (e.g., Wobus et al., 2011). In shelf seas the combination of highly energetic mixing induced by tides and dramatic changes in bathymetry, together with the euphotic zone being in close proximity to the seabed, lead to the potential for highly efficient C sequestration. Large-celled (> 5µm) phytoplankton species, such as diatoms, are thought to be particularly important for the export of POC (Legendre and Rivkin, 2002), and are commonly observed in shelf seas (e.g., Chapter 5). Indeed, a recent study estimates that nearly half of the biological pump transfer of C, in both dissolved and particulate pools, to the deep sea reservoir occurs at shelf sea regions (Jahnke, 2010).

Subsurface primary production in the shelf sea is now acknowledged to be as important as that generated during the spring bloom in terms of C fixation and the supply of organic C to the shelf sea ecosystem (Hickman et al., 2012; Simpson and Sharples, 2012). Furthermore, the presence of the sub-surface chlorophyll maximum (SCM) has been linked to CO_2 drawdown in shelf seas (Kitidis et al., 2012). Phytoplankton production and biomass is routinely monitored by remote sensing using surface maps of chlorophyll. However, these estimates of global primary production and phytoplankton biomass using satellites do not include the SCM (e.g., Behrenfield & Falkowski, 1997) as they are based on measurements of sea surface chlorophyll. Therefore, using satellite data to examine and quantify changes in

global primary production using satellites may be missing a considerable fraction of the water column primary production.

The turbulent supply of nitrate from below the thermocline is believed to limit the considerable production in the SCM (Rippeth et al., 2009). However the physical mechanisms that may influence this supply have not been fully quantified (Palmer et al., 2008). The internal tide and inertial oscillations are mechanisms which enhance shear at the pycnocline and potentially cause mixing (Rippeth, 2005). An upper estimate of the nitrate flux driven by the internal tide at the shelf edge during spring tides has been estimated as 9 mmol m^{-2} d^{-1} in the Celtic Sea (Sharples et al., 2007). A recent study by Tweddle et al. (2013) identify nitrate fluxes generated by internal wave mixing over banks in the interior of a shelf sea as supplying up to 50 mmol m^{-2} d^{-1} during spring tides. An important aspect of these internal wave-driven nitrate fluxes is that the higher fluxes are dominated by short-lived events of turbulent mixing at certain stages of the tidal cycle. These event-driven fluxes, generally associated with spring tides, have been estimated to support a significant fraction of new production on the shelf (Sharples et al., 2007; Tweddle et al., 2013). It is possible that these fluxes support the larger celled phytoplankton commonly seen at the base of the SCM, which are considered important for POC export (Legendre and Rivkin, 2002).

Two aspects of diapycnal nutrient fluxes to the SCM have been addressed in this thesis. First, wind-driven inertial oscillations are commonly observed in the ocean (Gill, 1982) and acknowledged to be an important mechanism for mid-water mixing (e.g., Simpson et al., 2002; Mackinnon and Gregg, 2005; Rippeth, 2005). Furthermore, wind-driven inertial oscillations have been identified as generating short-lived diapycnal mixing 'events' (Burchard and Rippeth, 2009). However, their influence on the turbulent supply of nitrate to the SCM phytoplankton community has not yet been quantified and has provided the main focus for the research described through this thesis. Second, there is a lack of evidence documenting the impact of diapycnal nitrate fluxes on primary production and community composition at the SCM. There are currently no estimates of the partitioning of fixed C into dissolved or particulate organic pools resulting from diapycnal mixing events, and yet this partitioning is a key uncertainty in current biogeochemical models (e.g. Blackford et al., 2004). This partitioning is particularly important in terms of

quantifying the export of C from the shelf, whether it is in dissolved or particulate form which controls the time scale of removal from the surface ocean and atmosphere. Research within this thesis has therefore expanded our knowledge of what impacts wind-driven nutrient pulses can have at the community level.

Here numerical, seagoing observational and experimental data have been used to investigate the hypotheses stated in section 1.5.

1) In tidally energetic shelf seas, new primary production in the SCM is sustained predominantly by diapycnal nitrate fluxes from the BML.

An important assumption underpinning previous work on rates of primary production in the shelf sea SCM is that a measurement of the diapycnal nitrate supply to the SCM quantifies the rate of new production within the SCM (e.g. Sharples et al., 2007; Tweddle et al., 2013); i.e. diapycnal nitrate fluxes dominate any other source of nitrate. Modelling of phytoplankton trajectories and growth within a tidally energetic shelf sea has, however, indicated that the transport of nitrate from the bottom mixed layer (BML) into the SCM within the cells of motile phytoplankton could be necessary for sustaining the SCM. Such transport would undermine the rationale behind measurements of diapycnal nitrate fluxes. The potential for phytoplankton to transport nutrients from the BML water to the SCM was investigated using a numerical model (Chapter 2). The model results showed that nutrient acquisition below the thermocline is unlikely to play a role in SCM maintenance in a tidally energetic shelf sea. Switching off nutrient assimilation below the thermocline produced no change in biomass at the SCM, suggesting that nutrient assimilation most likely takes place in the thermocline. Thus it is the physical supply of nitrate to the thermocline that is a key measurement for understanding shelf sea summer production. However, the model results also demonstrated that the turbulent-driven re-access of eroded biomass could play an important role in the maintenance of the SCM. The results of the model-based experiments in Chapter 2 for a tidally energetic shelf sea indicate that a measure of the diapycnal nutrient flux represents a real limit on the rate of primary production within the summer SCM.

An initial assessment of whether or not diapycnal nitrate fluxes could sustain known rates of primary production within the SCM was made using observations in the Western Irish Sea (WIS) (Chapter 3). There the diapycnal nitrate flux during a period of light winds and neap tides was measured, providing an estimate of the 'background' nitrate flux in the absence of any internal wave or inertial events in mixing. The nitrate flux measured in the WIS is the lowest observed in shelf seas to date (0.31 mmol m^{-2} d^{-1}; 95% C.I=0.22 to 0.43 mmol m^{-2} d^{-1}), and potentially drives 25 (95% C.I=17.0 to 34.3) mg C m^{-2} d^{-1} of primary production at the SCM. A small range in the confidence limits of the nitrate flux estimate indicated that there was little variability, and thus no evidence of mixing events at the time of sampling. By extrapolating the daily flux estimate over the summer (120 days) the background nitrate flux was estimated to supply 37.2 (95% C.I=26.4 to 51.6) mmol m^{-2} of nitrate annually to the SCM. Assuming Redfield proportions, this could support 3 g C m^{-2} y^{-1} of new production in the shelf sea. The contribution of this background nitrate flux to the total summer production was estimated to be between 7 and 30% using published primary production data from the Celtic Sea (Hickman et al., 2012) and WIS (Trimmer et al., 1999). This is equivalent to an *f*-ratio of between 0.07 and 0.3, which is lower than that observed in the shelf sea (0.3 to 0.5; Hickman et al., 2012). The implication is that the integrated new production driven by the background diapycnal flux of nutrients was significantly less than the new production expected over the summer period based on observations. Thus, this suggests that another source of nitrate is required, with the hypothesis (2) being that event-driven mixing, via the wind and/or non-linear internal waves, must be important for the supplying additional nitrate vertically into the SCM. Quantifying these event-driven fluxes is therefore important for estimating SCM primary production.

2) Diapycnal mixing events induced by wind-driven shear spikes will result in an enhanced supply of nitrate to the subsurface chlorophyll maximum.

The supply of nitrate to the SCM via wind-driven diapycnal mixing events was quantified in this study (Chapter 4). Wind-driven inertial oscillations were observed to provide the SCM with significant fluxes of nitrate over the background flux

during quiescent conditions. Using observations collected in June 2010 in the Celtic Sea during enhanced winds, measurements were made of the fluxes of nutrients into the thermocline driven by wind-driven inertial oscillations and their associated shear spikes (Chapter 4, Williams et al., *accepted*). Enhanced winds resulted in the shear vector within the thermocline rotating at the local inertial frequency (15.7 hours). The alignment of this vector and the wind direction corresponded with spikes of enhanced shear at the thermocline, agreeing with the observations of inertial oscillations made by Burchard and Rippeth (2009). These spikes of enhanced shear at the thermocline resulted in short-lived, intermittent turbulent dissipation spikes at the thermocline. During the period of inertial oscillations, the nitrate flux was estimated at 22 (2 to 81) mmol m^{-2} d^{-1}, which was a factor of 17 greater than the background nitrate flux into the SCM (1.3 mmol m^{-2} d^{-1}; 95% C. I=1.0 to 1.6 mmol m^{-2} d^{-1}). However, the sampling resolution of turbulent dissipation using the free-fall turbulence profiler did not capture the maximum wind-driven shear and potential peak in mixing, and thus we may have underestimated mixing from inertial oscillations. This study thus provides evidence that wind-driven inertial oscillations will supply the SCM with additional nitrate.

3) This nitrate flux will stimulate primary production in the phytoplankton community at the SCM.

The response of the plankton and bacteria community at the SCM to both 1) a wind-driven mixing event, and 2) isolation from background mixing were investigated experimentally in terms of the nitrate drawdown, primary production into dissolved and particulate pools (i.e., PP_{POC} and PP_{DOC} respectively), bacterial production and plankton species abundance and succession (Chapter 5). Currently, the experiment presented in Chapter 5 provides the only measurements on the response of the community at the shelf sea SCM to a mixing event as most studies have focused on the upwelling of nutrients from the BML into the nutrient limited surface mixed layer (SML) (e.g. Davidson et al., 2013).The findings from Chapter 4 indicated that wind-driven inertial oscillations will deliver nutrients to the base of the SCM, but that BML water is unlikely to be mixed through the thermocline and up into the nutrient limited surface layer. Thus the experimental set up presented in Chapter 5 was a representation of a wind-driven diapycnal mixing event that

supplied nutrients to the lower SCM and not the SML. This study highlighted that the plankton community at the SCM are rarely limited by nitrate due to the constant supply from the BML. Despite conducting an experiment that was equivalent to a nitrate flux of ~200 mmol m^{-2} d^{-1} into the SCM, the concentration in the experiment did not change significantly due to the concentration of nutrients already present in water collected from the SCM. However, the addition of water from the BML to water collected from the SCM increased the activity of bacteria. Dissolved organic matter concentrations are generally higher at the SCM than BML (Davidson et al., 2013), and this was the case in the Celtic Sea (A. Panton, personal communication; Davidson et al 2013). Furthermore the organic matter situated at the SCM is more labile in nature, and thus more bioavailable to bacteria, whereas organic matter in the BML generally represents non-labile fractions (Hansell, 2002). Bacteria upwelled from the BML are therefore likely to respond to the availability of fresh dissolved organic material by increasing their activity and potentially remineralising organic matter and releasing inorganic nutrients, which are available to autotrophs. Many studies focus on the turbulent supply of nitrate during mix events, whereas here the impact of mixing on the redistribution of autotrophs and heterotrophs (including bacteria and grazers) has been identified as important. In terms of C partitioning at the SCM, this study shows that in the shelf sea SCM the exudation of DOC may account for a significant fraction of fixed C in response to diapycnal fluxes (Chapter 5). When exposed to a mixing event, the drawdown of nitrate by the phytoplankton community at the SCM could be accounted for by gross carbon C fixation into dissolved and particulate organic pools according to the Redfield C:N ratio. However, this study found that it is possible that up to two thirds of carbon C fixed by the SCM community is exuded into DOC, and approximately 30% of the DOC enters the microbial loop to meet the bacterial carbon C demand. This has important implications for carbon C export from shelf seas, whether carbon C is exported to sediments off of the shelf in particulate form, physically exchanged in water containing DOC, or respired to CO_2. In an area supporting a large proportion of global fish stocks this also has important implications for higher trophic levels, which may be partially supported by C supplied via the microbial loop. Carbon C fixed by the community at the SCM may be exported off of the shelf as DOC during the exchange of waters between the shelf and the open ocean (Hopkinson et al., 2002; Hopkinson and Vallino, 2005). Therefore, the processes which exchange shelf

water such as downwelling, filaments, eddy exchange, cascading or transport through slope current bottom Ekman layer (Ivanov et al., 2004; Hill, 1998; Huthnance, 2001; 2009) may have a more significant role in shelf sea C export than previously acknowledged.

Without the diapycnal supply of BML water, the application of Redfield C:N ratio was shown to be inapplicable, and therefore the system was believed to become heterotrophic. Although there are a variety of reasons for this, this study hypothesised that the diapycnal mixing of BML water into the SCM introduces grazers and a different bacteria community, as well as constantly supplying nutrients. Additionally, mixotrophic ciliate species at the SCM were able to grow in the absence of diapycnal fluxes, perhaps due to exclusion of zooplankton grazers that reside in the BML. Consumption of organic C by mixotrophic ciliates may have contributed to the system switching from being autotrophic to heterotrophic when water from the SCM was isolated from BML water. Thus, Chapter 5 demonstrated that the DOC pool and heterotrophic consumption of organic C in the shelf sea is likely to be an important process to consider when assessing the impact of physical mixing mechanisms on the global C budget. However, there are few observations of bacterial activity, including production and respiration, in shelf seas.

4) Wind-driven inertial oscillations are significant for annual production in shelf seas.

Chapter 4 demonstrated, using documented observations (Sherwin, 1987), that approximately 9 wind-driven inertial events occur every summer, with each event potentially supplying an average of 22 (2 to 81) mmol m^{-2} d^{-1} of nitrate to the SCM over the time of the wind event (typically 1 to 2 days). The total supply of nitrate to the SCM during summer via wind-driven inertial oscillations was therefore estimated to be 197 (19 to 728) mmol m^{-2} y^{-1}, with the potential to support 15 (1.5 to 58) g C m^{-2} y^{-1} of nitrate-driven production annually in the SCM (Fig. 6.1). The total (new + regenerated) shelf sea summer production estimate extrapolated from Hickman et al. (2012) in the Celtic Sea is between 20 and 47 g C m^{-2} y^{-1}, thus wind-driven nitrate fluxes could support between 33% and 71% of the total summer SCM PP. These findings imply that between one to two thirds of the summer primary

production may be unaccounted for in models which do not simulate inertially-generated shear spikes correctly. For example, the NEMO (Nucleus for European Modelling of the Ocean) model is widely adopted for European shelf seas, and is unable to predict these stochastic mixing events driven by wind-driven inertial oscillations. More recently the POLCOMS (Proudman Oceanographic Laboratory Coastal Ocean Model) is being developed to accurately predict wind-driven inertial mixing events. In Chapter 3 this study estimated that the daily background diapycnal nitrate flux was of the order of approximately 0.3 mmol m^{-2} d^{-1}. By extrapolating this daily flux over the summer (120 days), the background diapycnal mixing can be expected to provide approximately 36 mmol m^{-2} y^{-1} of nitrate to the SCM (Fig. 6.1), which is capable of supporting ~3 g C m^{-2} y^{-1} of nitrate driven production. The background nitrate flux and wind-driven nitrate flux will occur over the entire shelf sea, and the potential nitrate driven production by the combination of both mechanisms accounts for between 38% and 90% of the total summer PP measured by Hickman et al. (2012). This suggests an *f*-ratio of between 0.38 and 0.9, and therefore indicates that a large proportion of summer PP is new production driven by the turbulent supply of nitrate to the SCM, which is largely influenced by wind driven mixing. Alternatively, this may suggest that the documented PP estimates by Hickman et al. (2012) do not reflect an average summer PP responding to several episodic wind events, and are thus underestimated. This is discussed further in the following section.

Therefore, the research presented here has supported the overarching hypotheses of this thesis (section 1.5):

- *In tidally energetic shelf seas, sustaining primary production in the SCM is controlled by diapycnal nitrate fluxes from the BML*.
- *Diapycnal mixing events induced by wind-driven shear spikes do result in an enhanced supply of nitrate to the subsurface chlorophyll maximum.*
- *The wind-driven flux stimulates primary production in the phytoplankton community at the SCM.*
- *And, wind-driven inertial oscillations are significant for annual production in shelf seas.*

This thesis has identified and quantified the importance of wind-driven inertial oscillations for the diapycnal supply of nitrate to the SCM, and demonstrated the potential importance of these short-term mixing events in sustaining primary production during the summer in shelf seas. Background diapycnal mixing does not provide the SCM with the nitrate needed for the measured summer production and the acquisition of nutrients below the thermocline is not significant for maintenance of the SCM. This study has also highlighted that diapycnal mixing events may affect the distribution of grazers and bacteria in the SCM, which is also likely to influence primary production and the partitioning of C. Furthermore, this study has illustrated that a significant amount of PP may be exuded into the DOC pool and the estimate of PP from the Celtic Sea that is referred to here (Hickman et al., 2012), is a measurement of PP_{POC}. Short-falls and accuracy of PP measurements are discussed further in the following section.

With these first estimates of the flux of nitrate supplied by wind-driven inertial oscillations, event-driven mixing is firmly acknowledged as providing significant fluxes of nitrate to SCM in shelf seas, via internal tidal waves at the shelf edge (Sharples et al., 2007) and over banks (Tweddle et al., 2013), and wind driven inertial oscillations (this study). Biogeochemical numerical models do not incorporate event-driven mixing generated by these processes, and thus may not accurately estimate primary production in shelf seas. An example of a shelf sea biophysical model which is unable to predict wind-driven inertial mixing events is provided by Sharples & Simpson (2012), the implementation of this model for exploring shelf sea primary production has been well documented (Sharples & Tett, 1999; Sharples et al., 2006; Sharples, 2008; Simpson and Sharples, 2012)).

Shelf sea annual nitrate-driven production can be roughly approximated by considering nitrate driven production occurring during the spring bloom and at the SCM during summer. The contribution of each diapycnal mixing mechanism to total nitrate driven production in shelf seas can be approximated by taking into account the background nitrate flux from this study, the flux driven by the internal tide (Sharples et al., 2007; Tweddle et al., 2013) and the flux driven by inertial oscillations from this study. Figure 6.1 provides a schematic of all documented

diapycnal mixing mechanisms in the shelf sea and associated nitrate supply (mmol m^{-2} y^{-1}).

The nitrate flux driven by non-linear tidal internal waves at the shelf edge in the Celtic Sea has been documented as being up to approximately 9 mmol m^{-2} d^{-1} during spring tides, and 1.3 mmol m^{-2} d^{-1} during neap tides (Sharples et al., 2007). The mean daily nitrate flux driven by spring-neap modulated internal waves at the shelf edge is therefore approximately 5.2 mmol m^{-2} d^{-1}. Extrapolating this over the summer period (120 days), indicates that the internal tide may supply on average up to 618 mmol m^{-2} y^{-1} over the region near the shelf edge, which accounts for approximately 6% of the area of the Celtic Sea (Fig. 6.1). Following Redfield C:N proportions (6.6:1), this nitrate supply can potentially drive up to 49 g C m^{-2} y^{-1} of new production at the shelf edge over the summer (Fig. 6.1). Mixing events generated by tidal flow over a bank are estimated to reach up to 50 mmol m^{-2} d^{-1} during spring tides (Tweddle et al., 2013), with a background nitrate flux of ~1 mmol m^{-2} d^{-1}. Using a similar approach, the mean tidally modulated nitrate flux generated over a bank is estimated to be 25 mmol m^{-2} d^{-1}. Over the summer period this is extrapolated to provide up to 3120 mmol m^{-2} y^{-1} of nitrate to the SCM over banks, which occupy approximately 10% of the shelf (Sharples et al., 2013). Using the Redfield C:N ratio, fluxes over banks are capable of supporting 247 g C m^{-2} y^{-1} of production annually (Fig. 6.1).

For the Celtic Sea it is possible to extrapolate these estimates of nitrate driven production provided in Fig. 6.1 over the area that each mechanism occurs, and thus assess their relative contributions to annual nitrate driven production. The Celtic Sea has a surface area of approximately 93500 km^2. The annual nitrate driven production consists of that occurring in both the spring bloom and the summer SCM. An estimate of the nitrate-driven production occurring over the entire Celtic Sea during the spring bloom can be made by assuming a surface mixed layer depth of 20 m with a nitrate concentration of 7 mmol m^{-3} at the initialisation of stratification (Hydes et al., 2004). This equates to a nitrate supply of 140 mmol m^{-2} of the Celtic Sea, giving a total of 1.3 $\times 10^{13}$ mmol of nitrate in the Celtic Sea SML at the onset of stratification. This entire amount of nitrate in the surface mixed layer is believed to be assimilated during the spring bloom to support nitrate-driven production. Assuming the Redfield C:N ratio this is equivalent to 1×10^{12} g C of nitrate driven

production occurring over the spring bloom (Table 6.1). During summer, the nitrate supplied via background mixing (36 mmol m^{-2} y^{-1}; Fig. 6.1) and wind-driven inertial oscillations (198 mmol m^{-2} y^{-1}; Fig. 6.1) will occur over the entire Celtic Sea also. Extrapolation of the nitrate flux generated from background mixing during summer over the entire Celtic Sea area gives 3.4×10^{12} mmol y^{-1}, which is capable of supporting 2.7×10^{11} g C y^{-1} of nitrate-driven production at the SCM (Table 6.1). Extrapolation of the annual nitrate flux resulting from wind-driven inertial oscillations (Fig. 6.1), over the entire Celtic Sea area gives 1.9×10^{13} mmol y^{-1}, which is capable of supporting 1.5×10^{12} g C y^{-1} (Table 6.1).

Process	**Total nitrate supplied in Celtic Sea (mmol y^{-1})**	**Potential nitrate driven production (g C y^{-1})**	**%age contribution to annual new PP**
Spring bloom	1.3×10^{13}	1×10^{12}	19%
Background flux	3.4×10^{12}	2.7×10^{11}	5%
Wind-driven inertial oscillations	1.9×10^{13}	1.5×10^{12}	28%
Non linear internal tidal waves	3.5×10^{12}	2.7×10^{11}	5%
Bank generated	2.9×10^{13}	2.3×10^{12}	43%
Total	**6.8×10^{13}**	**5.3×10^{12}**	

Table 6.1: Contributions to annual new production by documented processes in the Celtic Sea estimated by their nitrate supply.

Bank generated mixing will occur over 10% of the Celtic shelf sea (9350 km^2), as this is the area approximated to be occupied by banks (Sharples et al., 2013). Extrapolating the estimate of the annual nitrate supply via bank generated nitrate fluxes (3120 mmol m^{-2} y^{-1}), over an area of 9350 km^2 (10% of the area of the Celtic Sea) gives a total nitrate supply of 2.9×10^{13} mmol y^{-1} (Table 6.1). This is capable of supporting 2.3×10^{12} g C y^{-1} of nitrate driven production in the Celtic Sea.

Non linear internal tidal waves are generated at the shelf edge, which occupies approximately 6% (5600 km^2) of the Celtic Sea. Extrapolation of annual nitrate supplied by the internal tide over the area where this mixing occurs in the Celtic Sea gives 3.5×10^{12} mmol y^{-1}, which may potentially support 2.7×10^{11} g C y^{-1} of nitrate driven production (Table 6.1). The summary of these estimates are presented in Table 6.1 for comparison.

Thus for the Celtic Sea, the turbulent supply of nitrate from wind-driven inertial oscillations may support approximately 28% of the annual new production. Bank generated mixing appears to play a dominant role in supporting nitrate driven production in shelf seas (43% contribution to cumulative nitrate driven production). Inaccurate representation of shelf sea bathymetry and wind forcing in shelf sea models (e.g., the POLCOMS and NEMO shelf sea models), therefore may mean that up to 71% of new production in the shelf sea is not accounted for.

Nitrate supplied to the SCM via the mechanisms outlined in Fig. 6.1 does not reach the surface mixed layer during summer and thus is assumed to be assimilated by the SCM community. Additionally, in contrast to the spring bloom, PP occurring at the SCM is not visible at the sea surface, and thus satellite based measurements of PP are missing a significant proportion of annual nitrate driven production (e.g. Behrenfeld and Falkowski, 1997). Table 6.1 indicates that the spring bloom accounts for roughly 19% of annual nitrate driven production, and thus 81% may be unaccounted for via satellite based measurements of PP.

If the nitrate supplied by the mechanisms outlined in Fig. 6.1 were in excess of phytoplankton requirements, nitrate would be measurable in the surface mixed layer, which it is not. Bottle measurements of primary production do not take into account the intermittent fluxes outlined here, and are thus isolated from potential sources of nitrate. Measurements of PP may therefore be underestimated as a result of this isolation. This thesis has also highlighted the importance of the DOC pool in shelf sea production. We have shown that up to two thirds of C fixed by phytoplankton may be exuded as DOC. Most estimates of primary production are based on the measurement of ^{14}C assimilated into biomass (i.e., the particulate primary production; PP_{POC}), and does not account for the C exuded into the dissolved pool. The estimate of primary production used in Chapters 3 and 4 to

quantify the relative contributions of mixing processes to primary production (Hickman et al., 2012) is based on PP_{POC} measurements. Thus Chapters 3 and 4 could well be underestimating the summer primary production and consequently overestimating the contribution of mixing processes to total primary production in these chapters. However, the estimate calculated above in Table 6.1 of annual nitrate driven production in the Celtic Sea indicates that wind-driven inertial oscillations may be responsible for roughly a third of all nitrate driven production.

It is important to note that the results presented in this study are limited in time and space and extrapolation of isolated primary production rate measurements to cumulative annual primary production estimates may present inaccuracies. The variability of turbulence at the thermocline has been highlighted in this study. It is likely that measurements of turbulent dissipation could be underestimated. The findings here have highlighted the importance of sampling resolution in terms of quantifying turbulent fluxes of properties due to the stochastic and short-lived nature of mixing events. Additionally, the shelf sea has an irregular bathymetry, the importance of which for nitrate fluxes has been recently highlighted by Tweddle et al. (2013). The magnitude of wind-driven inertial oscillations are likely to vary depending on where in the shelf sea turbulence and nitrate are measured, the extrapolation of nitrate flux estimates over the entire shelf may be ambitious.

The findings on carbon partitioning by the SCM community documented here are based on the measurements from experimental incubations, which have numerous well-acknowledged short-falls (Karl and Dore, 2001). The SCM is not a homogenous ecosystem, and patchiness in phytoplankton, particulate organic matter and grazers are inevitable. Furthermore, the time and space scales of physical and biological process vary enormously (Dickey, 1991). Thus the sampling of 'snap-shots' of water from one location and the extrapolation of those measurements is indeed ambitious.

Irrespective of these limitations, wind-driven inertial oscillations increase the turbulent supply of nitrate significantly. Storms over the North Atlantic increase when the North Atlantic Oscillation (NAO) index is strongly positive (Dawson et al., 2002). The frequency and intensity of storms over the North Atlantic may change in the future due to the North Atlantic Oscillation varying (Hu and Wu, 2004). It is

possible that these future changes may result in an increase in intermittent inertial mixing events. The work in this thesis has demonstrated that wind-driven inertial oscillations are an important mixing process, and need to be considered in order to gain accurate shelf sea C fixation rates. Thus future numerical models need to accurately represent event-driven mixing in order to accurately quantify the shelf sea primary production. At present this stochastic events are not captured in physical models of the coastal or shelf seas (e.g., POLCOMS) Furthermore, the partitioning of C into dissolved and particulate fractions by the SCM has been shown here to vary significantly. Additional research needs to be applied to the partitioning of C into dissolved and particulate pools by the SCM community, which has been shown here to be sensitive to diapycnal fluxes. The potential for mixotrophic species has only been touched on in this thesis, although mixotrophs have been documented as being an abundant SCM species (Chapter 5). The triggers for changes in mixotrophic C acquisition strategies is an important factor to take into account when considering the importance of turbulent nutrient supply and C flow in shelf seas. Additionally, the focus of much scientific literature has been on the nutrients that are supplied by turbulent mixing, this thesis proposes that the mixing of BML water also has important implications in terms of introducing different bacteria communities to euphotic zone. Further research on the importance of the heterotrophic community (including bacteria and mixotrophic plankton) to primary production at the SCM is therefore needed.

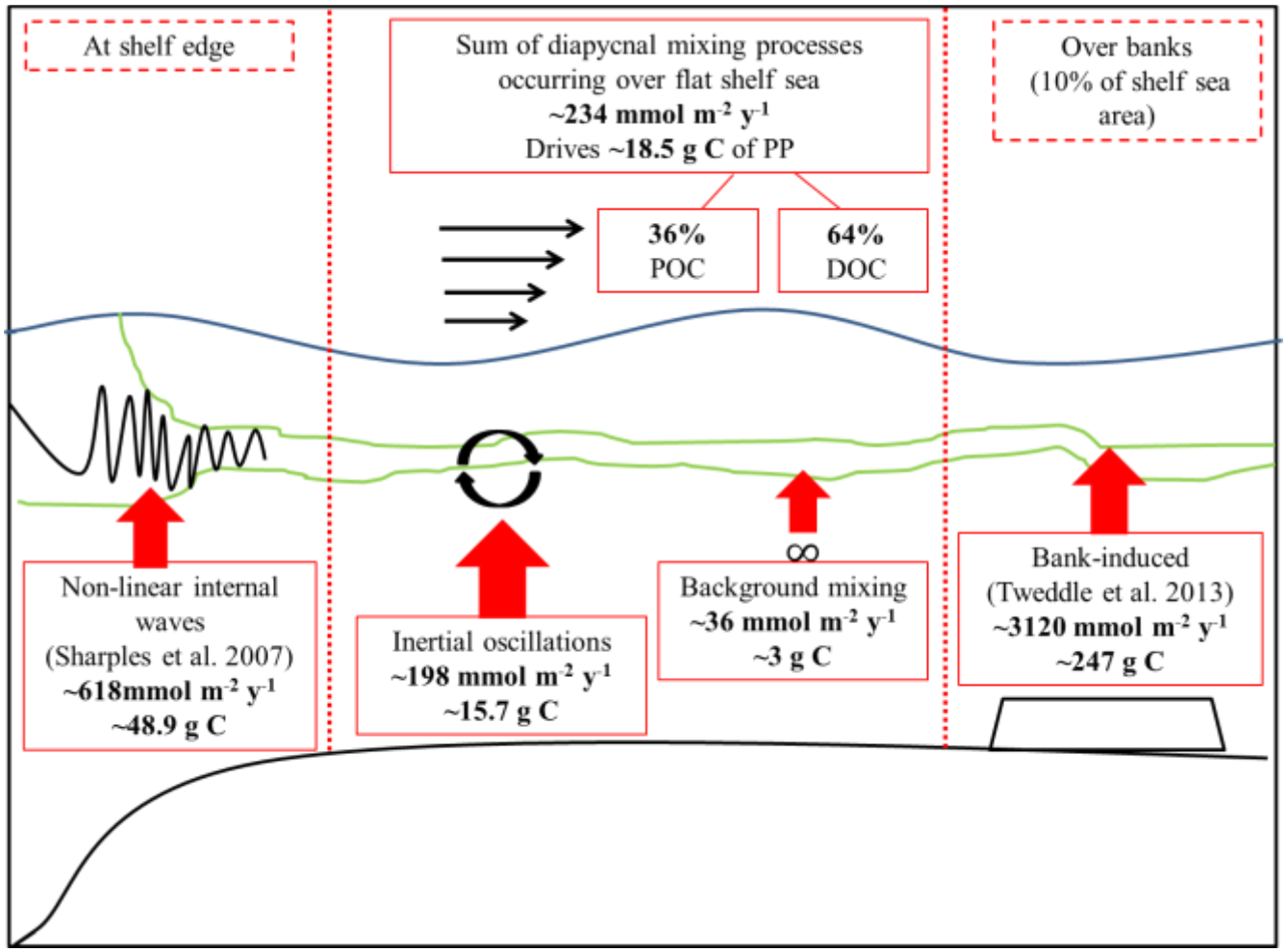

Figure 6.1: Schematic of various mixing processes contributing to the annual diapycnal flux of nitrate (mmol m^{-2} y^{-1}) to the shelf sea subsurface chlorophyll maximum, and the potential summer carbon fixation (g C) associated with this nitrate supply.

References

Behrenfeld, M. J., and P. G. Falkowski. 1997. Photosynthetic rates derived from satellite-based chlorophyll concentration. Limnol. Oceanogr. 42(1):1-20. Doi: 10.4319/lo.1997.42.1.0001

Blackford, J. C., I. Allen, and F. Gilbert. 2004. Ecosystem dynamics at six contrasting sites: A generic modelling study. J. Mar. Sys. 52: 191-15.

Burchard, H., and T. P. Rippeth. 2009. Generation of bulk shear spikes in shallow stratified tidal seas. Amer. Met. Soc. **29**:969-985, doi: 10.1175/2008JPO4074.1

Canadell, J. G., C. LeQuere, M. R. Raupach, C. B. Field, E. T. Buitenhuis, P. Ciais, T. J. Conway, N. P. Gillett, R. A. Houghton, and G. Marland. 2007. Contributions to accelerating atmospheric CO2 growth from economic activity, carbon intensity, and efficiency of natural sinks. PNAS. 104(47):18866-18870.

Davidson, K., L. C. Gilpin, R. Pete, D. Brennan, S. McNeill, G. Moschonas, and J. Sharples. 2013. Phytoplankton and bacterial distribution and productivity on and around Jones Bank in the Celtic sea.*in press*.

Dawson, A. G., K. Hickey, T. Holt, L. Elliot, S . Dawson, I. Foster, P. Wadhams, I. Jonsdottir, J. Wilkinson, J. McKenna, N. Davis, and D. Smith. 2002. Complex North Atlantic Oscillation (NAO) Index signal of historic North Atlantic storm-track changes. The Holocene. 12:363.

Dickey, T. 1991. The emergence of concurrent high resolution physical and bio-optical measurements in the upper ocean and their applications. Rev. Geophys. 29: 383-413.

Eppley, R. W., O. Holm-Hansen, and J. Strickland. 1968. Some observations on the vertical migration of dinoflagellates. J. Phycology. 4: 333-340.

Fraga, F., F. Perez, F. G. Figueiras, and A. F. Rios. Stoichiometric variations of N, P, C and O2 during *Gymnodinium catenatum* red tide and their interpretation. Mar. Ecol. Progr. Ser. 87: 123-134.

Gill, A. E. Atmosphere-ocean dynamics. Academic Press. London 1982.pp 323-345.

Hansell, D. A. 2002. DOC in the global ocean carbon cycle. In D. A. Hansell and C. A. Carlson (eds), *Biogeochemistry of marine dissolved organic matter*. Academic Press, San Diego, pp. 685-715.

Heaney, S. I., and R. W. Eppley. 1981. Light, temperature and nitrogen as interacting factors affecting diel vertical migrations of dinoflagellates in culture. J. Plankt. Res. 3(2):331-344.

Hickman, A. E., C. M. Moore, J. Sharples, M. I. Lucas, G. H. Tilstone, V. Krivtsov, and P. Holligan. 2012. Primary production and nitrate uptake within the seasonal thermocline of a stratified shelf sea. Mar. Ecol. Progr. Ser. **463**:39-57.

Hill, A. E., A. J. Souza, K. Jones, J. H. Simpson, G. I. Shapiro, R. McCandliss, H. Wilson, and J. Leftley. 1998. The Malin cascade in winter 1996. J. Mar. Res. 56(1):87-106.

Hopkinson, C. S., and J. J. Vallino. 2005. Efficient export of carbon to the deep ocean through dissolved organic matter. Nature **433**: 142-145

Hopkinson, C. S., J. J. Vallino, and A. Nolin. 2002. Decomposition of dissolved organic matter from the continental margin. Deep-Sea Res. II **49**: 4461-4478

Hu, Z. Z., and Z. H.Wu. 2004. The intensification and shift of the annual North Atlantic Oscillation in a global warming scenario simulation. Tellus A 56:112–124

Huthnance, J. M. V. A. Hendrik, M. White, D. E. Barton, B. LeCann, E. Coelho, E. Alvarez, P. Miller, and J. Vitorino. 2002. Ocean margin exchange – water flux estimates. J. Mar. Syst. 32(1-3):107-137.

Huthnance, J. M. 2009. Accelerating dense-water flow down a slope. J. Phy. Oceanogr. 39(6):1495-1511.

Hydes, D. J., R. J. Gowen, N. P. Holliday, T. Shammon, and D. Mills. 2004. External and internal control of winter concentrations of nutrients (N, P and Si) in north-west European shelf seas. Estuar. Coast. Shelf Sc. **59**: 151–161.

Ivanov, V. V., G. I. Shapiro, J. M. Huthnance, D. L. Aleynik, and P. N. Golovin. 2004. Cascades of dense water around the world ocean. Progr. Oceanogr. 60:47-98

Jahnke, R. A. 2010. Global Synthesis, p. 597-615. *In* K. K. Liu, L. Atkinson, R. A. Quinones and L. Talaue-McManus [eds.], Carbon and Nutrient Fluxes in Continental Margins: A Global Synthesis. Springer-Verlag.

Karl, D. M., and J. E. Dore. 2001. Microbial ecology at sea: sampling, subsampling and incubation considerations. In "Methods in Marine Microbiology". J. H. Paul. (Eds), pp 13-39. Academic Press.

Kitidis, V., N. J. Harman-Mountford, E. Litt, I. Brown, D. Cummings, S. Hartman, D. Hydes, J. R. Fishwick, C. Harris, V. Martinez-Vicente, E. M. S. Woodward, and T. J. Smyth . 2012. Seasonal dynamics of the carbonate system in the western English Channel. Cont. Sh. Res. **42**:30-40.

Legendre, L., and R. B. Rivkin.2002. Pelagic food webs: responses to environmental processes and effects on the environment. Ecology. Res. 17(2):143-149.

Mackinnon, J., and M. C. Gregg. 2003. Mixing on the late-summer New England shelf – solibores, shear and stratification. J. Phys. Oceanogr. **33**: 1476-1492

Palmer, M., M. E. Inall, and J. Sharples. 2013. The physical oceanography of Jones Bank: A mixing hotspot in the Celtic Sea. Progr. Oceanogr. (*in press*).

Rippeth, T. P. 2005. Mixing in seasonally stratified shelf seas: a shifting paradigm. Philos Trans A Math Phys Eng Sci. 363(1837): 2837-2854.

Rippeth, T. P., P. J. Wiles, M. R. Palmer, J. Sharples, and J. Tweddle. 2009. The diapycnal nutrient flux and shear-induced diapcynal mixing in the seasonally stratified western Irish Sea. Cont. Sh. Res. **29**:1580-1587.

Ross, O. N., and J. Sharples. 2008. Swimming for survival: A role of phytoplankton motility in a stratified turbulent environment. J. Mar. Sys. 70: 248-262.

Sharples, J., J. F. Tweddle, J. A. M. Green, M. R. Palmer, Y. Kim, A. E. Hickman, P. M. Holligan, C. M. Moore, T. P. Rippeth, J. H. Simpson, and V. Krivstov. 2007. Spring-neap modulation of internal tide mixing and vertical nitrate fluxes at a shelf edge in summer. Limnol. Oceanogr. **52**:1735–1747, doi:10.4319/lo.2007.52.5.1735.

Sherwin, T. J. 1987. Inertial oscillations in the Irish Sea. Cont. Sh. Res. **7**:191-213.

Simpson, J. H., and J. Sharples. 2012. Introduction to the shelf seas. In: Introduction to the physical and biological oceanography of shelf seas. Cambridge University Press, Cambridge, pp.

Trimmer, M., R. J. Gowen, B. M. Stewart, and D. B. Nedwell. 1999. The spring bloom and its impact on benthic mineralisation rates in western Irish Sea sediments. Mar. Ecol. Progr. **185**: 37–46., doi: 10.3354/meps185037.

Tsunogai, S., S. Watanabe, and T. Sato. 1999. Is there a 'continental shelf pump' for the absorption of atmospheric CO2? Tellus. 51B:701-712.

Tweddle, J. F., J. Sharples, M. R. Palmer, K. Davidson, and S. McNeil. (2013). Enhanced nutrient fluxes at the shelf sea seasonal thermocline caused by stratified flow over a bank. Progr. Oceanogr. *In press*.

Williams, C. A. J., J. Sharples, M. Green, C. Mahaffey, and T. P. Rippeth. (2013). The maintenance of the subsurface chlorophyll maximum in the western Irish Sea. Limnol. Oceanogr. Fluids & Environments. **3**: 61–73.

Wobus, F., G. Shapiro, M. A. M. Maqueda, and J. M. Huthnance. 2011. Numerical simulations of dense water cascading on a steep slope. J. Mar. Res. 69(2-3):391-415